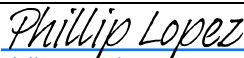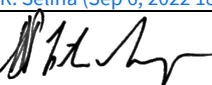# Front End Conceptual Design Description

020.30.05.00.00-0006-DSN

Status: **RELEASED**

PREPARED BY	ORGANIZATION	DATE
W. Grammer, S. Sturgis	Antenna Electronics IPT, NRAO	2022-07-26

APPROVALS	ORGANIZATION	SIGNATURES
P. Lopez, Antenna Electronics IPT Lead	Antenna Electronics, ngVLA/NRAO	*Phillip Lopez* Phillip Lopez (Sep 6, 2022 12:30 MDT)
T. Kusel, Systems Engineering	ngVLA System Engineering, NRAO	Thomas Kusel (Sep 6, 2022 20:36 GMT+2)
R. Selina, Project Engineer	ngVLA Project Office, NRAO	*R. Selina* R. Selina (Sep 6, 2022 18:03 MDT)
W. Esterhuyse, Telescope Project Manager	ngVLA Project Office, NRAO	

RELEASED BY	ORGANIZATION	SIGNATURE
W. Esterhuyse, Telescope Project Manager	ngVLA Project Office, NRAO	

Change Record

Version	Date	Author	Affected Section(s)	Reason
A	2019-07-24	A. Lear	All	Prepare PDF for approvals & release.
A.01	2022-01-25	A. Lear	All	Revised document number, approval queue for CoDR.
A.02	2022-03-08	W. Grammer	All	Initial draft of CoDR version
A.03	2022-03-09	A. Lear	All	Formatting, copy edits.
B	2022-05-30	W. Grammer	All	CDR version, most internal RIDs done
C	2022-07-21	W. Grammer	All	Post-CDR; RIDs addressed; resubmitted as C

Table of Contents

1 Introduction

1.1 Purpose

This document lays out a detailed conceptual design for the Front End subsystem and its components. This document will be part of the review package for the ngVLA System Conceptual Design Review (CDR).

1.2 Scope

This document covers the Front End subsystem in its entirety, as well as some details on the ngVLA 18-meter antenna optics. This includes key components and their functions; the design approaches, tradeoffs, and associated risks; and the interfaces to other defined subsystems. It does not include specific technical requirements, precise details of the interfaces, or schedule and budgetary details; however, references to these are provided as available.

2 Related Documents and Drawings

2.1 Applicable Documents

The following documents may not be directly referenced herein, but provide necessary context or supporting material.

Ref.	Document Title	Rev./Doc. No.
AD01	W. Grammer and R. Selina, "ngVLA Receiver Configuration Trade Study"	ngVLA Electronics Memo #13
AD02	18-Meter Antenna Optics Definition	020.25.01.00.00-0006-DSN

2.2 Reference Documents

The following documents are referenced within this text:

Ref.	Document Title	Rev./Doc. No.
RD01	Front End Reference Design Description	020.30.03.00.00-0002-DSN
RD02	Front End Technical Requirements	020.30.05.00.00-0003-REQ
RD03	R. Lehmensiek, "ngVLA: Structural Deformed Analyses", EMSS Antennas (Pty), 10 Dec. 2020	EMSS# EA-NGV-DR-06 Ref.: NRAO PO# 368286
RD04	R. Selina, "System-Level Cost Comparison of Offset and Symmetric Optics."	ngVLA Antenna Memo #1
RD05	R. Selina, "System-Level Evaluation of Aperture Size."	ngVLA Antenna Memo #2
RD06	R. Selina et al., "Antenna Optical Design Alternatives."	ngVLA Antenna Memo #3
RD07	ngVLA Optical Reference Design: Analysis of the ngVLA Antenna Optical Design #6 with Ideal and Actual Feed.	020.25.01.00.00-0001-REP
RD08	R. Lehmensiek and D. I. L. de Villiers, "An Optimal 18 m Shaped Offset Gregorian Reflector for the ngVLA Radio Telescope," *IEEE Trans. Antennas Propag.*, vol. 69, no. 12, pp. 8282–8290, Dec. 2021.	
RD09	R. Lehmensiek, "Final Report: ngVLA: 18-meter Antenna Optics Design," EMSS Antennas (Pty), 19 Oct. 2021.	EMSS# EA-NGV-DR-05 Ref.: NRAO PO# 368286

Ref.	Document Title	Rev./Doc. No.
RD10	W. Zhong et al., "1.2-4.2 GHz Spline QRFH for ngVLA", Caltech, 19 Nov. 2017	(no formal doc#)
RD11	R. Lehmensiek et al., "Deriving an Optimum Mapping Function for the SKA-Shaped Offset Gregorian Reflectors," *IEEE Trans. Antennas Propag.*, vol. 63, no. 11, pp. 4658–4666, Nov. 2015.	
RD12	S. Weinreb et al., "Cryogenic 1.2 to 116 GHz Receiver for Large Arrays," EuCAP, 12 Apr. 2018.	
RD13	J. Flygare, "ngVLA QRFH Demonstrator, 1.2 – 4.2 GHz simulated on both the SKA and ngVLA#6 reflector", OSO/Chalmers, 3 Aug. 2018.	(no formal doc#)
RD14	H. Mani and S. Weinreb, "Wideband Prototype Front-end for the ngVLA, Development Report," NRAO Socorro Colloquium, 25 Jan. 2019.	
RD15	S. White, private communication, 8 Feb. 2022.	
RD16	B. Simon, "Feed window and mechanical design," GBO Ultra-wideband Receiver Rebaseline Review, 22 Apr. 2021.	(no formal doc#)
RD17	R. Lehmensiek, "ngVLA: Band 1 Feed Study Interim Report," EMSS Antennas (Pty), 26 Nov. 2021.	EMSS# EA-NGV-DR-08 Ref.: NRAO PO# 371918
RD18	R. Lehmensiek, "ngVLA: Band 1 Feed Study," EMSS Antennas (Pty), 10 Feb. 2021.	EMSS# EA-NGV-DR-07 Ref.: NRAO PO# 368286
RD19	SOW: Band 1 Feed Design Study Phase 2.5.	020.30.05.01.01-0003-SOW
RD20	A. Dunning et al., "Design of a Band 2 Feed Horn for the ngVLA," CSIRO, 30 Oct. 2019.	(no CSIRO doc#) Ref.: NRAO PO# 365028
RD21	A. Dunning et al., "An Ultra-Wideband Dielectrically Loaded Quad-Ridged Feed Horn for Radio Astronomy," IEEE-APS Topical Conference on Antennas and Propagation in Wireless Communications (APWC), 2015.	
RD22	A. Dunning et al., "Offset quad ridged ortho-mode transducer with a 3.4:1 bandwidth," Proc. Asia Pacific Microwave Conf., 2013.	
RD23	SOW: ngVLA Band 2 Feed Horn: Phase 2 Design Studies.	020.30.05.02.01-0001-SOW
RD24	C. Granet, "R&D Collaboration with CSIRO for Design of a Band 2 Horn for the ngVLA: Preliminary Design Study," Lyrebird Antenna Research Pty Ltd, 30 Sept. 2019.	LAR# ER_0166_rev_1 Ref.: NRAO PO# 365028
RD25	R. Lehmensiek, "Final Report: ngVLA Feed Feasibility Study," EMSS Antennas (Pty), 7 Feb. 2019.	EMSS# EA-NGV-DR-01 Ref.: NRAO PO# 362812
RD26	ngVLA Antenna Electronics Block Diagram.	020.30.00.00.00-0005-BLK
RD27	R. Rayet, "ngVLA Front-end Receivers Thermal Study Initial Analysis Report," Callisto France S.A.S, 11 July 2018.	Callisto REP/1406/4366 Ref.: NRAO PO# 360198
RD28	A. Simone, "ngVLA Front-end Receivers Thermal Study Dewar B update," Callisto France S.A.S., 14 Feb. 2020.	Callisto REP/1406/4770 Ref.: NRAO PO# 367434
RD29	Front End Cascade Analysis Tool.	020.30.05.00.00-0004-GEN
RD30	B. Butler et al., "ngVLA Antenna Noise Temperature Calculation."	ngVLA Memo #96
RD31	S. Hesari et al., "NRC Q-band / Band-5 receiver development for the ngVLA," NRC Herzberg Astronomy and Astrophysics Research Centre, Oct. 2021	NRC# HAA-RIT-NGVLA-001-REP-A

Ref.	Document Title	Rev./Doc. No.
RD32	F. Jiang et al., "Cryogenic LNA Development for ngVLA Band 1, 3, 4, and 5 Receivers," NRC Herzberg Astronomy and Astrophysics Research Centre, Oct. 2021	NRC# HAA-RIT-NGVLA-003-REP-A
RD33	D. Henke et al., "Octave Band Receiver for ngVLA," NRC Herzberg Astronomy & Astrophysics Research Centre, Oct. 2021	NRC# HAA-RIT-NGVLA-002-REP-A
RD34	S. Hesari, private communication, 27 May 2022.	

3 Subsystem Overview

3.1 High Level Description

The basic purpose of the ngVLA Front End subsystem is the reception and amplification of incoming signals from astronomical sources collected by the antenna optics, over a broad frequency range. The ngVLA science goals require continuous frequency coverage from 1.2–116 GHz, with a gap at the atmospheric absorption band between ~50–70 GHz. This will be implemented in six, single-pixel, cryogenically-cooled receiver bands, with all but the largest consolidated into a single cryostat. Both cryostats are integrated into a temperature-controlled enclosure located on the antenna feed arm at the secondary focal point. Two-axis lateral translation of the enclosure is proposed for both band selection and focus adjustment.

3.2 Design Driving Requirements

Given the extremely low input levels, high gain is required, with the lowest possible added instrumental noise for maximum sensitivity. Optimizing overall sensitivity in each receiver band, while minimizing the total operating cost are the primary design goals: therefore, receivers must be cryogenically cooled, and multiple bands integrated into a common cryostat to maximize overall reliability. The receivers must also have exceptional temporal gain and phase stability, and high linearity.

Use of feed horn designs that have broad bandwidth and high aperture efficiency are also key to meeting these goals. Compact feed designs are also preferred, as they can be integrated into the receiver cryostat and cooled, further reducing the system noise. Total mass is an important concern, given that the antenna optics places the Front End package on a movable platform within the feed arm, rather than at a fixed location under the main reflector as on the VLA antennas.

A subset of the key requirements that drive the design, along with their associated technical risk levels for not being met, are listed in Table 1 below.

Parameter	Summary of Requirement	Reference	Risk Level
Optimum sensitivity	Overall sensitivity should be maximized for each band, to minimize total # of antennas required for science goals.	FED0001	Low
Optimum running cost	Limit annual maintenance cost to 5% of construction, by reducing cryocooler count per antenna to the minimum required.	FED0002	Low
Receiver gain	> 30 dB, between feed horn input and cryostat output. Ensures IRD contribution to T_{SYS} is < 1 K.	FED0401	Low to Moderate
Receiver sensitivity	Band 1: T_{RX} < 11.8 K max, 9.7 K avg. Band 2: T_{RX} < 15.1 K max, 12.1 K avg.	FED0201 FED0202	Low Low

	Band 3: T_{RX} < 17.8 K max, 15.1 K avg.	FED0203	Low
	Band 4: T_{RX} < 18.2 K max, 16.0 K avg.	FED0204	Moderate
	Band 5: T_{RX} < 24.9 K max, 21.1 K avg.	FED0205	Low
	Band 6: T_{RX} < 69.0 K max, 49.0 K avg.	FED0206	Low
Aperture efficiency	Band 1: 0.65 min (full), 0.77 min (80%)	FED0311	Moderate
	Band 2: 0.90 min (full), 0.92 min (80%)	FED0321	Moderate
	Band 3–6: 0.92 min (full), 0.94 min (80%)	FED0331	Low
Gain and bandpass stability	Normalized G_{TC} < 0.26 dB/K	FED0402	Low
	Each channel: < 0.013 dB over 60 minutes	FED0406	Moderate
	Pol-to-pol: < 0.026 dB over 5 minutes	FED0407	Low
Receiver dynamic range	Band 1: 46 dB min	FED0501	Low
	Band 2: 41 dB min, 42 dB goal	FED0502	Moderate
	Band 3: 39 dB min, 42 dB goal	FED0503	Low
	Band 4: 36 dB min, 42 dB goal	FED0504	Low
	Band 5: 33 dB min, 42 dB goal	FED0505	Moderate
	Band 6: 31 dB min, 42 dB goal	FED0506	High
Reliability	MTBM > 8800 hours, excluding cryocoolers	FED4004	Low
Total mass	140 kg max, excluding cryocoolers	FED0033	Moderate
Cryostat overall leak rate	< 10^{-8} std. cc He / sec (total for each cryostat)	FED2205, FED2215	Low to Moderate

Table 1: Key Front End Requirements, taken from [RD02]

3.2.1   Receiver sensitivity

Sensitivity of the Front End is quantified by the receiver noise temperature, T_{RX}. It includes all cryogenically cooled RF components in a receiver band (feed horn, OMT, LNAs, etc.), along with the infrared filter(s), vacuum window, and radome cover. To achieve optimum sensitivity, components must have low insertion loss (especially those ahead of the LNA) and for the LNA specifically, very low added noise.

3.2.2   Aperture efficiency

The feed and optics are assumed here to be perfectly aligned on the optical boresight, with no mechanical distortions from gravity, temperature, or wind. Optical surfaces are assumed to be perfectly smooth (i.e., unity Ruze efficiency term), and with negligible conductor loss. Blockage and polarization effects on overall efficiency are also assumed to be negligible in this case.

3.2.3   Gain and bandpass stability

To reduce gain and bandpass variation to the required levels, servo loop stabilization of the LNA bias current over temperature may be required. Closed-loop regulation of the cold stage temperature, using a variable-speed cryocooler, a small heater, or perhaps both, can further enhance temporal stability. Reducing RF mismatch and standing waves within the receiver chain will improve bandpass stability.

3.2.4   Receiver dynamic range

Receiver dynamic range is defined as the difference at the receiver output between the system noise on cold sky and the 1 dB compression point, assuming an input of broadband noise with a flat spectral noise characteristic across the full bandwidth of the receiver. A derating factor of 5 dB is applied, to account for the lower compression point with broadband noise versus narrowband (CW) output.

3.2.5 Cryostat overall leak rate

Principal contributors are: the number of feed horn windows along with their material type, diameter, and thickness; number and type of RF penetrations (coax or waveguide); number and size of service panels; and other factors, such as the gasket/O-ring types use, and the vacuum solenoid valve rating.

3.3 Key Technical Risks

Much of the Front End design uses existing and proven technology, so the overall level of associated technical risk is low to moderate. However, there are aspects of the subsystem design, production, and maintenance where failures could have significant consequences, such as loss of science capability, large schedule slips, or cost overruns. Here are a few of these that have been identified:

1) **Excessive sag and/or twisting of the antenna feed arm during translation of Receiver enclosure for band selection**. Although this is technically a structural issue with the antenna, the consequences would fall on the optical system; namely, a loss in aperture efficiency, significant pointing error, and a possible degradation in polarization performance. Mitigation of the first two is possible: some of the aperture efficiency loss due to gravitational sag is recoverable by adjusting the focus [RD03], and systematic pointing errors can be compensated for in the pointing model. However, twisting of the feed arm could cause rotation of the polarizations on the sky, an effect more difficult to remove, if at all.

   If structural changes to the feed arm are insufficient to reduce or eliminate these issues, the only other alternatives are a significant reduction in mass of the cryostats, or rearranging receivers to limit total translation, or perhaps both. Either would entail a major redesign of the cryostats and positioners, posing a significant technical as well as a schedule risk.

2) **Heavy reliance on commercial vendors for key receiver components like LNAs**. The large number of antennas in the ngVLA results in ~600 production LNAs needed per receiver band, including sufficient receiver and component spares. In contrast with past projects at NRAO, where most if not all LNAs were designed and built in-house, many if not all of these devices will likely be sourced from outside vendors or project partners. This presents a potentially significant cost and schedule risk, if for instance the supplier is unable to complete an order or deliver to schedule, or has unforeseen performance or quality issues. All of these scenarios are possible, and mostly beyond our control.

   A way to mitigate these risks is to develop reliable alternate sources for LNAs and other critical components. These could be in-house (the CDL), other project partners, vendors, or even university labs. This would require advance planning and additional funding, but would alleviate the risks associated with reliance on a single source for a critical component in multiple bands.

3) **Vulnerability of the Receiver enclosure to damage during transport**. Unlike on the VLA, individual ngVLA receivers or cryostats will not be swapped out in the field, but rather the entire Receiver enclosure would be replaced in the event of a component failure within (the cryocoolers being one notable exception). While in some ways simpler, the large size and mass of the enclosure and the delicate electronics within makes it riskier to handle and transport, especially on unpaved or gravel roads where vibration and repeated shocks could easily cause damage. To minimize these risks, specially-outfitted maintenance/transport vehicles equipped with suitable lifting devices will be needed, along with well-documented removal and installation procedures that include specific cautions on handling and transport.

4   Concept Development

The overall Front End subsystem concept and configuration have not changed in a major way since the so-called "reference" design phase, documented in [RD01]. However, there have been significant advances on the antenna optics and with wideband feed horns, which are summarized in detail in the following sections. A separate initiative by the NRC HAA (Canada) was undertaken to develop receiver components for the proposed ngVLA Band 5, as well as a study of octave-band receivers. Highlights from their work are shown in an appendix (Section 7.1), with a few comments and observations as well.

4.1   General Design Constraints

One key factor influencing the Front End subsystem design concept was the need to reduce the operating cost, particularly in the cryogenic system. The ngVLA as currently envisioned will have 263 antennas, more than nine times that of the present array but with an operations budget constrained to just three times that of the VLA and VLBA. It was immediately apparent that a system with many separately cooled receiver bands on each antenna (as implemented on the VLA and VLBA) would be inordinately expensive to build, operate, and maintain if scaled for the ngVLA. To attain the desired reduction in overall cost, two principal constraints were adopted during the reference design phase, reiterated below:

- **Maximize the fractional bandwidth of individual bands to the extent possible to reduce the total band count.** This is critical for bands at the low end of the frequency range: for example, an octave of bandwidth at the low end is 1.2 GHz, compared to 58 GHz at the high end. Low-frequency receivers (and feeds) also tend to be large and heavy, so reducing their number is critical to controlling the total cost and mass of the Front End package. However, the trade-off with wider bandwidth is degraded performance of the LNA and feed horn; i.e., a higher receiver noise temperature (T_{RX}) and a lower aperture efficiency (η_A). Taken too far, the additional antennas needed to recover the lost sensitivity would more than negate any cost savings from having fewer bands. To determine an optimum configuration for the ngVLA bands, a detailed design study was performed [AD01], and the final configuration from that study is presented in the following section.

- **Minimize the number of cryocoolers and cryostats required per antenna.** This is accomplished by packaging multiple receiver bands into a common cryostat. Benefits are a reduction in the total cryogenic load, and improvement of overall reliability by having fewer cryocoolers to wear out or fail. While relatively easy to accomplish for the high-frequency bands, it becomes impractical at low frequencies if the feed horn becomes much larger than its associated receiver. With high-gain feeds like those in the VLA antennas, receiver consolidation on all but the highest-frequency bands is not feasible for this reason. However low-gain feeds are much smaller, and could allow close spacing of receiver assemblies within a common cryostat. This obviously influences the optical and mechanical design of the antenna as well.

4.2   Optical System

The broad objective here is to obtain the optimum array sensitivity (generally expressed as Aeff/Tsys, the ratio of effective collecting area to system noise temperature) while remaining within the overall array construction and operating cost constraints. There is a complex interdependence between the antenna geometry and optics, feed horn type and size, and the total number of antennas and cryostats required. A number of design studies [RD04, RD05, RD06] were conducted to consider the tradeoffs between various

antenna geometries, aperture sizes, feed horn opening angles, and focusing/positioner concepts. The configuration adopted for the ngVLA optical system is described in the following subsections.

4.2.1 Antenna Geometry and Optics

The ngVLA main antenna will have a dual-offset Gregorian optical configuration, with an unblocked primary aperture of 18 meters, a secondary reflector chord length of approximately 3.33 meters, and a subtended half-angle at the secondary focus of 55 degrees. The secondary reflector has an added extension towards the bottom end to shield the feed horns from ground emission, thus reducing the antenna temperature. The appropriate choice of primary and secondary offset angles is effective in cancelling much of the cross-polarization response introduced by the offset geometry. The assumed feed arm position at low elevation angles is down (i.e., close to the ground), to allow for easier access to the secondary focus [AD02].

Optical shaping of both reflector surfaces is done to increase antenna forward gain, with acceptable trades in sidelobe levels and offset tolerances (scan loss, pointing error). The analytic mapping function used in the "reference" antenna design [RD07] was superseded in the conceptual antenna by one derived by an exhaustive parametric study of a parameterized aperture field distribution, using an actual corrugated feed horn radiation pattern and the secondary reflector extension [RD08]. The result is a fairly uniform illumination over almost all of the primary aperture, with a sharp roll-off near the edge. Total aperture efficiency was increased by ~6% and the sensitivity by ~12% over the previous mapping function [RD09]. Figure 1 and Figure 2 show optical ray trace diagrams of this system in the plane of symmetry [AD02].
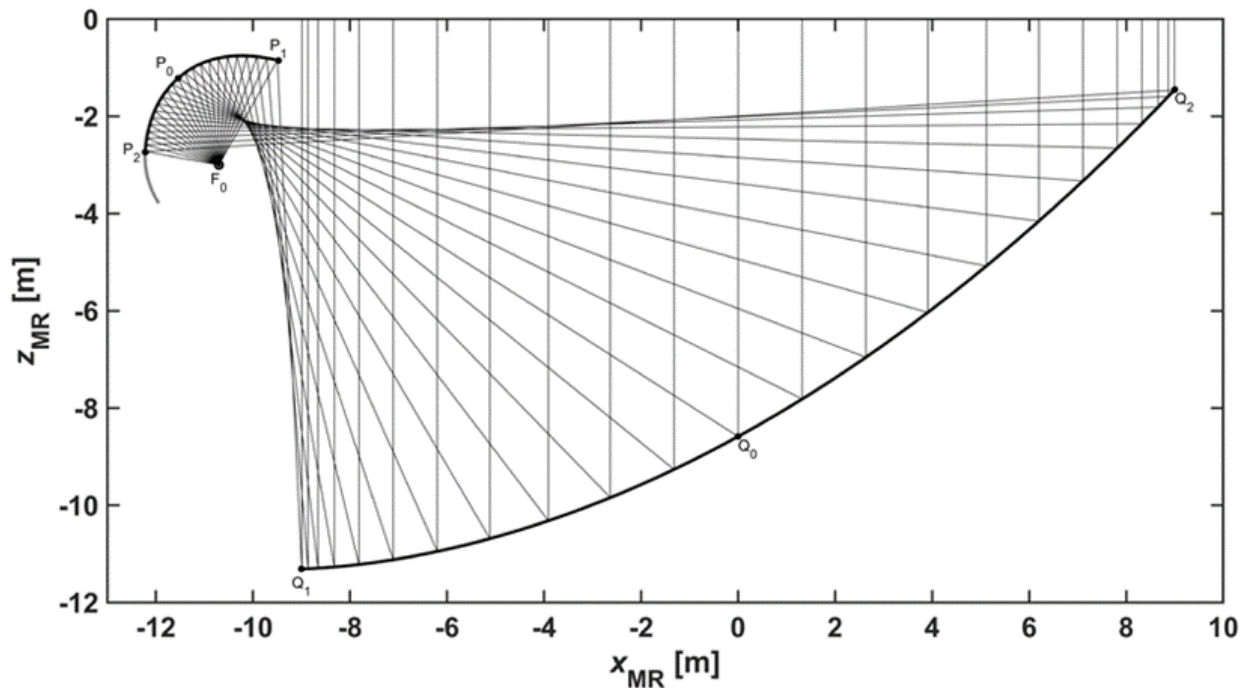

Figure 1: Optical ray trace of the ngVLA 18-meter antenna optics. The close spacing of rays at the edge of the primary aperture correspond to a sharp roll-off in illumination, reducing spillover while maximizing illumination efficiency.
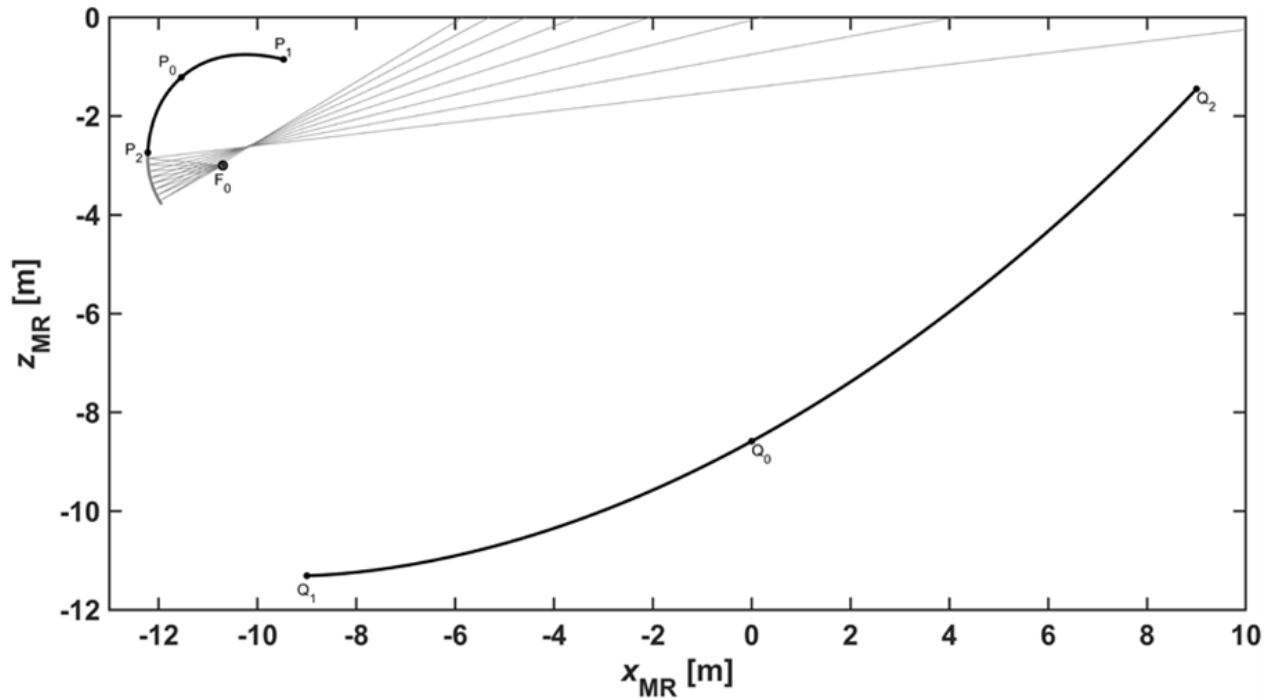
Figure 2: Optical ray trace of ngVLA 18-meter antenna secondary reflector extension. Spillover from the feed horn that would otherwise land on the ground is redirected toward cold sky, reducing the overall Tsys.

4.2.2   Feed Horns

Given the wide subtended (opening) angle at the secondary focus, feed horns matched to the ngVLA antenna optics will have relatively low gain compared to corresponding feed horns used in the VLA. Consequently, they will be far more compact, particularly in the upper decade of frequency coverage.

In the lower decade of frequency coverage (1.2–12.3 GHz), a quad-ridged feed horn (QRFH) was adopted as the best overall wideband, low-gain option. An all-metal QRFH can have reasonably good aperture efficiency and acceptable input match at bandwidth ratios up to ~3.5:1, depending on the horn and ridge taper profiles selected. Adding dielectric loading into the throat of the feed (e.g., a tapered cone or dowel, often with multiple layers) can extend the bandwidth ratio beyond two octaves. Therefore, full coverage of the lower decade is possible with just two receivers, rather than four as in the VLA [AD01].

In the upper decade of frequencies (12.3–116 GHz), optimum performance from the optics and receivers is needed to meet system sensitivity requirements. The feed horn type proposed for these bands is conical type with concentric corrugations, a highly compact design well suited for large opening angles [RD01]. Overall aperture efficiency is high, close to that obtained with an ideal Gaussian feed. The backlobe, spillover, cross polarization, and far-out sidelobe levels are lower compared to the QRFH, but over a narrower (octave) bandwidth [RD07].

Starting in 2019, a number of design studies were conducted on various feed horn options, with two still ongoing in their second round. Design and performance of each is presented in the following sections.

4.2.2.1   Caltech Band 1 Horn

The wideband feed horn included in the Front End reference design is a highly-compact QRFH designed by Caltech for 1.2–4.2 GHz, which overlaps ngVLA Band 1 (1.2–3.5 GHz). The feed opening angle and

ridge profiles were optimized for the SKA antenna optics, a shaped dual-offset Gregorian design very similar to the ngVLA main antenna [RD10, RD11]. A photograph of this feed is shown in Figure 3, with measurements of return loss at each of the ports. Plots of simulated aperture efficiency with and without an external cone around the feed are given in Figure 4 [RD12]. Maximum cross polarization over frequency was not reported for the feed horn alone, though in a separate unpublished memo, the intrinsic cross polarization (IXR) of this feed with the SKA optics was determined be >15 dB over the band [RD13].
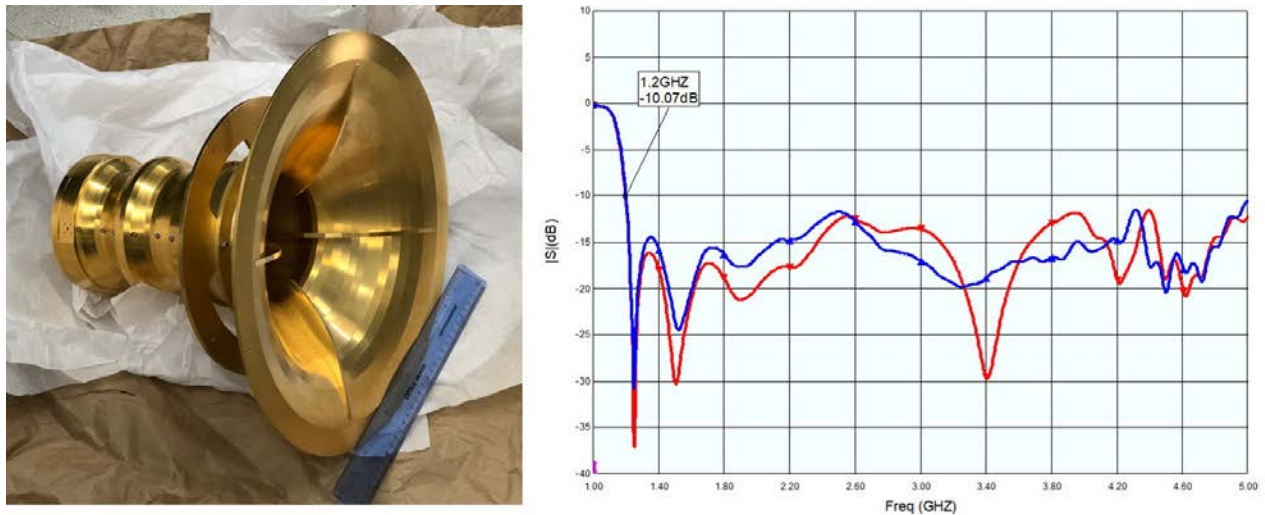
Figure 3: Band 1 feed prototype designed by Caltech, with measured return loss at each orthogonal port. The feed aperture diameter is ~350 mm, only 1.4 wavelengths at 1.2 GHz. Overall length is just ~300 mm.

Performance of the Caltech feed is remarkably good, given how small it is relative to the wavelength at 1.2 GHz. Port return loss is better than 10 dB over more than two octaves of bandwidth, and the aperture efficiency is fairly flat and reasonably good up to about 3.7 GHz. Spillover noise is quite high towards the low end of the band, likely due to the small electrical size of the aperture which tends to manifest as a higher backlobe in the radiation pattern. The external feed cone (a portion of which can be the cryostat vessel) appears to reduce the spillover noise significantly and with no adverse effect on aperture efficiency.

On the other hand, the influence of an external feed cone on the full radiation pattern is still unknown: while the backlobe may be reduced, there could be added sidelobes away from the boresight which could pick up RFI, a particularly bad problem in this band. And if the feed is coupling radiatively to the cryostat vessel as it appears, other pathologies may arise from this, such as excitation of resonant cavity modes in the cryostat vessel, evident as gain suck-outs or as noise spikes in the receiver passband.

Another challenging problem is designing a suitable vacuum window for the cryostat when the feed is cryogenically cooled, as it must be in this case. Because the quad ridges extend all the way to the horn aperture, a thermal break cannot be placed within the feed horn to allow the large aperture section to be placed outside of the cryostat. Hence the required window becomes quite large, and the force on it is enormous: over 1 metric ton at the VLA site elevation. The cryostat eventually built around this feed [RD14] used as a vacuum window a single layer of Mylar film ~0.36 mm thick clamped to the cryostat cylinder flange. It actually performed quite well under repeated cycling in the lab, though the deflection at the window center under vacuum was very noticeable (~50 mm). The RF loss was also low. However, Mylar degrades with long-term exposure to ultraviolet rays: the Mylar dust covers used on the VLA Ka- and Q-band feed apertures literally disintegrate after several years in the field, even though they are under a protective radome. Condensation and ice accumulation on the window (due to close proximity and

direct exposure to the cooled feed surfaces) is also a serious issue, even under ambient laboratory conditions [RD15]. This could be mitigated by adding a thick layer of expanded foam insulation between the feed horn and window. However, the additional space required above the feed horn for the insulation would significantly increase the window (and cryostat) diameters due to the large opening angle of the beam, adding extra volume and mass.
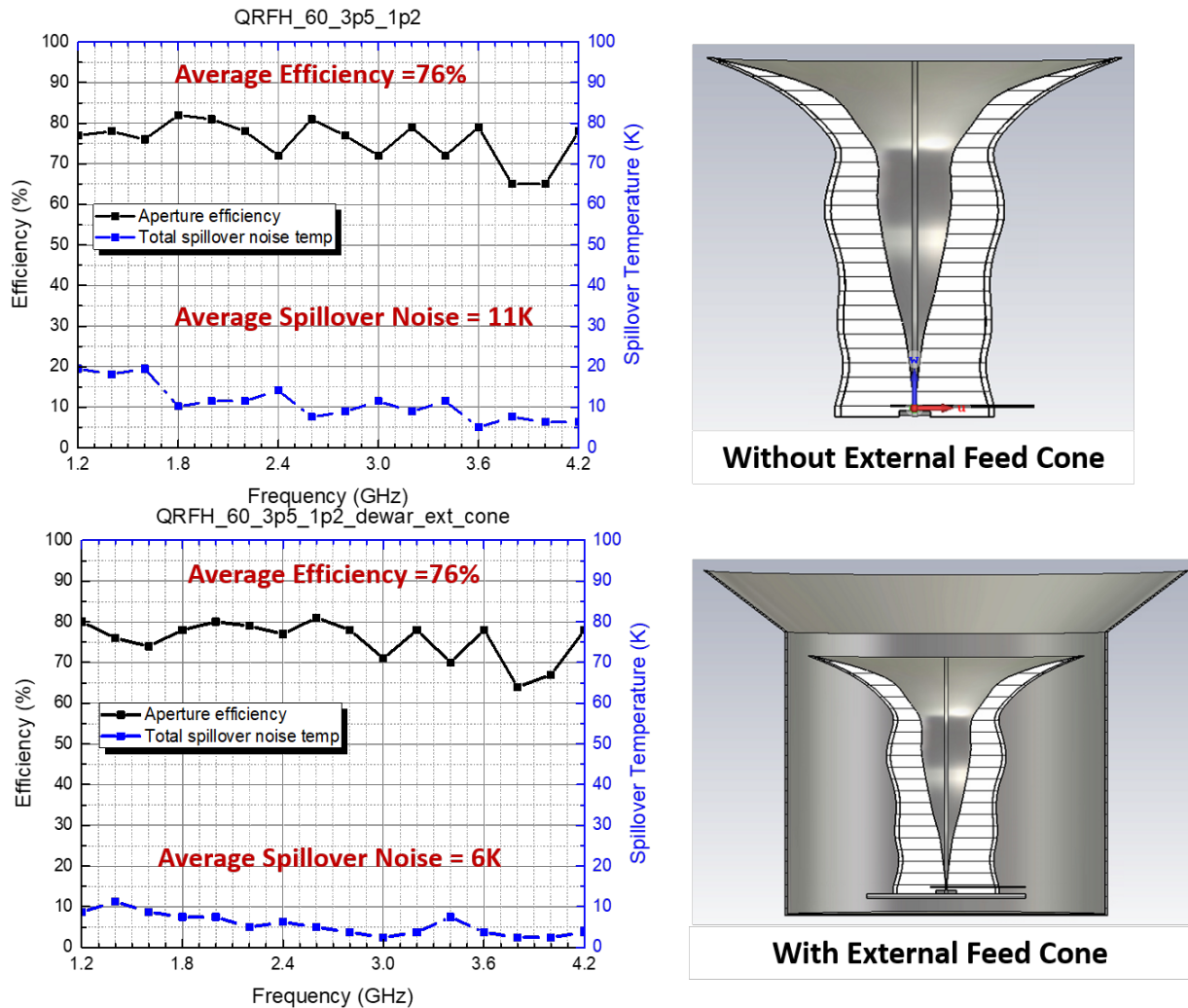
Figure 4: Simulated aperture efficiency of the Caltech feed horn with a dual-offset Gregorian shaped antenna. The external shield serves to redirect the backlobe away from the ground and toward cold sky, reducing spillover noise. Antenna elevation in these cases is 90 degrees (zenith).

Other window materials were investigated, in particular the vacuum-infused quartz fabric/epoxy laminate developed by a team at the Green Bank Observatory for a similar application [RD16]. While it is extremely durable, moderate in cost, and amenable to mass production, measurements of a prototype and related analyses [RD15, RD17] indicates the RF mismatch and attendant passband ripple may be quite high with this approach at frequencies above 2 GHz.

In summary, the potential performance issues of this feed horn combined with the difficulty of designing a large, mechanically robust vacuum window with good RF performance present moderately high technical risks, and ones without a clear path for mitigation short of a totally new feed design.

4.2.2.2   EMSS Band 1 Horn

An alternative to the Caltech Band 1 QRFH is currently at an advanced stage of development, after a series of design studies by EMSS Antennas [RD18, RD17]. Figure 5 shows a cross-sectional view of this feed horn in its current form. It is also a quad-ridged design, but with ridges that terminate ahead of the flared horn section. A thermal gap transition is added at this point to allow the large flared horn to be located outside of the cryostat, reducing the size of the cryostat. The horn/ridge profiles are splines defined by 20 total points, the coordinates of which were numerically optimized for high sensitivity and low mismatch. Finally, a highly compact balun is used for transitioning to the coax outputs from the polarizer (OMT) section.
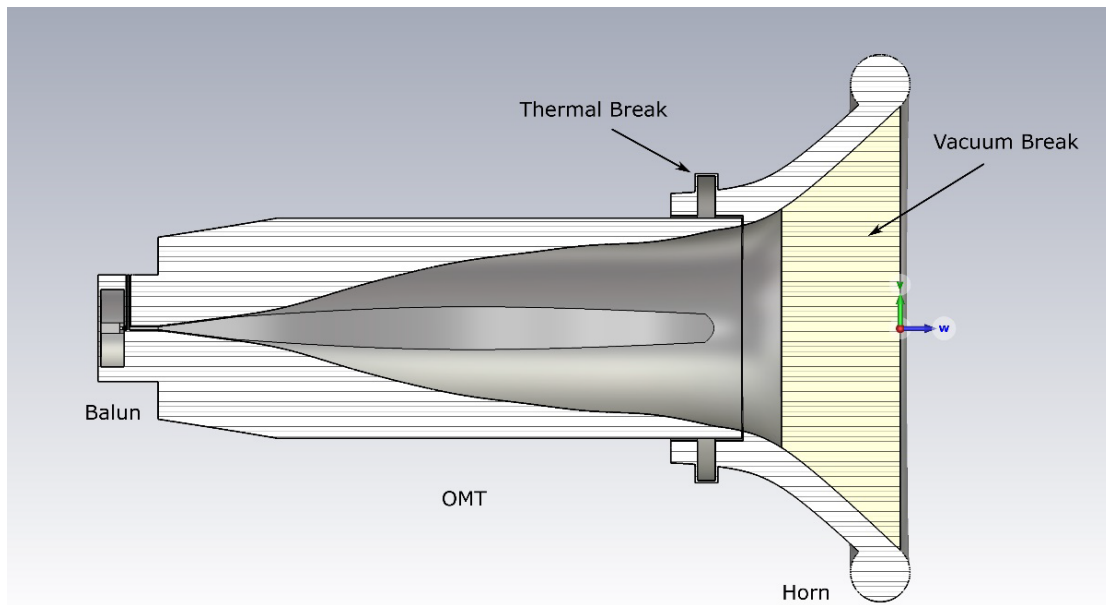
Figure 5: Cross-sectional view of the EMSS Band 1 feed horn concept. The origin point shown near the feed aperture plane coincides with the approximate phase center location at the upper band edge frequency.

The vacuum window is a thick wedge of closed-cell expanded foam (Divinycell H80, $\varepsilon r = 1.1$) bonded to the flared horn. It's simple, inexpensive, fairly robust, and addresses the problems of condensation and RF mismatch associated with the previous vacuum windows. The minimum thickness required for an adequate safety factor and for insulation from the cold surfaces on the vacuum side will be determined in a future mechanical and thermal analysis of the structure. Leak rate and outgassing tests of the foam will need to be conducted to verify its suitability as a vacuum window. A thin UV-protective film or coating on the outside may also be required to mitigate long-term degradation from exposure to sunlight. Nevertheless, given an almost identical material was used for windows on the VLA L-band and S-band receivers, we have high confidence this window design will in the end perform very well.

Plots of the simulated output return loss and total aperture efficiency are given in Figure 6. Port match is excellent, better than 20 dB return loss at all but the band edges. Aperture efficiency is quite high at midband but rolls off toward the band edges, especially above 3 GHz. The low end could be improved by relaxing the size constraint on the feed aperture outside diameter (450 mm); however, this is unlikely given the space constraints on the antenna feed arm where the Front End receivers are located. The high-end roll-off could be addressed by addition of dielectric within the ridged and/or horn sections: this is the subject of a proposed follow-on study that will be conducted later this year [RD19].
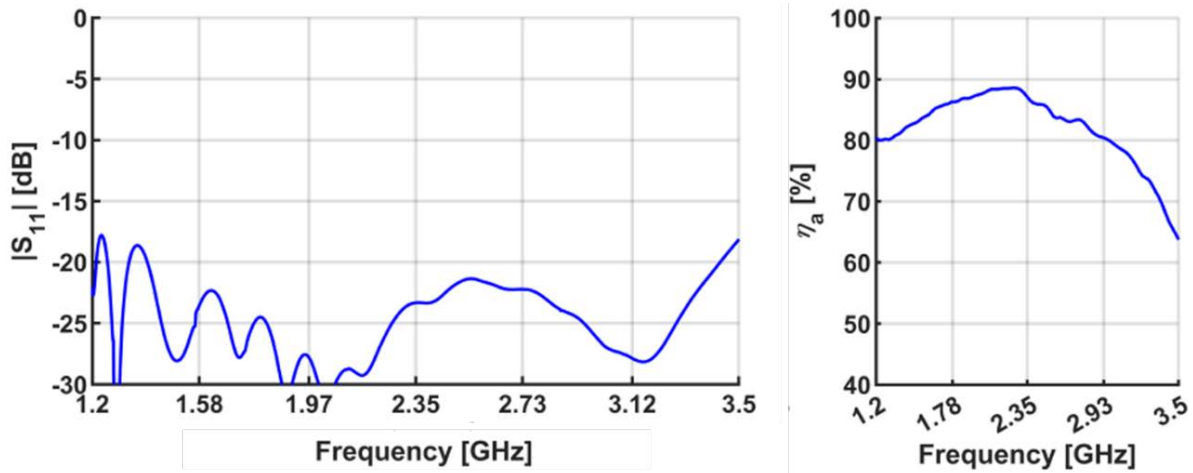
Figure 6: Simulated output return loss and aperture efficiency of the EMSS Band 1 feed horn concept. The ngVLA conceptual antenna optics were assumed for the calculation.

Figure 7 plots the spillover noise temperature and cross polarization levels relative to the main beam versus frequency, calculated with the ngVLA 18-meter conceptual antenna optics. Even in the worst case, there is a significant improvement in spillover performance from the Caltech QRFH, assuming both feeds are in free space (i.e., no external shield). This is partly due to the lower backlobe of the EMSS horn, but also because of the secondary reflector extension included in the ngVLA antenna. The roll-off in Tspill over the upper half of the band tracks with the aperture efficiency change: the main lobe of the feed progressively narrows, which under-illuminates the antenna reflectors. Maximum cross polarization levels are at an acceptably low level, better than –21 dB across the band.
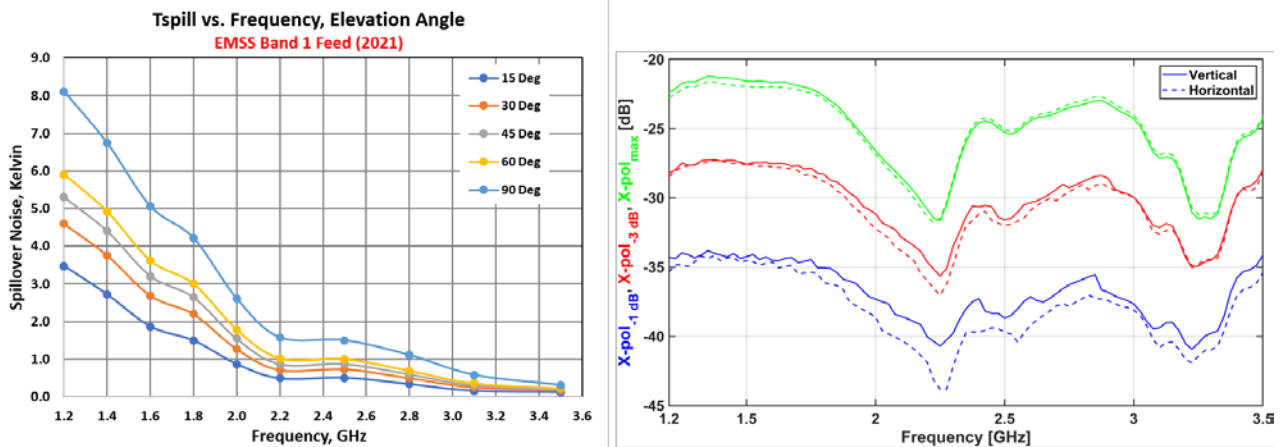
Figure 7: Spillover noise temperatures versus frequency and antenna elevation angle (left), and maximum cross polarization versus frequency (right), for EMSS Band 1 feed horn with ngVLA main antenna.

One potentially serious issue noted with the EMSS feed horn is the presence of two sharp resonant spikes in the passband at ~1.3 and 1.6 GHz. These are caused by a trapped TE_{21L} higher-order mode in the ridged section. Coupling to this undesired mode is enhanced by asymmetries in the 2-port balun and ridged structures, also degrading the isolation between the ports. Figure 8 shows the change in the simulated port match and coupling, as a function of various offsets applied to a ridge on only one side. This offset

can be the result of accumulated worst-case fabrication and assembly tolerances in the ridge section. Note that while the port match is fairly insensitive to tolerance offsets, the port isolation is exceedingly sensitive to even small errors, with rapid degradation across the band and large resonant spikes appearing for offsets as low as 50 μm (~0.002"). This implies the production fabrication and assembly tolerances would need to be several times better than this level to achieve acceptable yield, perhaps < 10 μm (< 0.0004"). While this is technically possible, it would be better to redesign the OMT section so that it has less inherent sensitivity to asymmetries or errors due to tolerances.
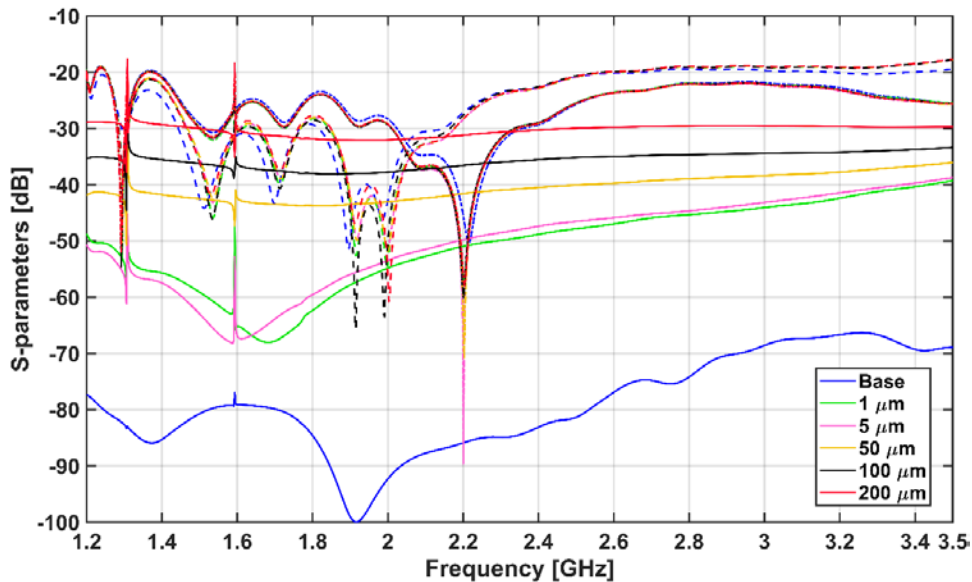
Figure 8: S11 (dash), S22 (dash-dot), and S21 (solid) for the EMSS QRFH with a 2-port balun. One ridge is offset by the distance given in the legend, degrading port isolation and enhancing the trapped-mode resonances.

While it is possible to reoptimize the horn and ridge profiles to eliminate these trapped-mode resonances, both the aperture efficiency and input match are severely compromised [RD17]. An alternative solution is to tweak the profiles so that both resonances fall at frequencies coincident with known RFI sources such as GPS, without significantly impacting the overall feed horn performance. The balun could also be replaced by a dual-ridged OMT with offset ports: this design could reduce the resonances and preserve port isolation while also being less sensitive to asymmetries introduced by manufacturing tolerances. These possible solutions are currently under investigation as part of a follow-up design study [RD19].

In summary, the EMSS feed horn appears to be a viable replacement for the Caltech QRFH. It addresses the most serious deficiencies due to its lower backlobe/spillover, and lower chance of cavity modes or other pathologies when enclosed in a cryostat. The presence of trapped modes in the OMT is a concern, but we are confident these can either be eliminated or reduced to a very low level. A priority for further development would be to improve the efficiency at the high end of the band, possibly with a small amount of dielectric loading in the horn, as mentioned earlier.

4.2.2.3 CSIRO Band 2 Horn

A variation on the standard QRFH designed under contract by CSIRO [RD20] is the leading candidate for use on ngVLA Band 2 (3.4–12.3 GHz). It is derived from an earlier ultra-wideband feed horn built for the Parkes telescope [RD21]. Figure 9 shows detailed cross-sectional views of this feed horn concept, including principal dimensions of the various parts. Though significantly larger than a similarly scaled Caltech QRFH, this feed horn is sufficiently compact to share a cryostat with other higher-frequency receiver bands. As with the EMSS feed horn, the ridges terminate ahead of the aperture section so a

thermal gap can be inserted, reducing the size and mass of the cooled assembly. In place of the smooth flared horn section, corrugations are used here. These improve the aperture efficiency and reduce spillover at the low end of the band. On the opposite side, an OMT section provides transitions to the offset coaxial outputs, via stepped ridged waveguide transitions [RD22].

A very notable addition is a cooled dielectric spear placed in the ridged section of the feed. It has a series of concentric grooves of varying depths machined into it, effectively producing a layered structure with different dielectric constants. The spear is made from PTFE, which has very low loss at cryogenic temperatures, and also the optimum dielectric constant needed with the feed opening angle used in the ngVLA antenna optics. A thick, semi-domed foam vacuum window is bonded over the corrugations, additionally serving as a thermal barrier for the dielectric spear to keep it colder. A thin outer layer of PTFE serves solely as an environmental barrier for the foam window.
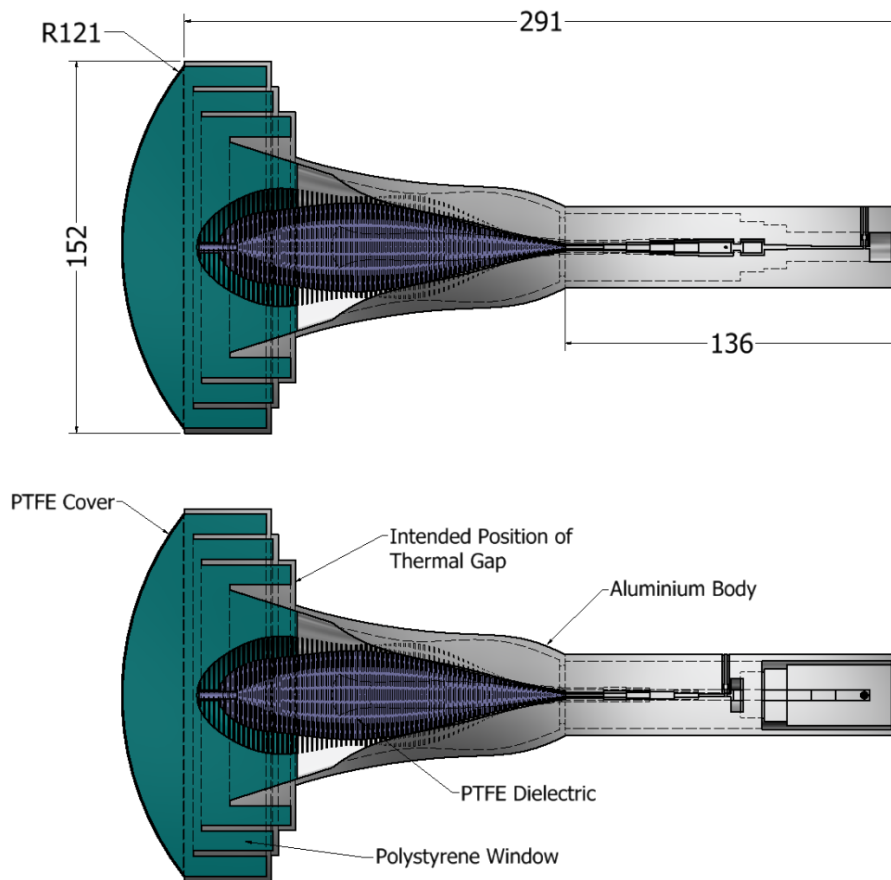
Figure 9: Cross sectional views of the CSIRO Band 2 feed horn, with the dielectric spear and foam vacuum window. Note the location of the thermal gap at the first corrugation: only the ridged horn and polarizer sections will be inside the cryostat. All dimensions shown are in millimeters.

Figure 10 and Figure 11 show the simulated performance of this feed horn with the earlier ngVLA reference antenna optics [RD20]. The initial results are excellent: return loss of the combined feed and OMT is >17 dB, aperture efficiency is uniformly high (~86–88% at all but the band edges), the maximum cross polarization level is –24 dB, and spillover noise is < 9 K in the worst case. With the horn design re-optimized for the conceptual antenna optics, efficiency and spillover are likely to be even better: this work is currently underway as a follow-up design study by CSIRO [RD23].
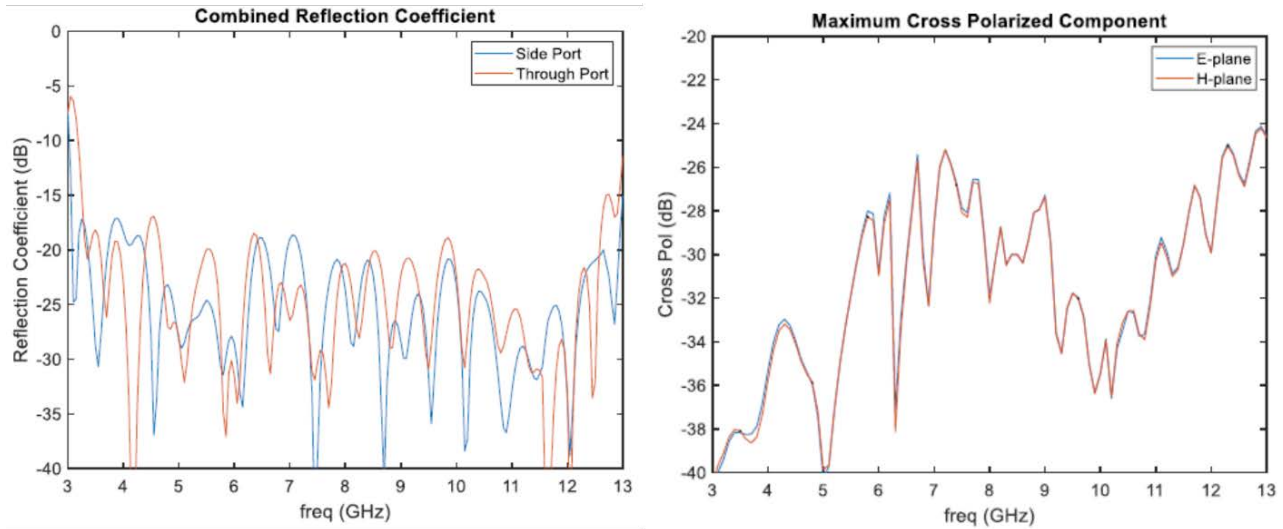
Figure 10: Simulated return loss and cross polarization versus frequency of the CSIRO Band 2 feed horn concept, using the reference antenna optics.
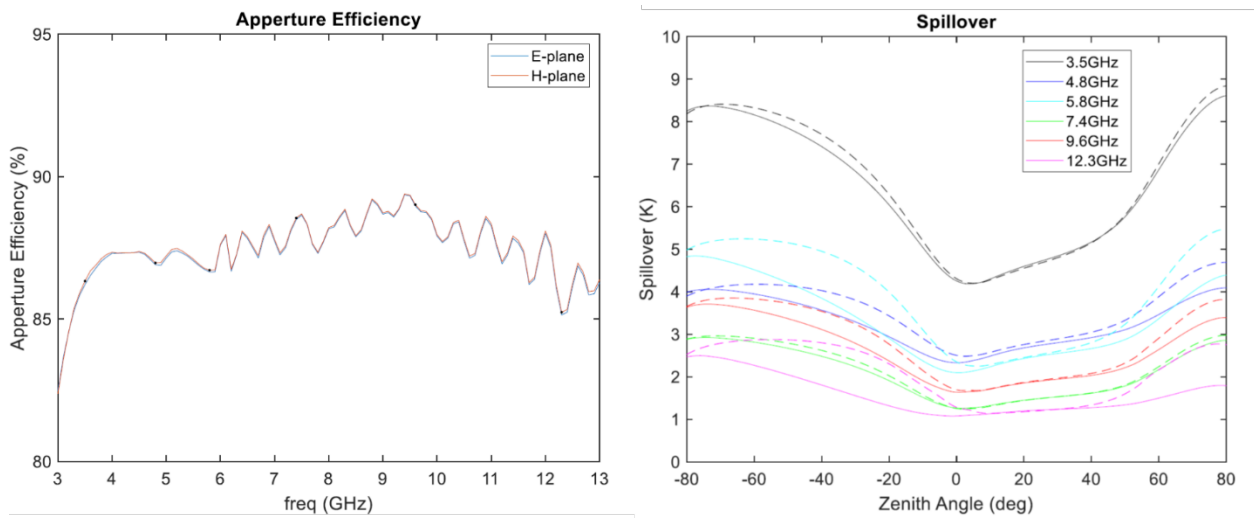
Figure 11: Simulated aperture efficiency and spillover noise of the CSIRO Band 2 feed horn concept, using the reference antenna optics. Negative zenith angles correspond to the "low" feed arm configuration used on the ngVLA. The solid and dashed lines in the spillover plot refer to the two orthogonal orientations of the feed horn relative to the antenna. They differ because the feed beam width is slightly wider in the H-plane than in the E-plane at certain frequencies.

In the initial design study, no in-band trapped-mode resonances in this feed horn were observed. However, given that the OMT and feed sections were designed and analyzed separately, there is still a small possibility of trapped higher-order modes appearing when they are joined. Thus, an electromagnetic analysis of the full feed assembly is necessary to identify these modes, and more accurately model other parameters such as cross polarization. In addition, there are a number of other potential issues that have not been investigated, or items to revisit:

- The antenna optical design and sky brightness model need to be updated, and the combined feed and antenna performance analyses rerun. This should include full-hemisphere radiation patterns, to verify the far-out sidelobe levels are within specification.
- There was also no analysis of manufacturing tolerance sensitivity on performance, which is essential given the large production quantity required.
- Detailed mechanical design and RF simulation of the thermal gap transition is still pending.
- Though a detailed thermal analysis was performed as part of the initial study, it assumed the OMT was at 70 K. Another thermal analysis with the OMT at 20 K needs to be performed.
- Mechanical means for support and alignment of the dielectric spear need to be fleshed out.

All of the above tasks are part of an ongoing follow-up study [RD23], which will conclude later this year.

4.2.2.4   LAR Band 2 Horn

In parallel with the CSIRO dielectric-loaded feed study reported above, a wideband feed horn concept was developed by Lyrebird Antenna Research (LAR), under a subcontract through CSIRO, as an all-metal alternative for Band 2 [RD24]. Figure 12 shows cutaway views of this horn, along with dimensioned axes to indicate the approximate scale. Instead of a tapered ridged waveguide section as in the QRFH, excitation is via a coaxial waveguide which tapers to a point. Not shown are the required OMT, coax line transitions, and 180° hybrid couplers necessary for even-mode (balanced) excitation to generate a pure TE_{11} mode at the end of the taper. These would approximately double the length of the integrated feed horn structure, to ~400 mm.
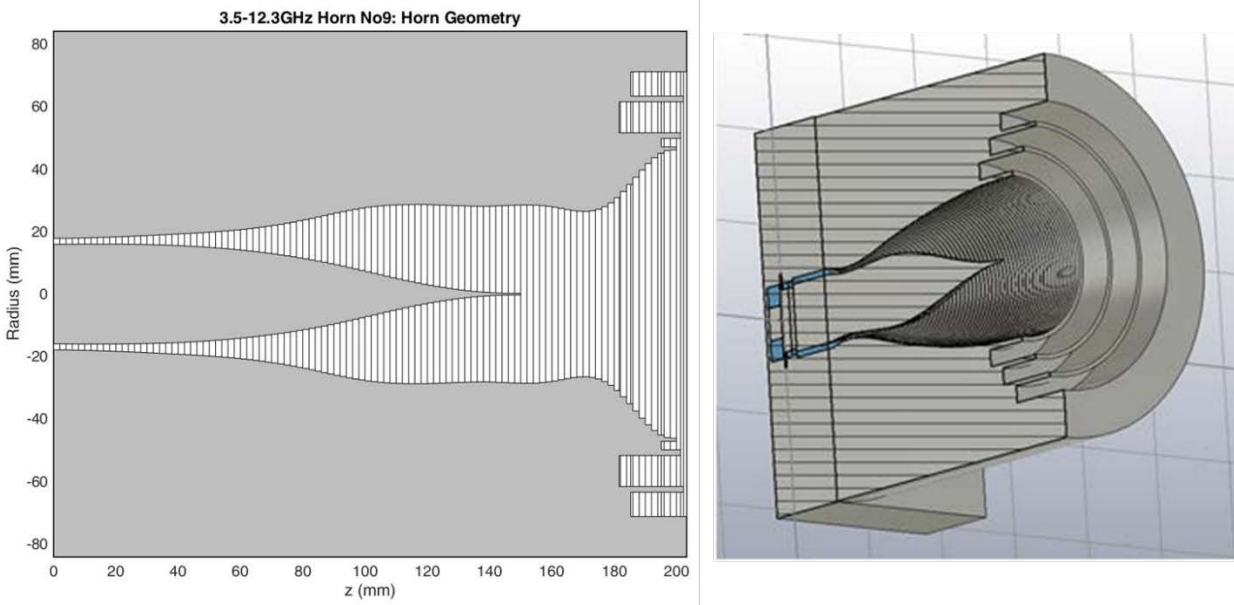
Figure 12: LAR Band 2 'bullet' feed horn concept. The OMT needed for driving the coaxial waveguide input on the left side is not shown here; a preliminary 4-port balanced design from LAR was ~200 mm long.

Selected plots of the simulated RF performance using the reference antenna optics are shown in Figure 13. While the input match looks quite good, the OMT is not included and would contribute some mismatch. Efficiency is reasonably high up to about 9 GHz, but then rolls off steadily to below 60% by 12.3 GHz; this seems to indicate a fundamental bandwidth limitation of the horn design. Antenna temperature is reasonable, considering the lack of a spillover shield in the reference antenna optics: given the cosmic background at 4.8 GHz is 4 K to ~8 K from zenith to 15 degrees elevation, this works out to an

approximate spillover noise of 6 K to ~12 K over the same range. While this is better than the Caltech QRFH, the CSIRO horn outperforms it.
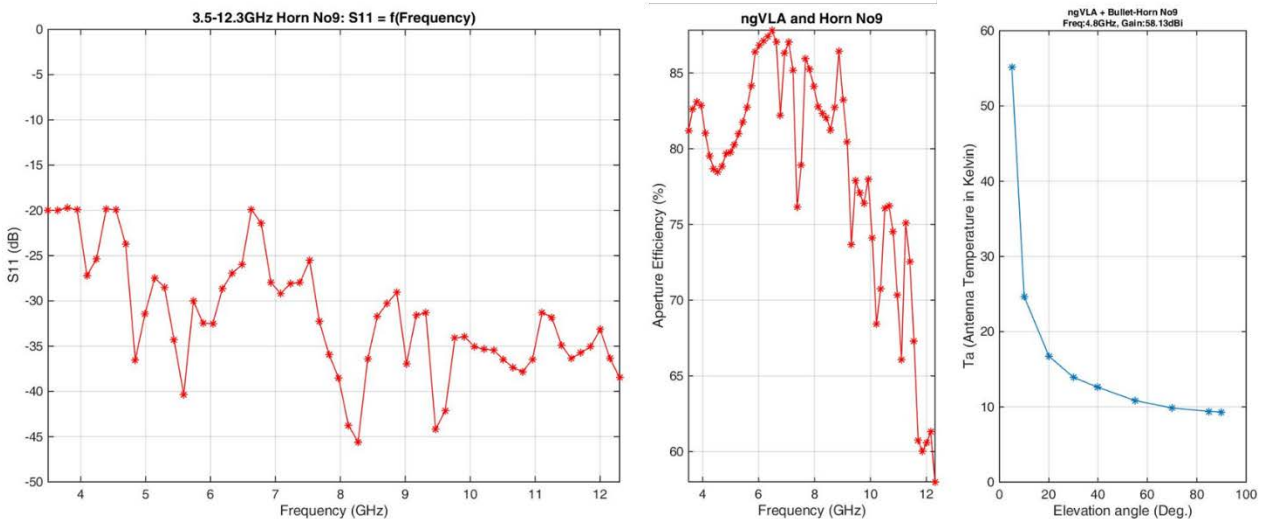
Figure 13: Simulated return loss and aperture efficiency versus frequency, and antenna temperature (worst case, at 4.8 GHz) versus tipping angle, for the LAR feed horn with earlier ngVLA antenna optics.

From [RD24], the worst-case cross polarization for the feed alone was −16 dB, but on average was around −20 dB; with the antenna optics, it would likely be lower. Far-out sidelobe levels peaked at ~0 dBi at 4.8 GHz, and steadily decreased again at higher frequencies.

Given the apparently inherent bandwidth limitations of the bullet feed horn, the complexity and size of the required excitation network, and overall in-band RF performance inferior to the CSIRO feed option, we decided not to pursue further development of this concept for ngVLA Band 2.

4.2.2.5 Corrugated Feed Horns

As noted in Section 4.2.2, an octave-bandwidth corrugated feed horn will provide superior overall RF performance compared to a wideband QRFH, and is the preferred choice for Bands 3–6. The original Cortes and Baker 8-corrugation feed used in the reference design [RD01] was replaced with a simpler 6-corrugation design by EMSS, and re-optimized together with the conceptual antenna optics to maximize overall sensitivity [RD09]. This was done at Band 4 frequencies, but the same feed horn design can be scaled for use on Bands 3, 5, and 6.

A 3D mechanical rendering of this horn is given in Figure 14, cut away to show the relative width and depth of the six corrugations. Compared to the Cortes horn, the aperture diameter is 29% larger, while the length is 16% shorter. The corrugation walls are also relatively much thinner: in an actual feed these may need to be thicker for ease of manufacturing. However, an extensive tolerance analysis performed on a very similar feed design indicated that feed performance is fairly insensitive to wall thickness [RD25].

Simulated optical and RF performance of the feed horn with the antenna optics at Band 4 are plotted in Figure 15 and Figure 16. The aperture efficiency is ~6-7% higher, and spillover noise ~2 K less in the worst case across the band, as compared to the reference antenna optics and feed performance [RD07, RD09]. Maximum cross polarization is low, well below the goal of −30 dB for the high-frequency bands [RD02]; however, it should be noted that manufacturing tolerances on the feed as well a significant contribution from the OMT will degrade the overall cross polarization performance of the receiver.

The return loss gets worse at lower frequencies as the TE_{11} mode cutoff frequency is approached, but this could be improved by adding steps in the circular waveguide section. These would likely be needed regardless, to provide an impedance match to the OMT that follows.
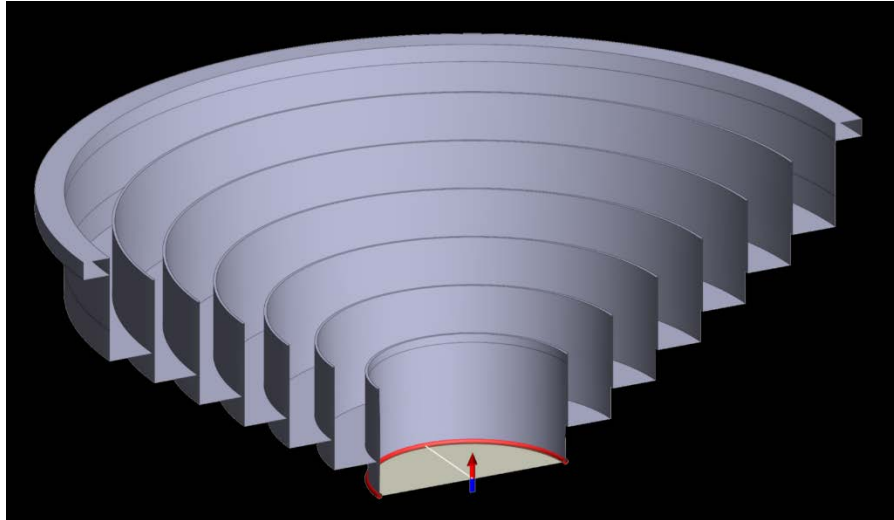
Figure 14: Corrugated feed horn design by EMSS, re-optimized for the current ngVLA antenna optics. A version with six corrugations is shown, but a simpler one with four corrugations can also be used with a slight penalty in performance.
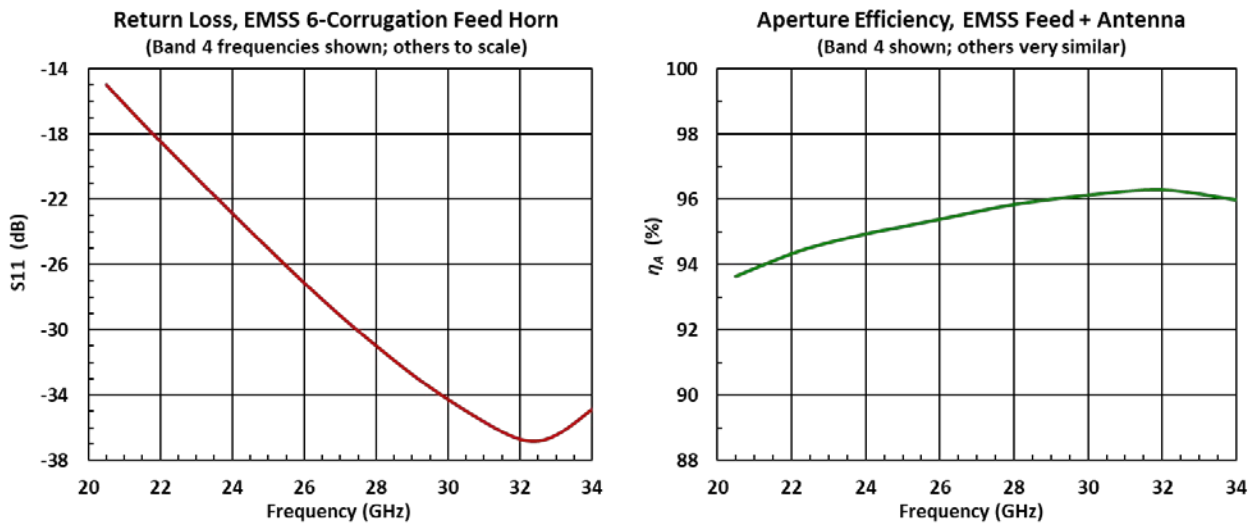
Figure 15: Simulated return loss and aperture efficiency versus frequency of the EMSS corrugated feed horn, using the ngVLA conceptual antenna optics. Performance at Bands 3, 5, and 6 is nearly the same, other than the frequency scale. Aperture efficiency shown does not include ohmic loss or roughness effects from the reflectors.
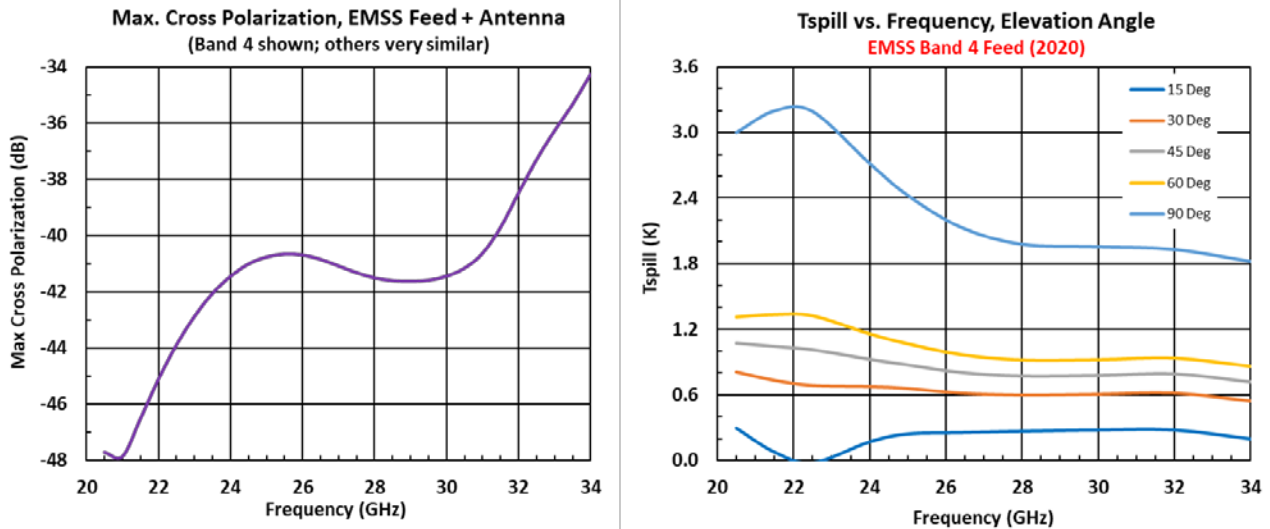
Figure 16: Simulated cross polarization level and spillover noise of the EMSS corrugated feed horn, using the ngVLA conceptual antenna optics. Again, performance at Bands 3, 5, and 6 is very similar, other than the frequency scale. The dip in spillover near 22 GHz for the 15-degree case is likely not real: accuracy is low due to high sky temperature.

The principal attributes of the scaled corrugated feed horn proposed for each of the high frequency ngVLA bands are given in Table 2. The dimensions on Bands 3, 5, and 6 are scaled from the original on Band 4 by the ratio of the lower band edge frequencies. These get quite small on Band 6: the entire feed is significantly smaller than the mating waveguide flange! Fabricating such a small structure in volume and to the required tolerances is challenging, but was determined to be feasible and cost effective [RD25].

Band #	f_L GHz	f_M GHz	f_H GHz	$f_H{:}f_L$	Feed Horn Properties					
					ϑ, deg	D	L	P.C.	WG I.D.	Temp, K
3	12.3	15.9	20.5	1.67	55	68.54	24.34	18.28	17.61	20
4	20.5	26.4	34	1.66	55	41.15	14.61	10.97	10.57	20
5	30.5	39.2	50.5	1.66	55	27.66	9.82	7.37	7.10	20
6	70	90	116	1.66	55	12.05	4.28	3.21	3.09	20

Notes:
1. All physical dimensions are given in millimeters.
2. 'ϑ' is the subtended half-angle of the secondary reflector at the secondary focus.
3. 'D' refers to the aperture diameter of the feed.
4. 'L' refers to the overall length of the feed along the optical axis, relative to the aperture plane.
5. 'P.C.' refers to the offset of the feed phase center along the optical axis relative to the aperture plane.
6. 'WG I.D.' refers to the inside diameter of the Bands 3-6 feed circular waveguide input.

Table 2: Frequency range and principal dimensions for the EMSS corrugated feed horns, Bands 3–6.

5   Concept Description

A conceptual design in the context of the ngVLA refers to an advanced design concept that is technically viable and can meet all the key subsystem requirements with only low to moderate associated technical risk. While the level of development and detail is less than in an actual preliminary design, progression to that stage is well defined and straightforward. The subsystem design is fairly stable by the end of the conceptual stage, but additional development effort and trade studies at the component level may still be required.

5.1   Subsystem Components

The Front End subsystem components are all located on the feed arm of the antenna. A pair of enclosures (Receiver, Auxiliary) provide environmental protection and temperature regulation for the subsystem and other associated components. The Receiver enclosure contains a pair of cryostats, each with cooled receiver and feed assemblies, the downconverter/digitizer (IRD) modules, and a cold plate for temperature regulation of the IRDs. It mounts atop a 2-axis lateral translation table, for moving the phase center of the desired band into the focal point. The Auxiliary enclosure houses the vacuum pump necessary for evacuation of the cryostats prior to cool-down, and other Front End support electronics not integrated into the cryostats (DC power supplies, monitor and control unit). It is mounted in a fixed location on the feed arm, adjacent to the Receiver enclosure.

A conceptual rendering of the subsystem enclosures is shown in Figure 17. Other associated elements (not shown) include the cryocooler helium lines, vacuum and glycol lines, and associated cable wraps.
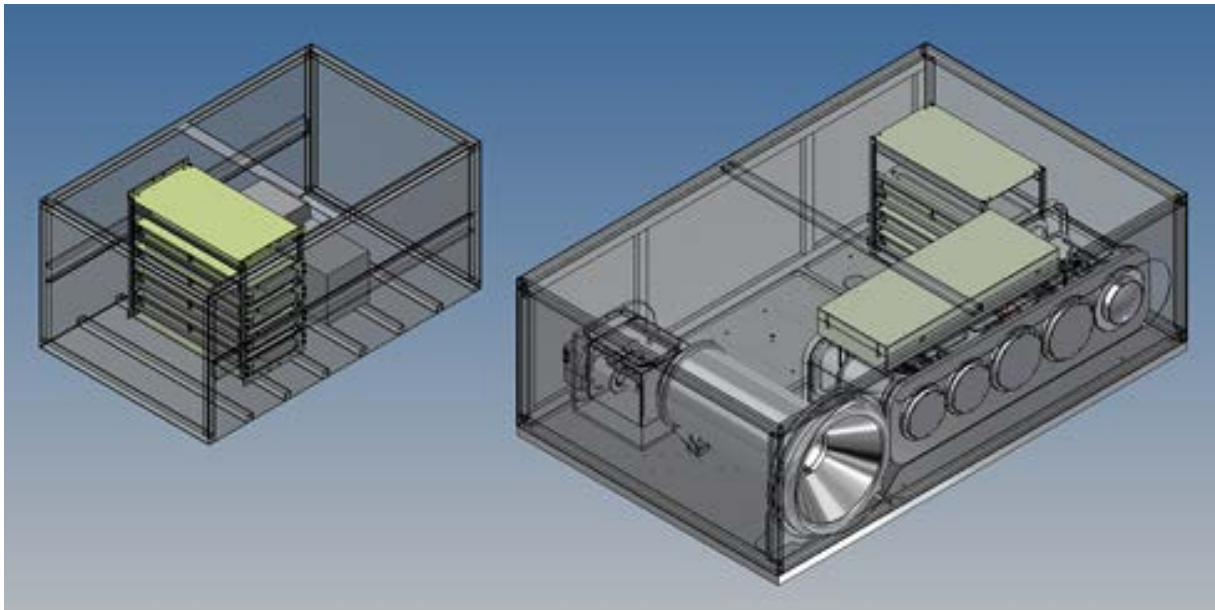
Figure 17: Front End subsystem: Receiver enclosure (R) and Auxiliary enclosure (L), with panels removed to show internals. Cryostats are arranged to allow band selection via a simple lateral translation of the Receiver enclosure. The IRD module (not part of the Front End subsystem) is shown above the larger cryostat.

Approximate dimensions and masses for the assembled Front End enclosures are:

- Receiver Enclosure: **1800 x 1150 x 600 mm** (L x W x H), total mass ~ **522 kg**
- Auxiliary Enclosure: **1200 x 750 x 565 mm** (L x W x H), total mass ~ **206 kg**

5.2 Receiver Configuration Overview

The proposed ngVLA Front End configuration is implemented in six independent receiver bands, each with its own feed. The upper five bands will be integrated into a single, moderately sized cryostat (B), while the lowest (Band 1) occupies a second, somewhat smaller cryostat (A). All feeds are sufficiently compact to be cryogenically cooled, reducing losses ahead of the cooled low-noise amplifiers (LNAs). Due to its size, only the ridged section of the Band 1 feed is cooled (to 80 K), while the feeds on the other bands are cooled to 20 K.

Table 3 shows the frequency range, bandwidths, and output characteristics for the six ngVLA bands. Coverage is continuous except for the expected break in the atmospheric absorption band at ~50–70 GHz. The large overlap at the boundary between Bands 4 and 5 was deliberate: it allows observations at ~30 GHz with higher sensitivity, away from a band boundary. Output polarization on all receivers is linear rather than left/right circular as on the VLA. This simplifies the receiver design, reduces the receiver noise, and maximizes the useable bandwidth in the all-waveguide receivers of Bands 3–6.

Output connectors are selected based on the ratio bandwidth and upper frequency limit of a receiver, and also the physical location (cooled OMT or warm cryostat wall). Components with coaxial connectors are necessary in Bands 1–2 because of the large ratio bandwidths, and are also compact with relatively low loss. In Bands 3–6 the smaller bandwidth ratios and higher frequencies permit all-waveguide receivers compact enough to fit within Cryostat B, with lower loss and added noise ahead of the LNA than in coax-based receivers. The rectangular waveguide size (WRxx) is chosen such that the receiver's upper band edge is just below the cutoff frequency of first higher-order mode (TE_{20}). This ensures propagation will be single-mode across the band, while keeping the lower band edge well above cutoff to minimize loss. In Bands 3–4, this leads to non-standard or custom waveguide sizes in the cooled components, which are justified given the noise performance gains and expected production volumes.

Band #	Cryostat	f_L GHz	f_M GHz	f_H GHz	$f_H : f_L$	BW GHZ	Output Type OMT	Output Type Cryostat	Output Pol.
1	A	1.2	2.0	3.5	2.92	2.3	SMA	SMA	Linear
2	B	3.4	6.5	12.3	3.62	8.9	SMA	SMA	Linear
3	B	12.3	15.9	20.5	1.67	8.2	WR56.3	SMA	Linear
4	B	20.5	26.4	34	1.66	13.5	WR34	2.92mm	Linear
5	B	30.5	39.2	50.5	1.66	20	WR22	WR22	Linear
6	B	70	90	116	1.66	46	WR10	WR10	Linear

Table 3: Key characteristics of the 6-band design configuration. The connector types shown are those expected, but could change slightly during the detailed design of the receivers and cryostats.

Approximate dimensions and masses of the Front End cryostats (without cryocoolers) are:

- Cryostat A (Band 1): **968 x 364 x 302 mm** (L x W x H), total mass ~ **49 kg**
- Cryostat B (Bands 2–6): **1143 x 466 x 305 mm** (L x W x H), total mass ~ **95 kg**

5.3 Receiver RF Block Diagrams

Figure 18 shows RF block diagrams of the Front End receivers. Each receiver has two orthogonally polarized outputs, which feed the Integrated Receiver Downconverter/Digitizer (IRD) modules. No

frequency conversion is performed on any of the bands in the Front End portion of the system. There will be at least one multi-stage LNA per channel, though the high frequency bands may require an additional cascaded amplifier to provide sufficient output power to be within the input dynamic range of the IRDs.

Each receiver contains a calibrated noise injection path ahead of the LNAs for self-calibration during observing. This is shown with a splitter and pair of directional couplers, all of which are cryogenically cooled. The noise source driving this path has an output level adjustable over a wide range (~30 dB on Bands 1–4, and ~15 dB on Bands 5–6), to accommodate solar observing modes. If possible, the noise sources will be integrated within the cryostats, to reduce the number of RF penetrations required and minimize the chance of mechanical and electrical damage. These will be under tight temperature control to minimize drift, but near ambient (not cooled).
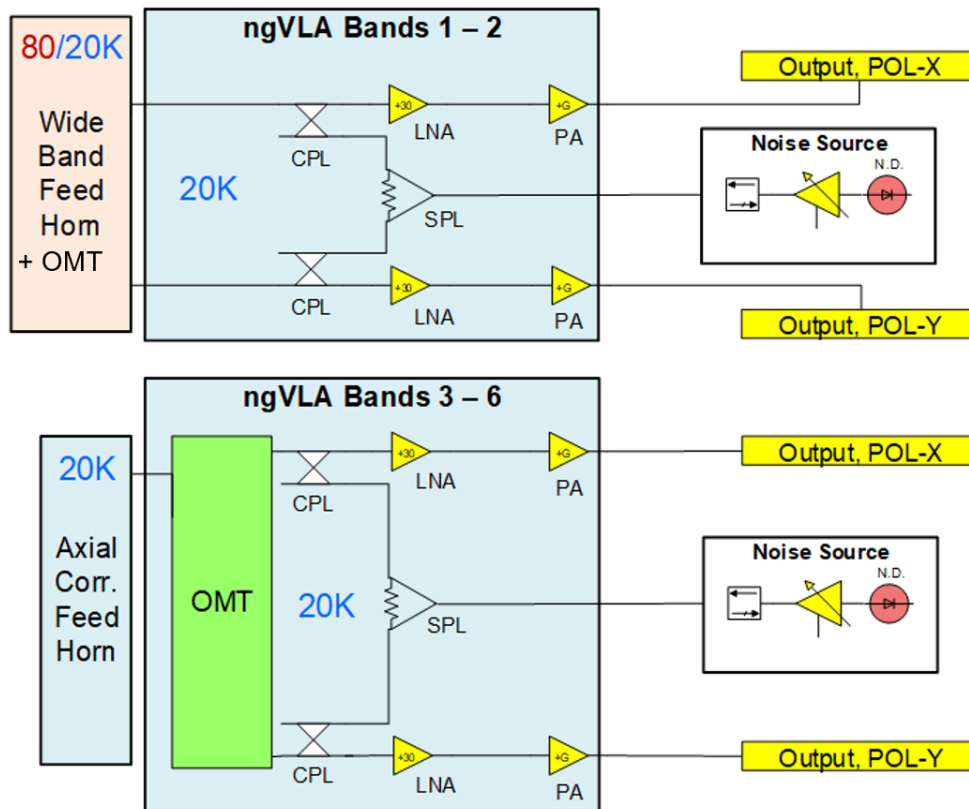
Figure 18: ngVLA Front End receiver block diagrams, Bands 1 & 2 (top) and Bands 3–6 (bottom). Note that the OMT is integral with the feed horn on Bands 1–2, bus is a separate waveguide component on Bands 3–6.

5.4   Receiver and Cryostat Support Electronics

Nearly all of the support electronics required for each receiver and the cryostat will be integrated into the vacuum space of the respective cryostat, to minimize the number of external interface connections required, and to save space and weight by eliminating packaging. The support electronics will provide the following functions [RD26]:

- DC bias/driver circuitry for LNAs, noise calibrator sources, and other active components
- RF output control/leveling for the noise calibrator sources
- Input signal conditioning from the cryostat and receiver cartridge temperature sensors
- Circuitry for any active temperature control required on the LNAs.

The support electronics are envisioned at present to be implemented on circuit cards, one per receiver band, each soldered directly to a pair of flexible flat ribbon cables (e.g., Kapton/copper) terminated with a Micro-D multipin receptacles. One cable containing the receiver analog I/O signals would plug into a mating connector on the cooled receiver cartridge. The second cable with analog and low-level digital I/O would plug into the corresponding noise calibration source, which would be at ambient temperature.

The hardware interface to each cartridge electronics card will be a synchronous serial I/O multi-drop bus, with separate data and clock inputs. Details of the interface are TBD, but it will likely use some standard form of differential signaling, with all embedded sequential logic externally clocked from the bus to eliminate internal clock oscillators that could cause interference. The communications protocol would include some form of addressing, to allow daisy-chaining of multiple cards onto a single I/O cable. This could possibly include a second redundant port for enhanced reliability.

Electrical connection to the cryostats is assumed to be via multi-conductor shielded cables, with a bulkhead receptacle/cable plug pair at each end. Specific details are undefined at present; however, these will likely consist of single, multi-pin round, twist-locking connector interfaces, with a hermetic glass seal for contacts on the cryostat receptacle side, to maintain vacuum integrity.

5.5 Receiver Packaging Concept

The size and shape of Cryostat A are largely driven by the Band 1 feed, which is by far the largest component. As evident in Figure 19, the LNAs and other RF components take up very little space by comparison. This rendering represents the worst case: depending on the outcome of an ongoing OMT design study [RD19], the overall feed horn length could remain as shown or be significantly shorter.
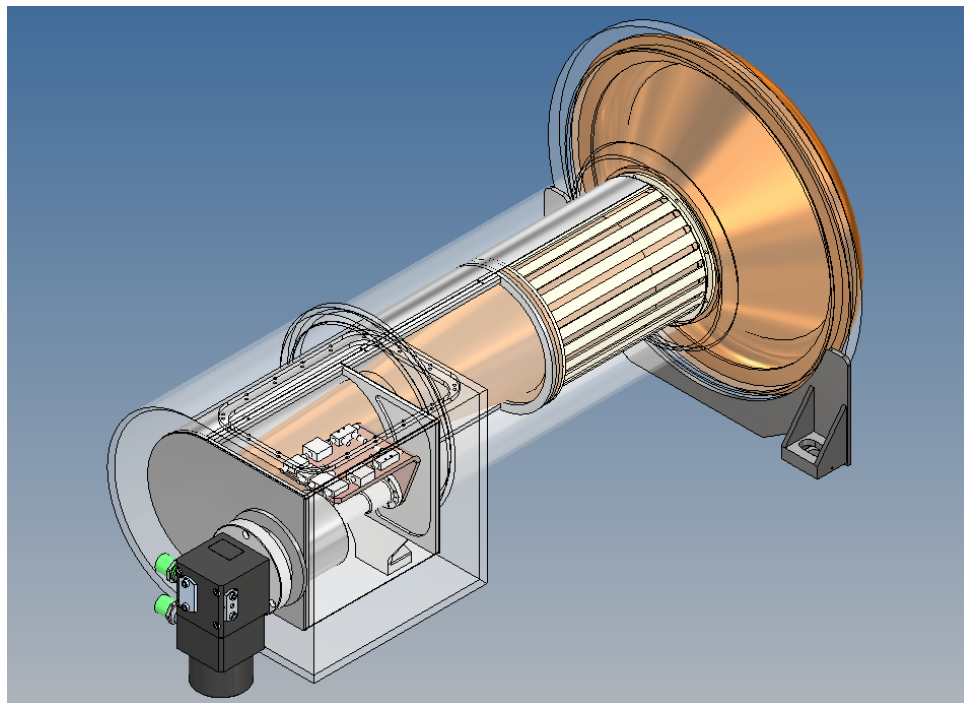
Figure 19: Cryostat 'A' (Band 1). The flared horn section of the QRFH is outside the vacuum space at ambient temperature. This reduces the cryostat mass, while adding a very small amount of additional noise.

A detailed rendering of Cryostat B from the top rear is shown in Figure 20, with the cryostat vessel made transparent to view the interior layout. The five receiver bands are arranged inline to allow band selection with linear movement along a single axis perpendicular to the optical boresight. Phase centers of all feeds are coplanar, and located such that focusing is possible within the ±100 mm adjustment range along the boresight axis. Receivers are placed within the cryostat in order by frequency, with Band 6 on the side closest to Cryostat A in the enclosure. The reasoning is to locate the highest frequency receivers near to the center of mass of the Receiver enclosure, which should minimize deformation (twisting) of the antenna feed arm along its axis when these receivers are moved into the focal point.
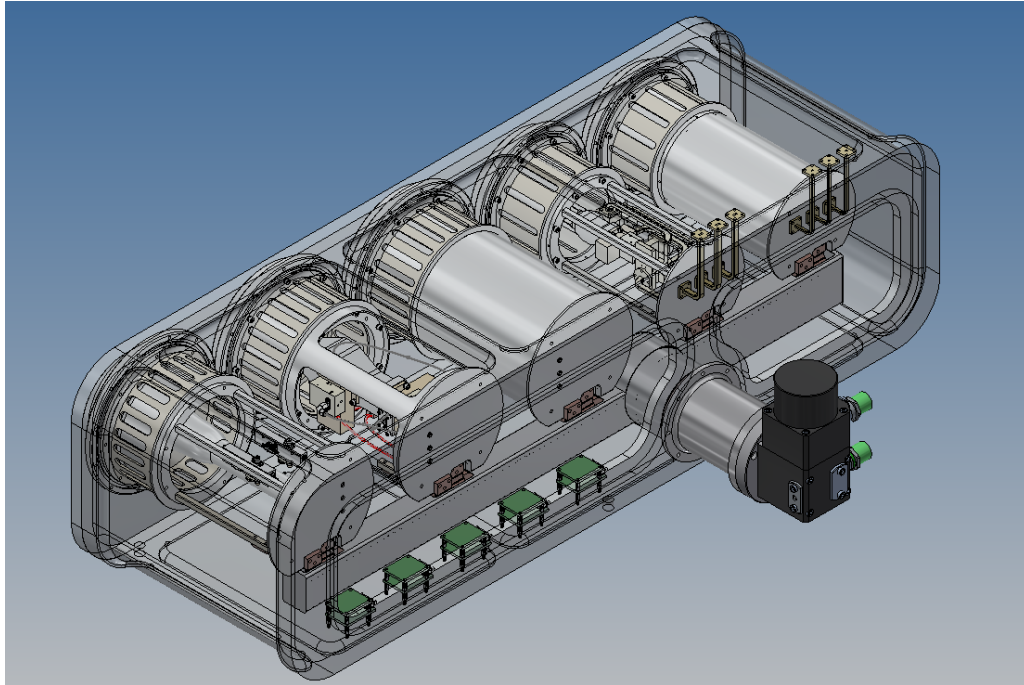
Figure 20: Cryostat B (Bands 2–6). The radiation shields are removed on several of the bands, to show the cooled electronics within. Support electronics are mounted on the vacuum side of a bottom access plate. Not shown here are the noise source modules.

Figure 21 gives an underside view of Cryostat B, which shows the thermal distribution bus structure attached onto the cold stages of the cryocooler. Its purpose is to provide a highly conductive thermal path from the dispersed receiver components back to the cold stages. It consists of two oxygen-free high-conductivity copper (OFHC) rails, each tied to the 20 K and 80 K stages of the cryocooler, enclosed in a radiation shield to minimize thermal loading of the 20 K rail. Figure 22 shows close-up views of the how the receiver electronics are attached to the distribution bus rails. Braided OFHC straps are used to provide a flexible connection with minimal thermal resistance.

The RF connections from the cooled receiver electronics out to the cryostat bulkhead (at ambient) must all have low thermal conductivity, to reduce thermal loading of the cold stages. This can be achieved with semirigid coax cable or waveguides made from thin-wall stainless steel, which are commercially available. A thin layer of gold or copper (~5 skin depths) is flashed onto the center pin of the coax or inside walls of the waveguides, to obtain low RF loss with only a small sacrifice in the thermal insulation. In a like manner, the DC and signal connections to cooled electronics use fine-gage alloy wire (BeCu, brass, or steel) for reduced thermal conductivity at cryogenic temperatures. These can be silver plated as needed, for solderability.
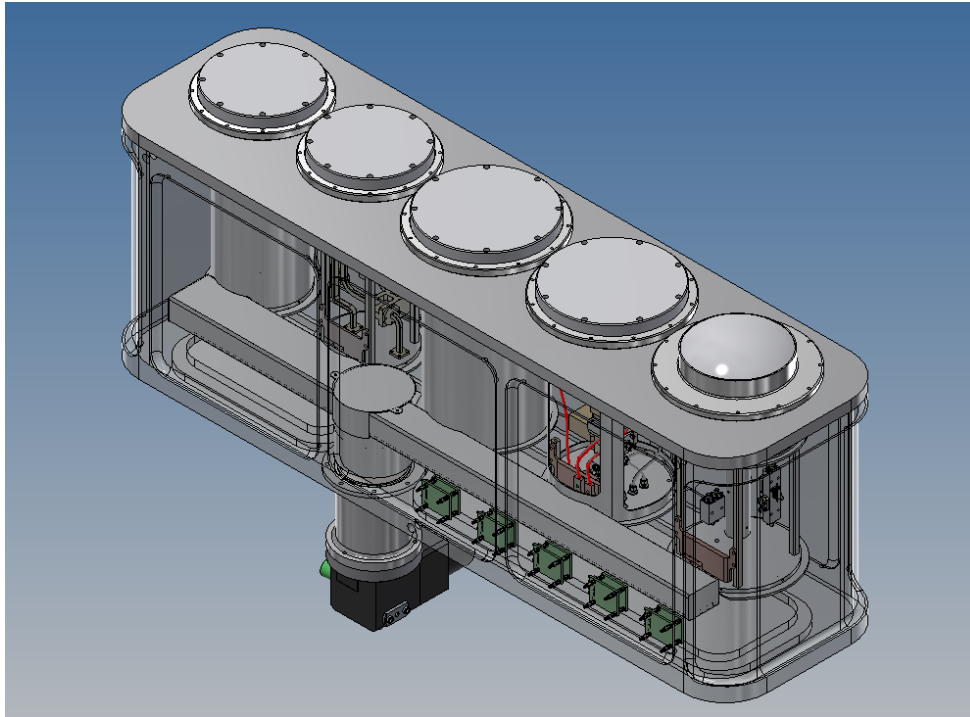
Figure 21: Bottom view of Cryostat B, showing the thermal distribution bus from the cryocooler cold stages.
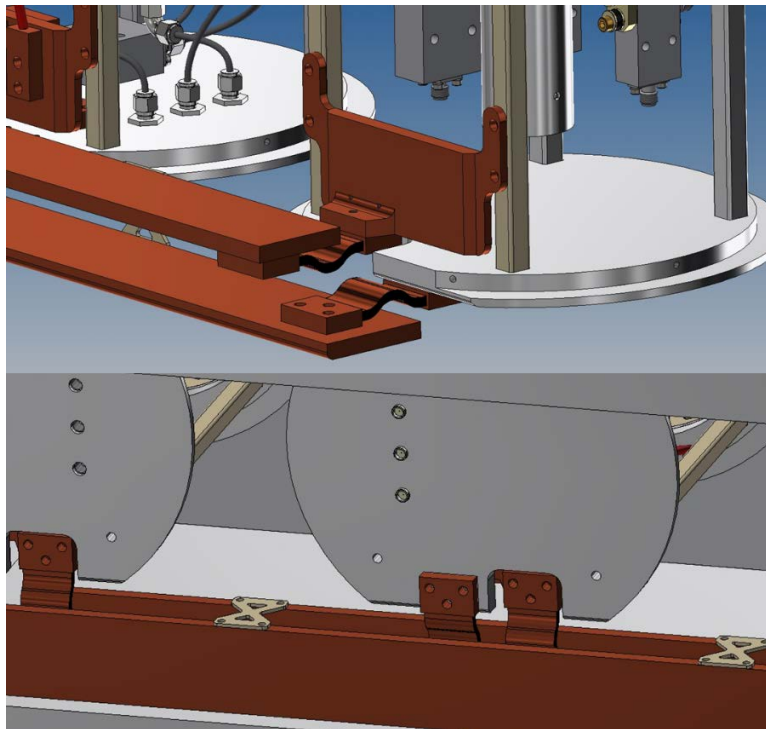
Figure 22: Detailed views of distribution bus connections to a receiver cartridge. These are made with short braided copper straps. The rails are supported and thermally isolated with hourglass-shaped G10 brackets.

Bias and sensor wiring harnesses, vacuum and cryocooler temperature sensors, receiver support electronics, and the mechanical and electrical interfaces to the IRD subsystem are all integral to the cryostats. Both cryocoolers face toward the rear of the receiver enclosure to facilitate their replacement in the field without requiring removal of either the cryostat or the enclosure.

Individual receivers in Cryostat B are designed as modular units or "cartridges" to facilitate efficient mass production and simplify servicing. The intent is to have two standard cartridge body sizes for all five bands, enabling the use of a common test cryostat for receiver development and production testing. Each receiver cartridge integrates a vacuum window, IR filter, feed horn, OMT, calibration couplers, and LNAs into a generic receiver cartridge body, which has its own radiation shield, RF/bias/sensor connector ports, and cold stage connections.

Installation or removal of a receiver assembly is through the front of the cryostat. The window flange incorporates an O-ring vacuum seal and dowel pins for alignment during installation. Removable panels at the rear of Cryostat B allow access to the cold stage ports (for connection to the thermal distribution bus), the receiver wiring harness connector (for connection to the support electronics), and the coax or waveguide ports of the receiver (for connection to IRD interface ports and noise source module).

A conceptual rendering of a representative receiver cartridge is shown in Figure 23, both fully assembled, and in a cutaway view. A closeup of the thermal gap assembly and feed horn can be seen in Figure 24.
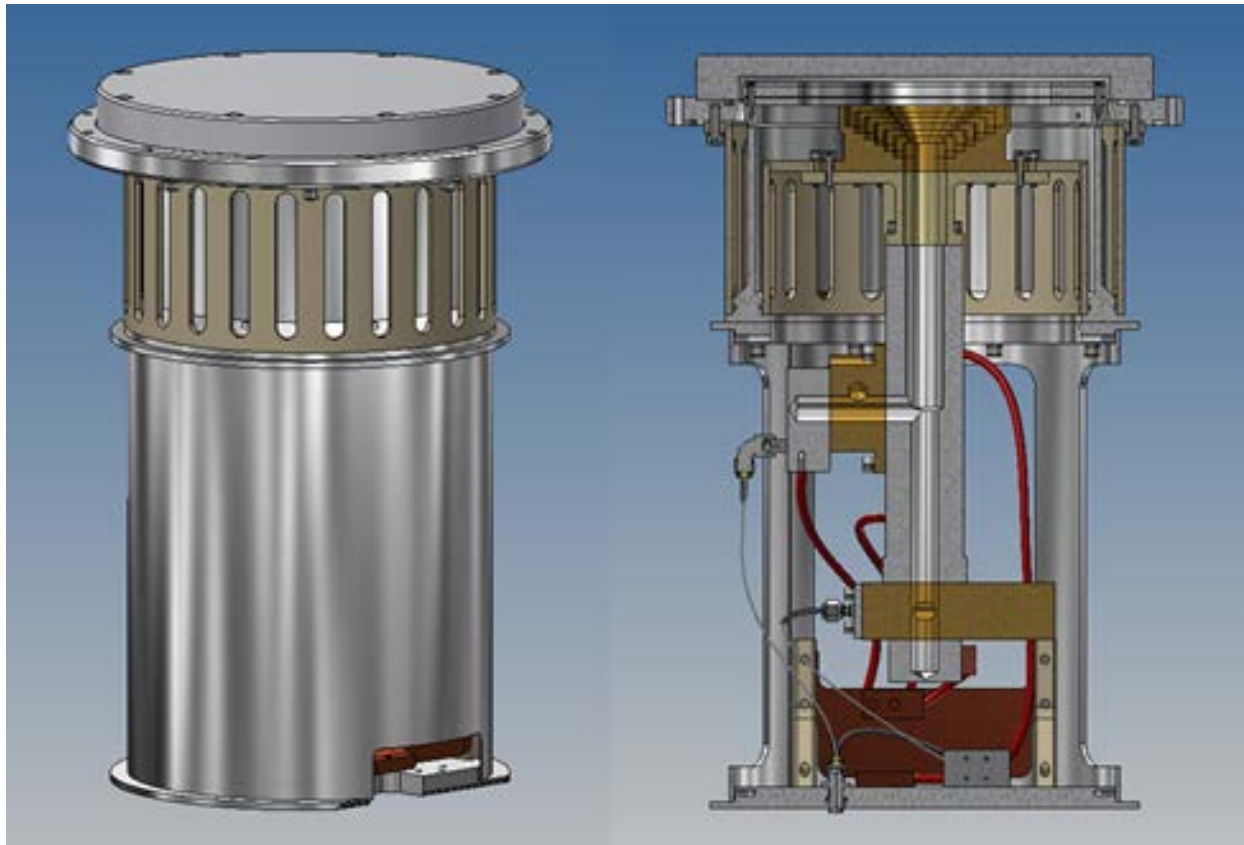
Figure 23: Receiver Cartridge, Cryostat 'B'. Band 3 model is shown; others are very similar. Other than the thermal gap assembly, the component shapes, sizes, and placement shown in the cutaway are notional, and do not necessarily represent actual designs for this or other bands.
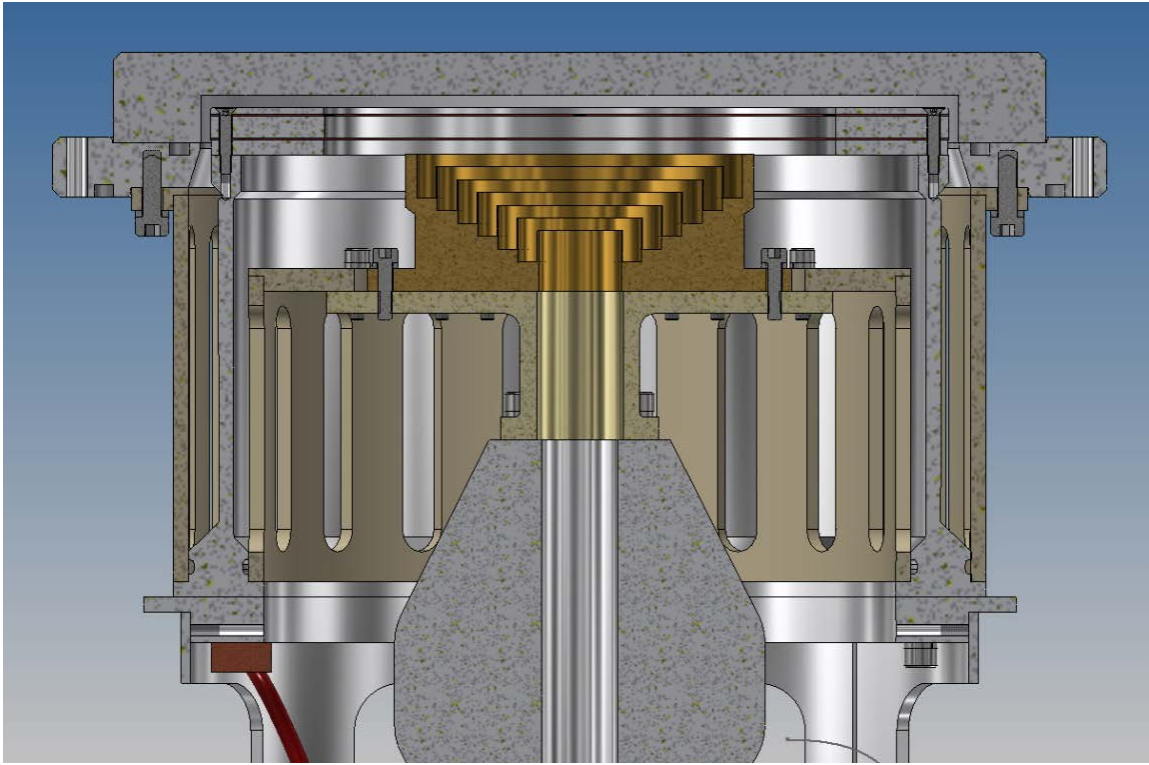
Figure 24: Close-in cutaway view of the receiver feed and thermal gap support structure. The nested, slotted G10 cylinders have the necessary strength and mechanical stability for securing the cold stage components and precisely locating the feed horn, while providing good thermal isolation of the cold stages from ambient.

5.6 *Cryocooler and Cryostat Thermal Modeling*

A variable-speed, two-stage Gifford-McMahon cryocooler was retained as the baseline option for cooling each cryostat. Both cryostats use the same model (Trillium 350CS), which is basically identical to the one used in the majority of the VLA receivers. It has 5W and 20W of cooling capacity on the 20 K and 80 K stages, respectively.

To validate the cryocooler selection, detailed thermal modeling and analyses of both cryostats under various conditions were performed by an outside vendor, using representative internal components from the original reference design [RD01]: LNAs, passive RF components, windows, IR filters, radiation shields, and output waveguides, cables, and wiring harnesses [RD27, RD28]. A graphical representation of the calculated heat flows between various components was produced for each receiver band as a visual aid. A diagram of a single case for Band 1/Cryostat A is shown in Figure 25; representations of the other five bands in Cryostat B are similar.

Table 4 briefly summarizes some of the thermal analysis results at several temperatures for Cryostat A, and with variations in shielding for Cryostat B. Overall, they are encouraging. Cryostat A is well within the cryocooler capacity even at 45 °C, so the risk in this case appears low. Cryostat B appears to have a very thin margin on the 1st stage for Case B1 (< 10%). However, this is at 40 °C: at the expected maximum ambient of 30 °C within the enclosure, margin on both stages should be adequate. Adding aluminized Mylar film over the thermal gap and extra layers of MLI can greatly reduce loading, as shown in Case B4.

The cryostat and receiver designs have evolved quite a bit since the thermal analysis was last iterated in 2020. We plan to update the thermal model to reflect the current design in the next phase, but are fairly confident the total thermal loads on this cryocooler will remain within the limits in both cryostats.
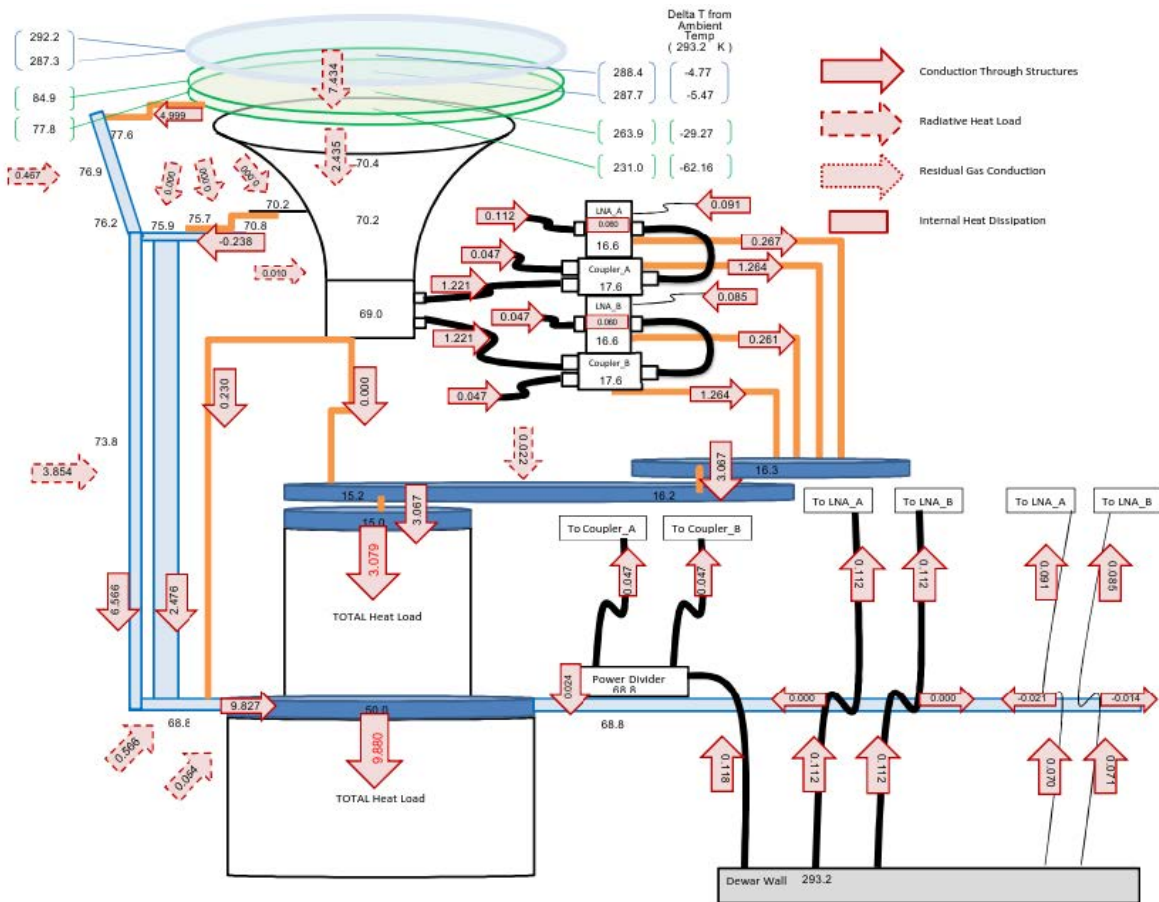
Figure 25: Graphical representation of heat flow results from modeling of the Band 1 receiver in Cryostat A, using the ThermXL® analysis tool. In this particular case, an ambient of 20°C and a cryostat pressure of 10⁻⁶ mbar was assumed, and 1st and 2nd stage temperatures of 50 K and 15 K, respectively.

Case	Ta, °C	MLI	TG shield	1st stage, W	2nd stage, W
A1	20	Yes	n/a	9.88	3.08
A2	45	Yes	n/a	14.22	3.39
B1	40	10 layers	(none)	18.8	3.4
B2	40	10 layers	Al / Mylar	17.4	3.7
B3	40	30 layers	(none)	17.9	4.1
B4	40	30 layers	Al / Mylar	11.8	3.5

Table 4: Thermal analysis results for Cryostats A and B. For each case, loading is worst case, over the full range of cold stage temperatures from 300 K down to 50 K / 15 K. 'TG shield' refers to a thermally floating shield of highly reflective film loosely wrapped around the G10 cylinder in the thermal gap assembly.

5.7 Maintenance Concept

A Line Replaceable Unit (LRU) is defined as the lowest level within a subsystem that can realistically be replaced in the field. Examples are plug-in modules or circuit cards, and units designed for periodic replacement such as battery packs. In the Front End subsystem, the cryostat would appear to be a

natural boundary for an LRU, as it is in the VLA. However, there are a number of difficulties with this concept, listed below:

1) Access to the cryostats is somewhat restricted, as they are packaged close together within a relatively compact enclosure rather than inside a receiver room as on the VLA. The accessible area on the feed arm around the enclosure may also not be sufficient to safely accommodate two technicians with their tools.

2) Integration of multiple receivers into Cryostat B and a large cooled feed horn into Cryostat A makes them heavier than most of the VLA receivers. Work safety requirements would mandate the use of lifting devices, regardless of access.

3) The receiver windows on Cryostat B are delicate and could potentially be damaged during removal or installation of the cryostat. Removing it together with the protective enclosure poses less of a risk in this regard.

4) Unlike on the VLA, Front End service will be conducted entirely in an outdoor environment, with exposure to wind and precipitation of all kinds possible. Opening the enclosure to the elements complicates maintenance, and should be avoided unless there is not a workable alternative (such as for a cryocooler swap).

Based on the above considerations, we decided that in the event of a component failure in any individual receiver, the entire Receiver enclosure should be swapped out as a unit, to minimize risks to personnel and damage to the equipment. While this might seem excessive, with proper equipment and engineered lift points on the enclosures, replacement at the enclosure level is actually simpler, quicker, and safer than at the cryostat level. It does subject the "good" cryostat to an extra temperature cycle it would otherwise not experience, but given that cryocooler swaps are likely to occur much more frequently than any receiver failures, this will have little impact on the long-term reliability of the cooled electronics.

The base of the Receiver enclosure is ~2.25 meters above ground level with the antenna pointed at the lower elevation limit (~12 degrees). This provides convenient access to the installed equipment, as shown in Figure 26. A small truck equipped with a telescoping boom lift should be more than adequate for removal and installation of either enclosure, with a step ladder or raised platform sufficient for personnel to access the lift points. Transport to and from the maintenance center would be in an enclosed cargo truck or trailer, specially outfitted to absorb any shocks or vibrations that could damage the receivers while in transit.

While the lower elevation limit provides easier access from the ground, one potential difficulty would be the slight forward tilt (~13 degrees) of the Receiver enclosure. It is aligned onto the two-axis positioner using tapered dowel pins at the interface. Installation may not be too much of a problem, but removal could be a little trickier and pose potential safety risks, both to the equipment and to personnel.

With the antenna at 25.2 degrees of elevation, the Receiver enclosure would be level, as shown in Figure 27. In this position the elevation stow pin can also be engaged to provide an extra margin of safety, though under conditions acceptable for maintenance this may not be required. However, the height of the Receiver enclosure from the ground is almost doubled (~4.47 meters), making access more complex. Both a boom truck and a bucket lift would likely be needed for service, with stricter safety protocols in place for working at the greater height. But it should still be feasible to have a two-person maintenance crew, given the bucket lift is operated by the rider and not from the ground.

In contrast with the Receiver enclosure, all LRUs within the Auxiliary enclosure will be field-replaceable. Hence there will be no need to remove the Auxiliary enclosure for routine maintenance.
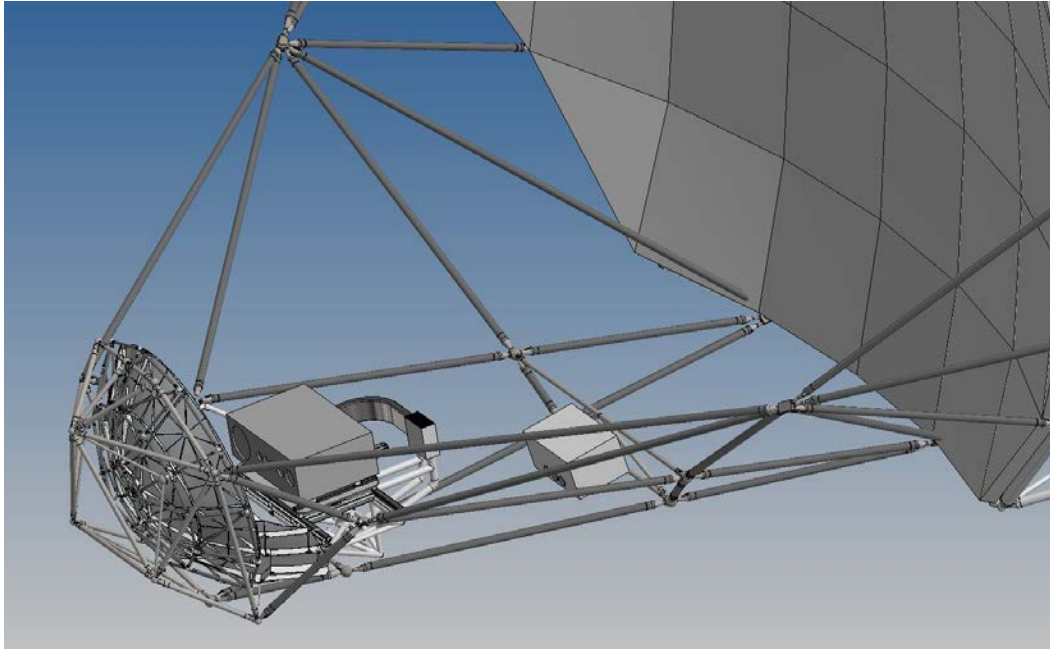
Figure 26: Antenna feed arm in position for service at the lower elevation limit (12 degrees), showing locations of the Receiver and Auxiliary enclosures. The service/transport vehicle (not shown) would park alongside the feed arm on a concrete or asphalt pad.
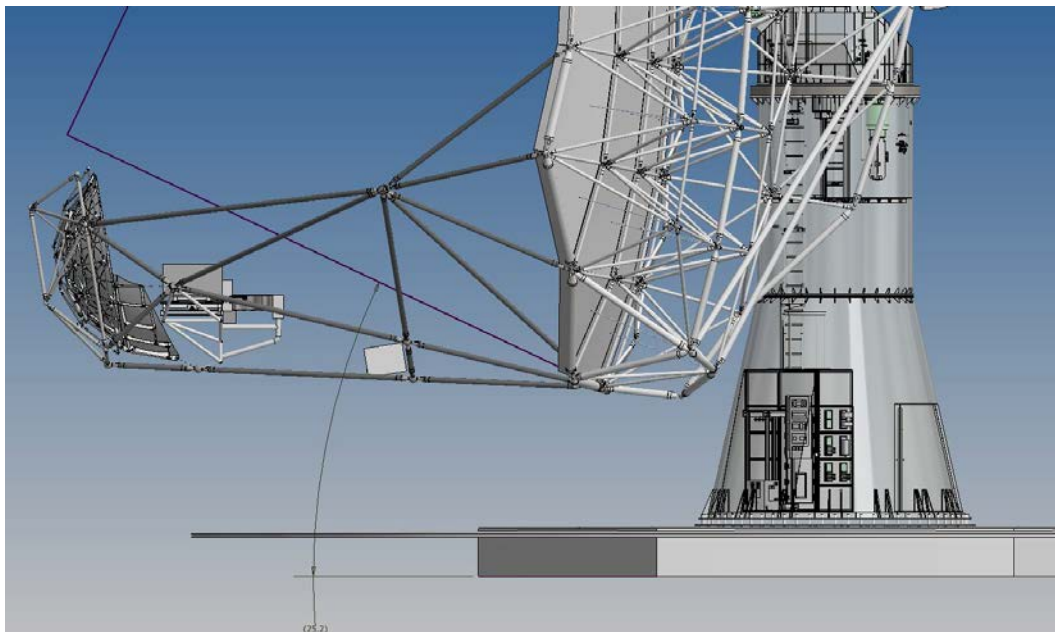
Figure 27: Alternative position for service, at 25.2 degrees elevation. The bottom of the Receiver enclosure is ~4.5m (> 14 ft) above ground level. Access would be via a bucket lift parked directly underneath, with a boom truck off to one side of the feed arm for lifting the enclosures.

6   Simulated Performance

6.1   Receiver Noise Temperature

A cascade gain and noise analysis [RD29] was performed for each of the six bands, using measured or simulated data on key components (LNAs, OMTs) and estimated numbers for the other components (feeds, windows, couplers, cables, waveguides) based on simplified analysis and on past experience. A uniform temperature of 20 K was assumed for almost all cooled receiver components in the signal path including the feeds. The only exception is on Band 1, where the ridged feed section and OMT was assumed to be at 80 K (the ambient flared horn section has a small contribution, and was omitted here). Components for the noise calibration injection are mostly at ambient, except for the power splitter which is assumed cooled to 80 K. Coax cables or waveguides that connect components at different temperatures are assumed for simplicity to have a uniform temperature at their average: while not exact, the resulting error and effect on the overall noise temperature is very small.

For the present, component RF mismatch and the ripple it adds to the cascaded noise and gain responses over frequency was omitted from this analysis. These will be added later, when component selection and design have advanced, and simulated or measured full 2-port S-parameter data becomes available.

Full results of the receiver cascaded analysis are shown in an appendix (Section 7.2; Table 8 through Table 13). From these, the simulated receiver noise temperatures across frequency for all six bands are plotted in Figure 28. As expected, noise temperatures increase steadily at higher frequencies, but seem to mostly flatten out in Bands 1–2, rather than decrease. This behavior can be explained by comparing the noise temperature of the LNA relative to the cascaded noise of all components before it in each of the cascaded noise tables. On the higher-frequency bands, the LNA contribution is comparable to or larger than the total of the passive components ahead of it (excluding the radome). However, on the lower-frequency bands the LNA contribution is overshadowed by these other components, especially on Band 1. The slight rise at the lower edge of Band 1 is due to the particular commercial LNA used, which can be redesigned for better low-frequency performance.
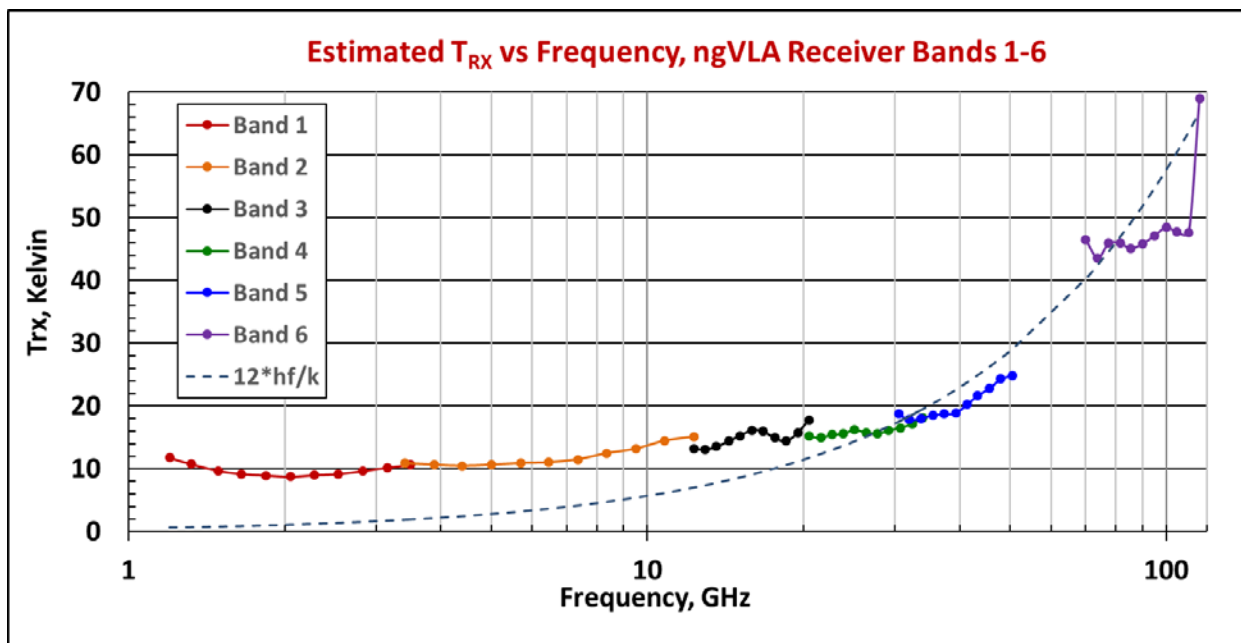
Figure 28: Receiver noise temperatures, ngVLA Bands 1–6.

It should be noted that with the off-the-shelf LNAs used on Band 1 and Band 4, the overall receiver gain is several dB under the expected 30 dB minimum. While they have acceptable noise performance, the lower overall gain of the receiver could result in a higher added noise contribution than desired (< 1 K) from the cascade with the IRD subsystem. Efforts will be undertaken in the detailed design phase to identify alternative devices with comparable noise temperature and higher gain. It should also be stated that the LNAs selected in the simulation are not necessarily final: these will be decided in the detailed design phase.

Table 14 in the appendix (Section 7.3) shows the manufacturer part numbers and measured data of all the LNAs used in the receiver cascade simulation.

6.2   Receiver Linearity

Both the linearity and the dynamic range (DR) of a receiver are primary a function of the LNA. As was stated in the previous section, the LNAs assumed here are representative choices only, not necessarily the final selections. In addition, data on the 1 dB output compression point of the vendor's devices are derived from estimates rather than actual measurements. Hence, any predictions of linearity and DR at this point in time are preliminary and subject to change.

That being said, the parameters related to receiver linearity (dynamic range, headroom, and input damage levels) were calculated from the receiver cascade and the preliminary LNA data [RD29]. These are presented below in Table 5, along with the associated technical risk in meeting the corresponding requirements for linearity from [RD02].

Band	LNA-based CW linearity data				Noise DR and HR (1%, IIP3)			
	P_{1dB}	P_{IIP3}	$P_{1\%}$	$P_{in,max}$	DR	$HR_{1\%}$	HR_{IP3}	Risk
#	dBm [1]	dBm	dBm	dBm [1]	dB	dB	dB	Level
1	-3.0	-18.6	-15.0	+10.0	59.2	52.2	73.8	Low
2	-10.0	-35.3	-22.0	+10.0	35.8	28.8	50.4	Mod.
3	-10.0	-32.9	-22.0	+10.0	38.2	31.2	52.8	Low
4	-12.0	-29.6	-24.0	+10.0	37.9	30.9	52.5	Low
5	-15.0	-38.4	-27.0	+10.0	26.1	19.1	40.7	Mod.
6	-15.0	-41.3	-27.0	+10.0	17.0	10.0	31.6	High

[1] Output 1 dB compression and input damage limit data are vendor estimates.
[2] Dynamic range (DR) is defined as the difference between the 1 dB compressed output and the output power on cold sky [RD02].
[3] Headroom (HR) is defined as the difference between the third-order intercept point (IP3) referred to the input, and the equivalent input system noise power [RD02].

Table 5: Estimates of receiver dynamic range, headroom, and input damage levels.

6.3   System Temperature

Simulated results of the system temperature are shown in Figure 29. Nominal observing conditions at the VLA site are assumed for Bands 1–5, and precision conditions (dry, nighttime winter) for Band 6 only. The antenna noise temperature is calculated over frequency and elevation angles for these conditions [RD09] assuming the sky brightness model in [RD30]. In addition, an added 1 K of noise was assumed as the contribution from the IRD subsystem (which was not included in T_{RX} above).

There is a very noticeable increase in system temperature for the lower half of both Band 1 and Band 2. This is due to the increased spillover noise of the wideband feeds (as seen in Figure 7 and Figure 11,

respectively), combined with an increase in receiver (LNA) noise, particularly on Band 1. The noise bump at ~22 GHz is from the well-known water vapor absorption line: the noise rapidly rises in Bands 5–6 at frequencies approaching the oxygen absorption band.
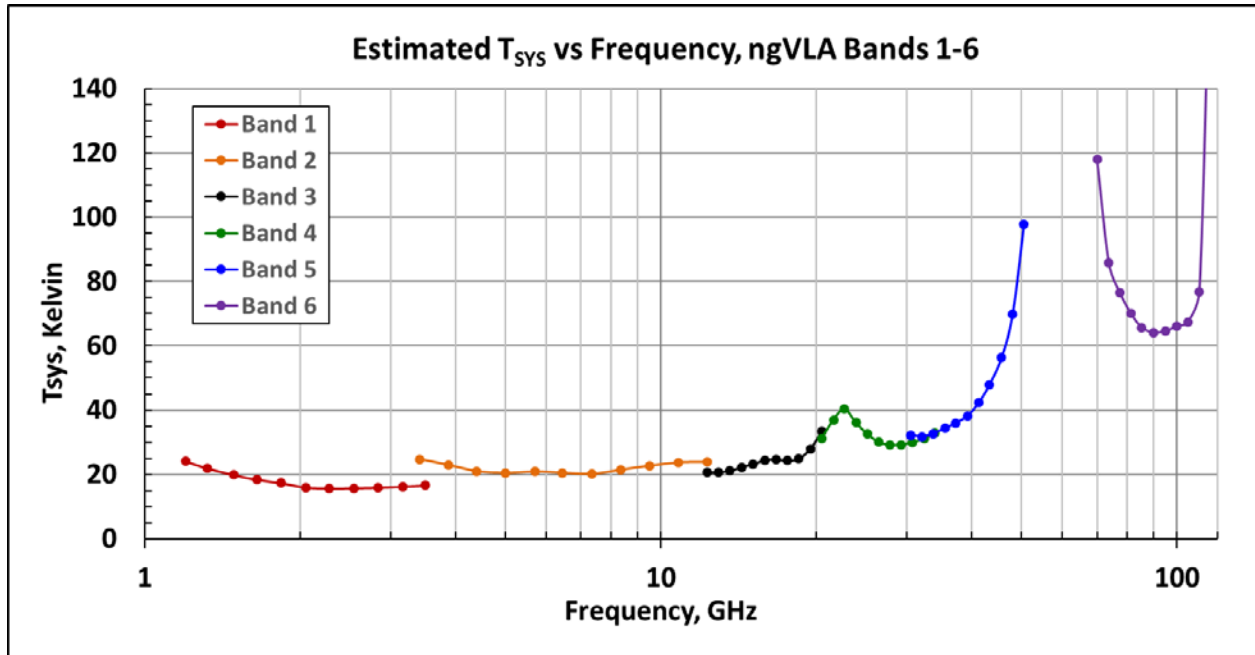
Figure 29: System noise temperatures, ngVLA Bands 1–6. An antenna elevation angle of 45 degrees is assumed; atmospheric PWV is 6mm for Bands 1–5, and 1mm for Band 6. A 1 Kelvin contribution from the IRD subsystem is also assumed and included here.

6.4 Antenna Sensitivity

Using collected estimates of feed + antenna aperture efficiency [RD29] combined with the estimated overall system temperature, the sensitivity metric A_{EFF}/T_{SYS} is calculated for a single ngVLA antenna. The results are plotted in Figure 30, over the full range of frequency and at five different elevation angles. Tabulated values of these results are given in Table 15 of the appendix (Section 7.4). The following are assumed:

- Unblocked dual-offset Gregorian antenna optics with an 18-meter primary aperture, as described in section 4.2.1. For now, no antenna deformation over elevation is assumed.
- Reflector surface roughness or small-scale deviation of 160 microns RMS.
- Precipitable water vapor (PWV) of 6 mm for Bands 1–5, and 1 mm for Band 6 alone.
- Nominal VLA site elevation of 2120 meters.

The roll-off in A_{EFF}/T_{SYS} seen at below 2 GHz is mainly due to the decreasing feed efficiency of the current Band 1 feed horn design, combined with higher T_{SYS}. Roll-off at the higher frequencies is caused by a combination of increasing receiver and sky temperatures (especially at low elevation) and decreasing aperture efficiency due to the effect of antenna reflector surface roughness (Ruze efficiency).

Gravitational deformation of the antenna optical surfaces, and of their locations relative to the feed horn and to each other, can have a significant effect on sensitivity at low elevation angles and at high frequencies. The former is beyond the scope of this document: however, analyses of the latter were performed at selected frequencies [RD03]. Offsets were applied to the feed and reflector positions along their reference axes, and the resulting aperture efficiency drop (scan loss) and beam squint (plate scale) were calculated.

Results on feed offsets alone are the most relevant here: a summary of these for various scan loss levels is given in Table 6. The calculated plate scale (~15 arcsec/mm) was largely independent of frequency and polarization.
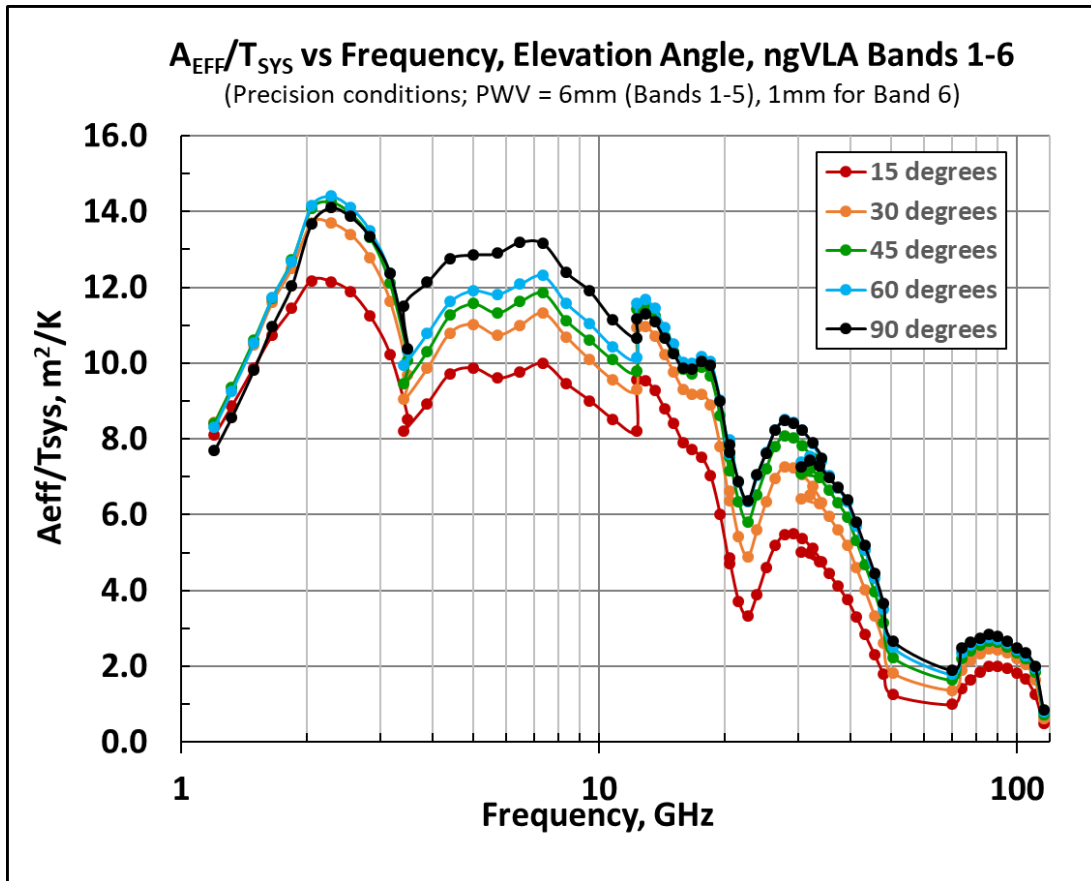
Figure 30: Relative sensitivity for a single ngVLA antenna vs. frequency and elevation angle, ngVLA Bands 1–6. There is no data between 50.5 and 70 GHz.

Frequency	X-Y Feed Offset, for Scan Loss of:		
(GHz)	2%	5%	10%
15	15.86	25.53	37.33
30	8.41	13.33	19.23
45	5.58	8.85	12.83
116	2.09	3.40	4.96

Table 6: Scan loss levels corresponding to feed horn lateral offsets (x,y) in millimeters, versus frequency.

7 Appendices

7.1 Receiver Component Development at NRC HAA

As an independent initiative, the NRC HAA in Victoria BC, Canada undertook advanced development of key receiver components for ngVLA. This includes design of feed horns, LNAs, OMTs, and vacuum windows, as well as a test cryostat and supporting electronics. Their work to date is described in a series of detailed design reports [RD31 – RD33] submitted to NRAO for inclusion in the conceptual design review documentation package. A very brief summary description of some of their component development work with excerpts from the reports are given here.

7.1.1 Feed Horn Development

The feed horn is corrugated design similar to the one described in Section 4.2.2.5, and tries to balance the goals of compact size, high performance, and ease of machining. Figure 31 shows this feed and its simulated return loss and aperture efficiency with the ngVLA optics design [AD02]. Performance is excellent, with a very flat efficiency and high return loss (> 30 dB) over 90% of the band. Diameter at the aperture for a Band 5 version is 38 mm, ~37% larger than the optimized EMSS feed listed in Table 2, which may be an acceptable trade on this band. The larger size helps improve relative efficiency and input match at the lower frequencies. Overall cross polarization is also less than -31 dB.
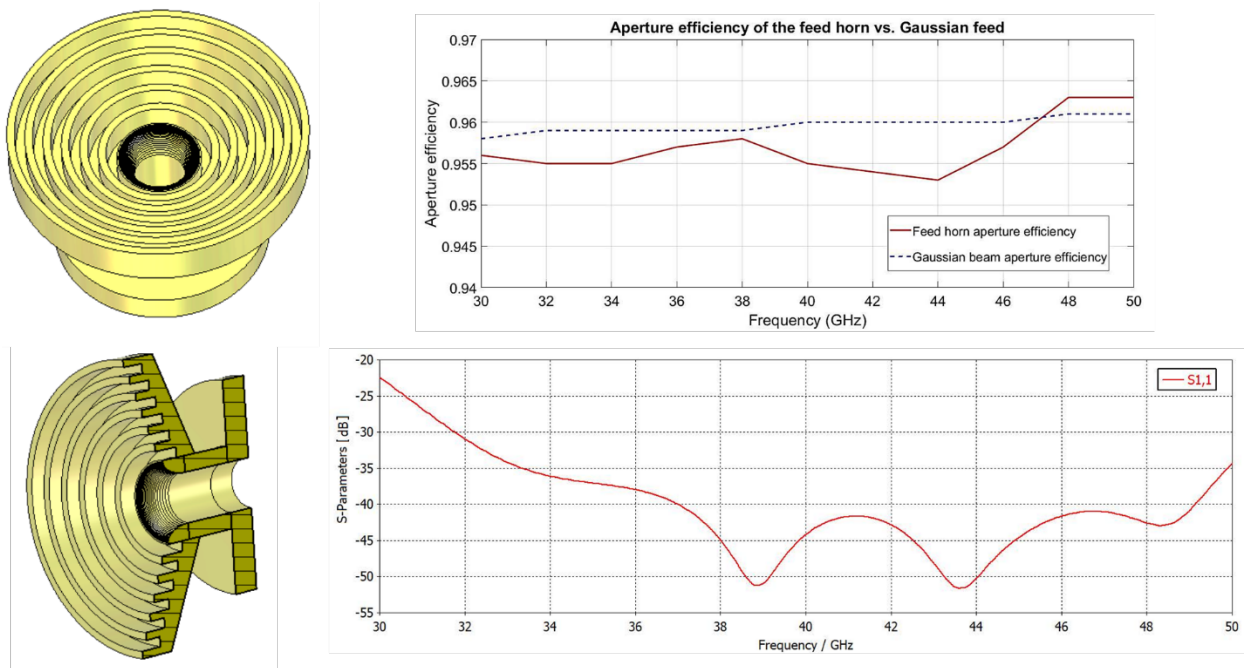
Figure 31 – NRC HAA corrugated feed horn for ngVLA Band 5. Overall and cross-section views are shown to the left; aperture efficiency and return loss over frequency are plotted on the right. Note the logarithmic taper between the waveguide section and corrugations, added to improve the input match.

7.1.2 Vacuum Window Development

A vacuum window concept developed for Band 5 is shown in Figure 32. It is made from a single block of high-density polyethylene (HDPE), with a pair of graded dielectric anti-reflection (AR) layers with a total thickness of ~10 mm on each side, for better matching over the full band. These consist of a hexagonal

grid of concentric circular bores, to produce the desired effective dielectric constant in each layer. A 'top hat' geometry was adopted to allow a smaller window diameter to be used without truncation of the feed horn beam by the cryostat wall.

Electromagnetic performance of this window is very good. There is a slight (~5 dB) increase in feed horn return loss in the central portion of the band with the window added. The calculated aperture efficiency using [AD02] is virtually the same as without the window, except for a roll-off of ~1% at the upper and lower band edges. Insertion loss is also very low, < 0.014 dB over the full band.
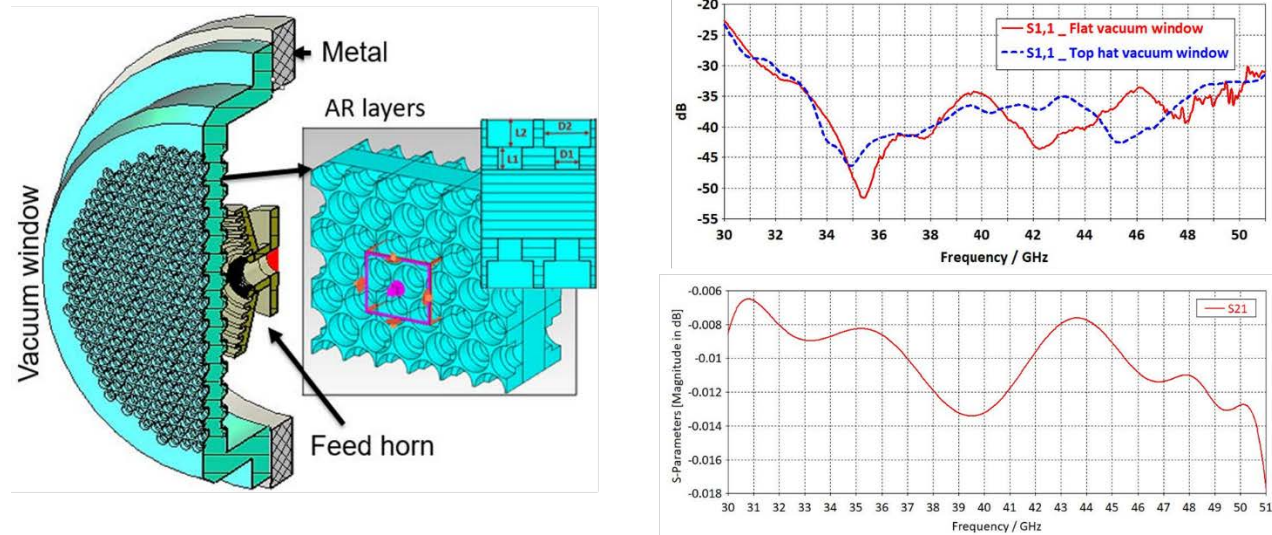
Figure 32 – NRC HAA vacuum window for ngVLA Band 5. Overall and cross-section views are shown to the left; simulated return and insertion loss over frequency are plotted on the right. The window would add ~1 K max. to the overall receiver noise, based on the insertion loss shown.

Modeling of stress and deflection was performed using FEA, with a total window thickness of 15 mm and a pressure differential of 1 atm. The maximum stress observed (3.5 Mpa) was in the window center; assuming a 5 Mpa limit, the safety factor is therefore ~1.4. Instantaneous deflection at the center was ~0.22 mm, and maximum (long-term) deflection of this material is estimated to be ~1 mm.

Two aspects not covered in the report are the predicted or measured leak rate of this window structure, and the UV resistance of the material. These could affect the expected vacuum life (i.e., the interval between cooldown cycles) and long-term durability of the Front End cryostat in the field.

7.1.3 OMT Development

Waveguide turnstile junction OMTs in four different mechanical configurations were designed as possible candidates in both ngVLA Bands 5 & 6. The first three (Figure 33) are variations on a single OMT, while the fourth (Figure 34) has an OMT integrated with a pair of 35 dB couplers and a two-way splitter, for noise calibration injection into the signal paths. Simulated performance for versions in both bands is very good: for Band 5, input return loss is generally better than 25 dB, max insertion loss is < 0.2 dB (OMT only), and output port isolation is > 70 dB over most of the band. The integrated coupler adds ~0.06 dB of loss in the signal path over the OMT alone, but the overall effect on receiver noise is minimal (~0.3 K, with it cooled to 20 K).
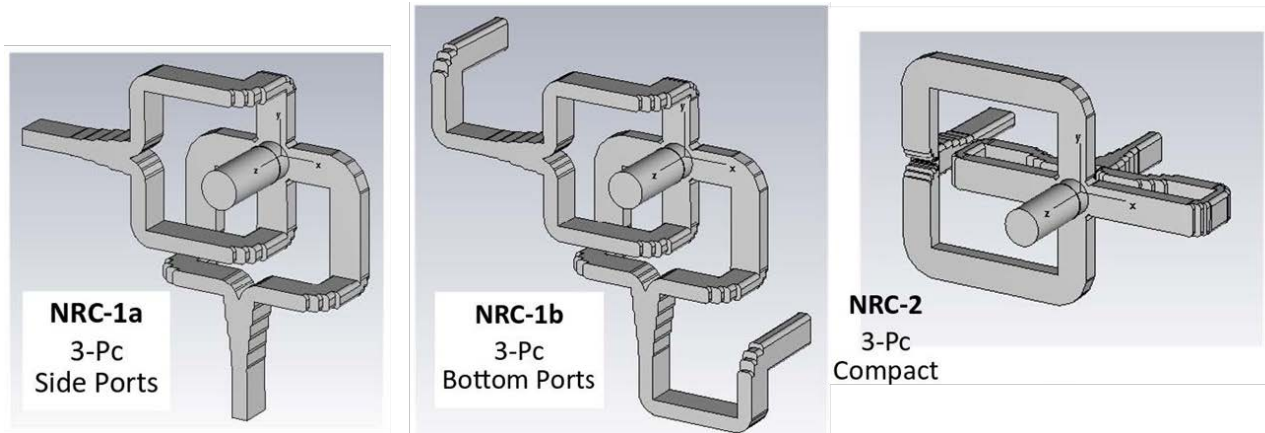
Figure 33 – Rendering of NRC HAA turnstile OMTs, with three different output port or size configurations. The input port to the feed horn is on the face of the central cylinder.
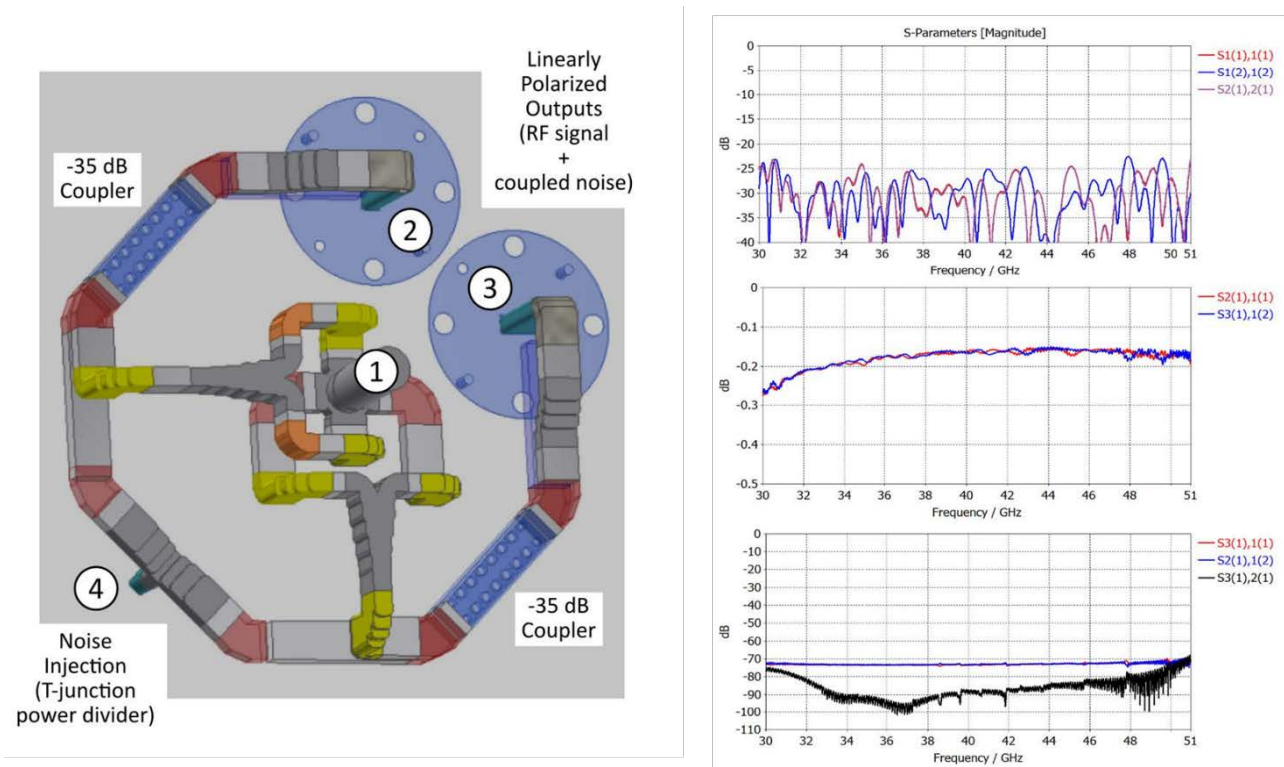
Figure 34 – (Left) Rendering of NRC HAA turnstile OMT integrated with noise calibration injection, for ngVLA Band 5. Mating WR22 waveguide flanges are shown on ports 2 & 3, to show their size and spacing. (Right) Simulated port return losses, thru path loss, and port isolation over frequency. Gold plated waveguide at 77 Kelvin was assumed for the simulated thru loss.

A variation on the above OMT was recently designed by NRC as their new baseline concept. Renderings of the waveguide structure and fabrication concept, and simulated RF performance data are all shown in Figure 35. In this version, the power combiners on each pair of ports from the turnstile junction were replaced with waveguide magic-T hybrid junctions. One advantage of the magic-T is it reflects back any higher-order modes propagating in from the feed horn. Another plus is the machined assembly will be more tolerant to misalignment and less likely to have dips in the response than the original design [RD34].

The RF performance of the new version is almost as good as the original. Insertion loss is only very slightly higher, and the port isolation is ~10 dB worse than before, but still very high (> 60 dB). The magnitude of the return loss is mostly unchanged over the band, but there appears to be much better tracking of the two ports across the band. The only apparent downside is the need to terminate 4th port of the magic-T, which adds two additional embedded terminations.
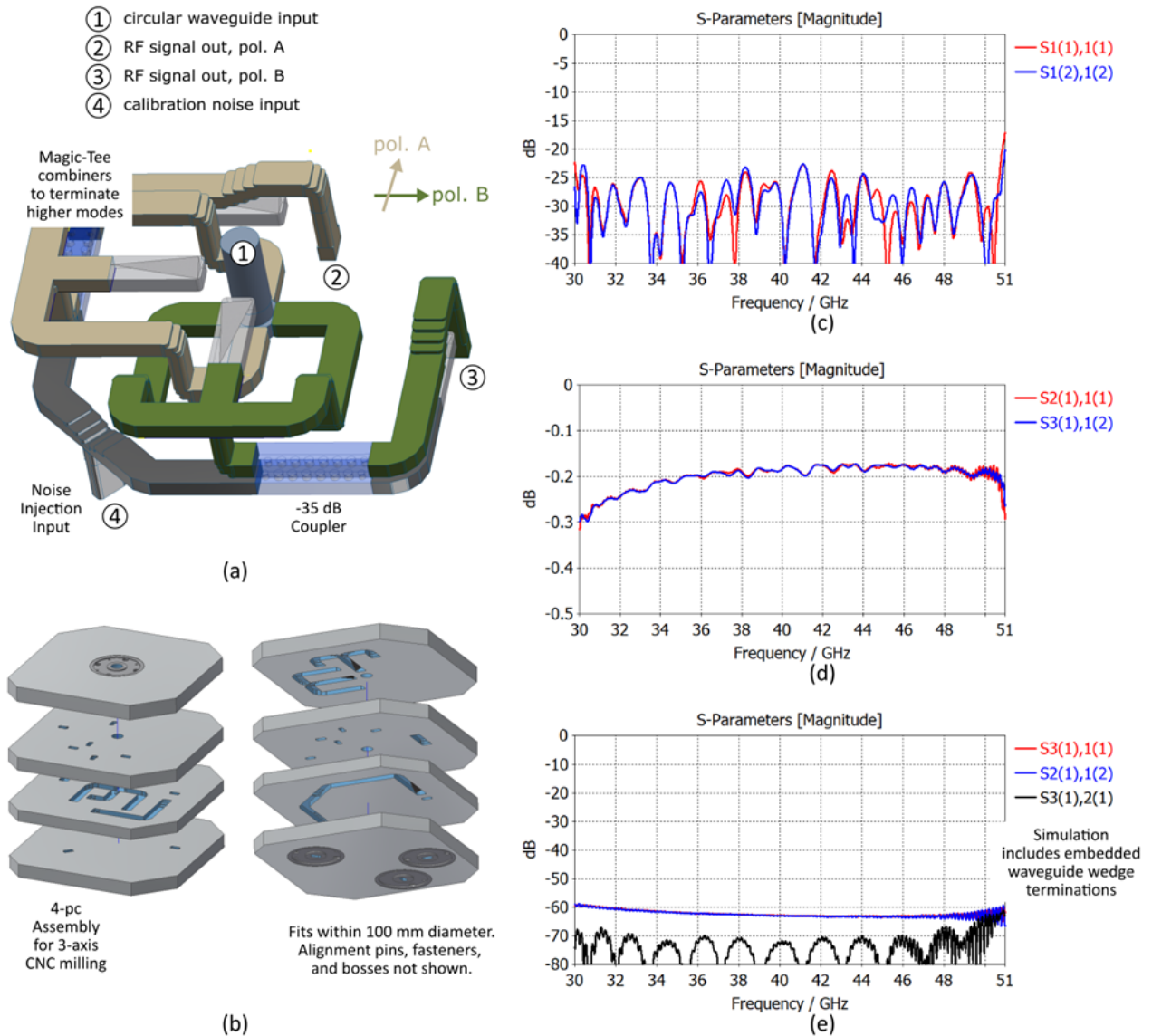
Figure 35 – (a) Rendering of updated Band 5 OMT assembly, with magic-T combiners and terminations. (b) Rendered views of proposed 4-piece layered assembly, showing input and output port flanges. (c-e) Simulated input return losses, thru path losses, port isolation, cross polarization leakage over frequency.

7.1.4 LNA Development

A two-stage GaAs HEMT LNA was designed for ngVLA Band 1. The amplifier is of hybrid construction, with discrete transistors and lumped-element passive components interconnected with wire bonds, mounted within a plated tellurium copper housing. The RF and bias connectors are SMA and Micro-D (MDM), respectively. Measured performance of the prototype is given in Figure 36 below. Input return loss is > 11 dB and gain > 34 dB, with an average noise temperature of ~1.6 K over the full band.
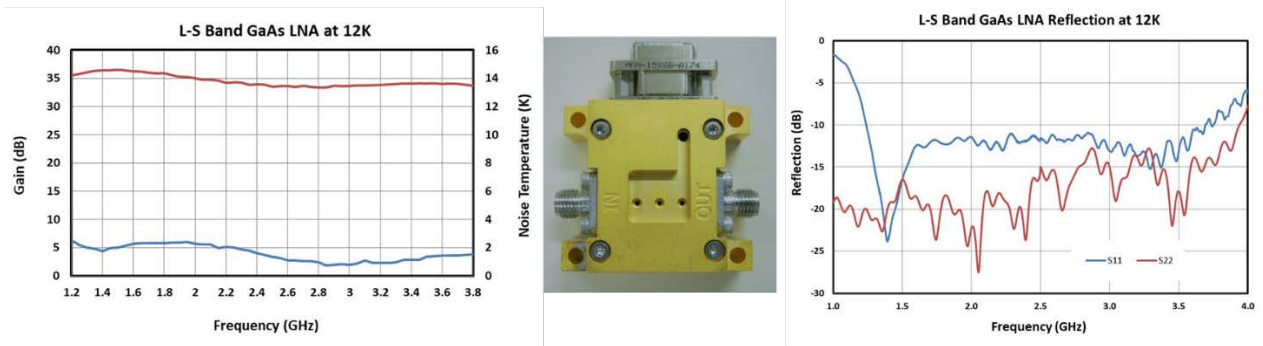
Figure 36 – NRC HAA prototype GaAs HEMT LNA for ngVLA Band 1 (center photo), flanked by plots of gain and noise performance (L) and input/output port return loss ®. Gain is on the red trace, noise temperature on the blue trace.

For ngVLA Band 3, a 4-stage hybrid InP HEMT LNA was designed using devices sourced from the NRC foundry in Ottawa. Simulation of the amplifier performance at ambient temperature yielded > 30 dB of gain and a maximum noise temperature of 60 K. The expectation is the noise temperature will be ~5 K at cryogenic temperatures (12 K). Figure 37 shows plots of the simulated performance over frequency.
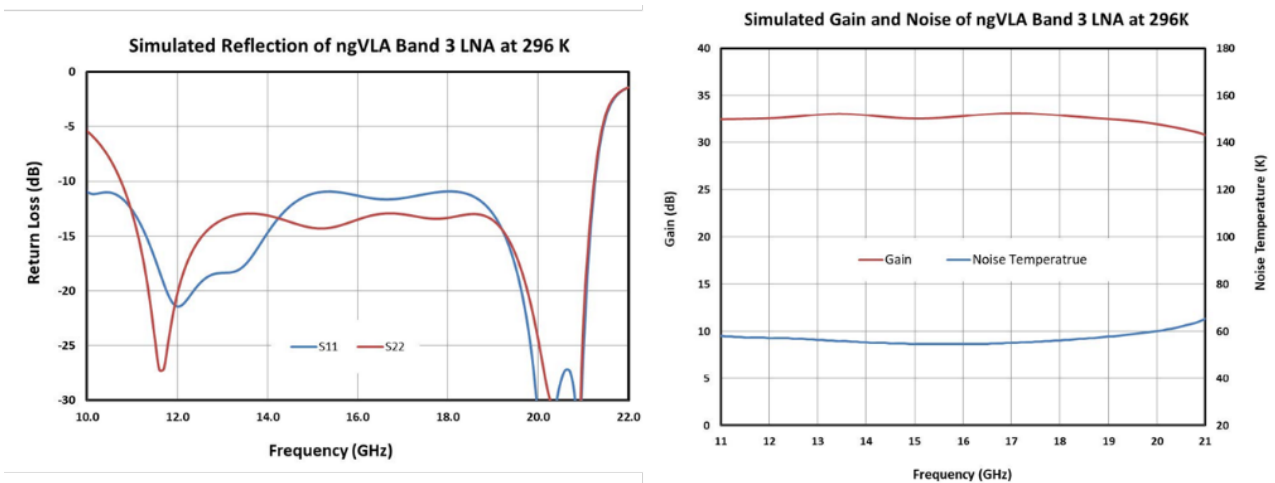
Figure 37 – Simulated ambient temperature gain and noise performance ® and input/output port return loss (L), NRC HAA InP HEMT LNA design for ngVLA Band 3. Input return loss is > 11 dB over the full band.

For ngVLA Bands 4 & 5, a pair of MMIC LNAs were designed using GaAs mHEMT technology with a gate length of 70 nm. The Band 4 unit is a 4-stage amplifier covering a full octave (18 – 36 GHz), and packaged with coaxial connectors. The Band 5 is a 5-stage design, with waveguide (WR22) ports. Figure 38 shows plots of the simulated RF performance at ambient temperature. At cryogenic temperatures (12 K), a noise temperature of ~9 K is expected on the Band 4 LNA, and ~14 K for the Band 5 LNA.
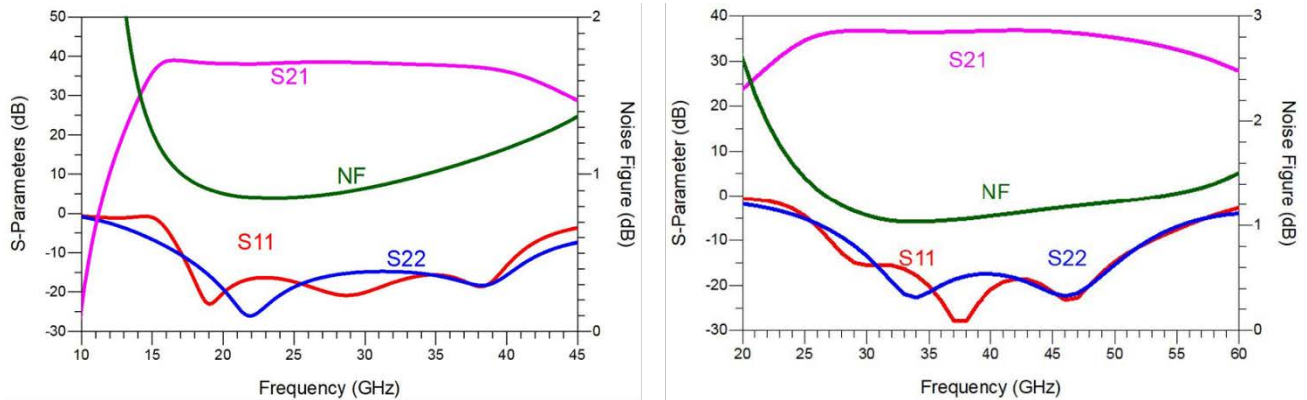
Figure 38 – Simulated RF performance of the GaAs mHEMT amplifiers for Band 4 (L) and Band 5 ®, at ambient temperature. The coax or waveguide launchers are included in the simulation. Gain equals or exceeds 35 dB across both bands, with return loss greater than 10 dB.

Currently, the Band 5 LNA is under fabrication at an outside foundry (OMMIC, in France), with the Band 4 LNA to follow afterwards. Future development plans are for InP MMIC versions of these designs, which would be fabricated at the Ottawa foundry. The measured performance of these will be compared against the GaAs version, and a final selection made.

7.1.5 Octave-Bandwidth Receiver Study

The bandwidth limitation for achieving optimum noise in a cryogenic receiver is generally ~1.7:1 bandwidth ratio. This is primarily driven by the single-mode range of OMTs implemented in standard rectangular waveguide. Performance of a corrugated feed horn (efficiency, input match), and the LNA (primarily the input match) also degrade at wider bandwidths.

The single-mode range limit of the waveguide turnstile OMT can be extended using ridged waveguide. Figure 39 shows a rendering of such an OMT and its simulated RF performance, designed to cover a full octave (25 – 50 GHz). The circular waveguide input is quad-ridged to support orthogonal polarizations; the rectangular outputs are single-ridge. As with a regular turnstile or Boifot OMTs, precise alignment, path symmetry, and adequate spacing are important for suppression of undesired higher-order modes. One possible concern is the sensitivity to small misalignments or gaps between the machined sections. Some additional analysis of these effects might be warranted.

The corrugated feed horn presented earlier was reoptimized for octave bandwidth with added ring loading and tapered quad ridges for compatibility with the quad-ridged OMT above. Figure 40 shows rendered views of the revised feed design, along with simulations of return loss and aperture efficiency using the ngVLA antenna optics, from 25 – 50 GHz. Maximum cross polarization over the band with the optics is -27 dB, about 4 dB worse than in the waveguide-bandwidth feed. Overall, performance is surprisingly good, with only a modest degradation from the baseline. One concern is the mechanical complexity of this design and possible difficulties in fabrication, particularly on the ring-loaded sections. An investigation into this would be useful, as well as a tolerance analysis to determine sensitivities.

An overall summary of performance and comparison against the waveguide-bandwidth component versions is given in Table 7. This includes results from window and LNA and overall receiver cascaded noise results.
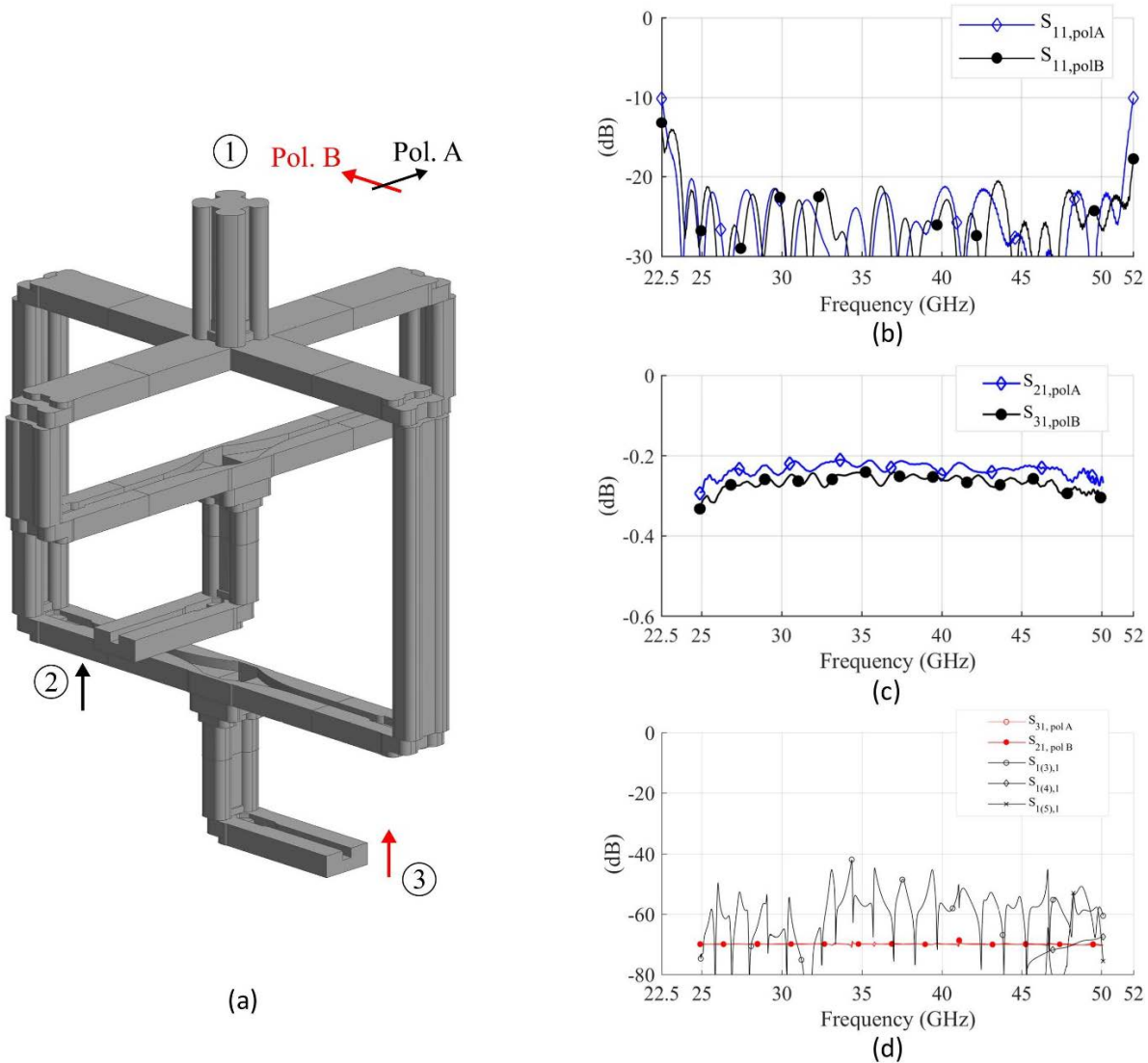
Figure 39 – An NRC HAA octave-bandwidth turnstile OMT, implemented using quad- and single-ridged waveguides. A rendering of the OMT layout is shown in (a), with simulations of input match, thru loss, and cross-polarization/high-order mode leakage plotted in (b), (c), and (d), respectively. Material conductivity assumed was for tellurium copper at ambient temperature.

Figure 40 – (Top) NRC HAA octave-bandwidth corrugated feed horn, with a quad-ridged circular waveguide output to match the OMT. (Bottom) Simulations of input match (L) and aperture efficiency ®, using the ngVLA antenna optics.

	Comments	
Component	**Standard Waveguide Band** (performance estimated at 30.5–50.5 GHz, unless otherwise noted)	**Octave Band** (performance estimated at 25–50 GHz, unless otherwise noted)
Window	Reflected Power: -30 dB (2 stepped holes, UHMWPE)	Reflected Power: -25 dB (2 stepped holes, UHMWPE)
Feed Horn	Reflected Power: -25 dB Phase Efficiency > 99.5% (fixed position) Simulated with ngVLA shaped reflector optics: Aperture Efficiency > 95% Cross-Pol < -30 dB	Reflected Power: -25 dB Phase Efficiency > 99.4% (fixed position) Simulated with ngVLA shaped reflector optics: Aperture Efficiency > 92% Cross-Pol < -25 dB
OMT	Reflected Power: -26 dB cross-pol isolation < -50 dB Insertion Gain > -0.25 dB	Reflected Power: -21 dB cross-pol isolation < -40 dB Insertion Gain > -0.35 dB
LNA	** simulated 30.5–50.5 GHz Input Reflected Power: -10 dB Output Reflected Power: -14 dB Gain > 30 dB	** simulated 18–36 GHz, MMIC Input Reflected Power: -10 dB Output Reflected Power: -10 dB Gain > 30 dB
	**(not enough information for cryogenic noise comparison; room temperature noise simulations appear even)	
Bandwidth	1.66:1	2:1, 20% instantaneous bandwidth increase
Receiver Noise	15–20 K[1] (20.5–34 GHz) 19–27 K[1] (30.5–50.5 GHz)	18–24 K[*] (18–36 GHz) 22–28 K[*] (25–50 GHz)
	[*]Octave band values are simulated or estimated. [1]From Table 7, NRAO Doc. 020.10.20.00.00-0001-REP-B-SYSTEM REFERENCE DESIGN, vol. 1, Jul. 2019.	

Table 7: Summary of NRC HAA component and receiver performance, octave versus waveguide bandwidth.

Title: Front End Conceptual Design Description	Owner: Grammer	Date: 07/26/2022
NRAO Doc. #: 020.30.05.00.00-0006-DSN	Version: C	

7.2 Cascaded Gain and Noise Tables, Bands 1–6

Band #: 1	Temp. Stage	Phys. Temp.	T-Line Len.	1.20				1.32				1.49				1.65				1.84				2.05			
Component Type	#	K	m	G, dB	Te, K	Gcas	Tcas	G, dB	Te, K	Gcas	Tcas	G, dB	Te, K	Gcas	Tcas	G, dB	Te, K	Gcas	Tcas	G, dB	Te, K	Gcas	Tcas	G, dB	Te, K	Gcas	Tcas
Lossless Input	1	20		0.00	0.00	0.00	0.00	0.00	0.00	0.00	0.00	0.00	0.00	0.00	0.00	0.00	0.00	0.00	0.00	0.00	0.00	0.00	0.00	0.00	0.00	0.00	0.00
Weather_Radome	5	300		0.00	0.00	0.00	0.00	0.00	0.00	0.00	0.00	0.00	0.00	0.00	0.00	0.00	0.00	0.00	0.00	0.00	0.00	0.00	0.00	0.00	0.00	0.00	0.00
Vacuum_Window	5	300		-0.02	1.38	-0.02	1.38	-0.02	1.38	-0.02	1.38	-0.02	1.38	-0.02	1.38	-0.02	1.38	-0.02	1.38	-0.02	1.38	-0.02	1.38	-0.02	1.38	-0.02	1.38
IR_Filter	4	190		-0.02	0.88	-0.04	2.27	-0.02	0.88	-0.04	2.27	-0.02	0.88	-0.04	2.27	-0.02	0.88	-0.04	2.27	-0.02	0.88	-0.04	2.27	-0.02	0.88	-0.04	2.27
Feed_Horn	3	80		-0.10	1.86	-0.14	4.15	-0.10	1.86	-0.14	4.15	-0.10	1.86	-0.14	4.15	-0.10	1.86	-0.14	4.15	-0.10	1.86	-0.14	4.15	-0.10	1.88	-0.14	4.17
Coax_141Cu	2	50	0.1	-0.04	0.47	-0.18	4.64	-0.04	0.50	-0.18	4.66	-0.05	0.53	-0.19	4.69	-0.05	0.56	-0.19	4.73	-0.05	0.60	-0.19	4.77	-0.06	0.64	-0.20	4.83
Cal_Coupler	1	20		-0.45	2.18	-0.63	6.91	-0.45	2.18	-0.63	6.94	-0.45	2.18	-0.64	6.97	-0.45	2.18	-0.64	7.01	-0.45	2.18	-0.64	7.05	-0.45	2.18	-0.65	7.11
Cal_Inj_Band1	4	190		0.00	0.19	-0.63	7.13	0.00	0.19	-0.63	7.16	0.00	0.19	-0.64	7.19	0.00	0.19	-0.64	7.23	0.00	0.19	-0.64	7.27	0.00	0.19	-0.65	7.33
LNA_Band1	1	20		26.00	3.96	25.37	11.70	27.02	3.07	26.39	10.71	27.61	2.13	26.97	9.66	27.43	1.64	26.79	9.13	27.12	1.40	26.48	8.89	26.80	1.16	26.15	8.68
Coax_086SS	4	190	0.4	-0.62	29.09	24.75	11.79	-0.65	30.53	25.74	10.78	-0.69	32.58	26.29	9.73	-0.73	34.53	26.06	9.20	-0.77	36.87	25.71	8.98	-0.82	39.34	25.34	8.77
Cascaded Values:						24.8	11.8			25.7	10.8			26.3	9.7			26.1	9.2			25.7	9.0			25.3	8.8

Band #: 1	Temp. Stage	Phys. Temp.	T-Line Len.	2.28				2.54				2.83				3.16				3.49			
Component Type	#	K	m	G, dB	Te, K	Gcas	Tcas	G, dB	Te, K	Gcas	Tcas	G, dB	Te, K	Gcas	Tcas	G, dB	Te, K	Gcas	Tcas	G, dB	Te, K	Gcas	Tcas
Lossless Input	1	20		0.00	0.00	0.00	0.00	0.00	0.00	0.00	0.00	0.00	0.00	0.00	0.00	0.00	0.00	0.00	0.00	0.00	0.00	0.00	0.00
Weather_Radome	5	300		0.00	0.00	0.00	0.00	0.00	0.00	0.00	0.00	0.00	0.00	0.00	0.00	0.00	0.00	0.00	0.00	0.00	0.00	0.00	0.00
Vacuum_Window	5	300		-0.02	1.38	-0.02	1.38	-0.02	1.38	-0.02	1.38	-0.02	1.38	-0.02	1.38	-0.02	1.38	-0.02	1.38	-0.02	1.38	-0.02	1.38
IR_Filter	4	190		-0.02	0.88	-0.04	2.27	-0.02	0.88	-0.04	2.27	-0.02	0.88	-0.04	2.27	-0.02	0.88	-0.04	2.27	-0.02	0.88	-0.04	2.27
Feed_Horn	3	80		-0.11	1.98	-0.15	4.26	-0.11	2.08	-0.15	4.37	-0.12	2.20	-0.16	4.49	-0.13	2.34	-0.17	4.62	-0.13	2.48	-0.17	4.77
Coax_141Cu	2	50	0.1	-0.06	0.68	-0.20	4.96	-0.06	0.72	-0.21	5.11	-0.07	0.76	-0.22	5.28	-0.07	0.81	-0.24	5.47	-0.07	0.86	-0.25	5.67
Cal_Coupler	1	20		-0.45	2.18	-0.65	7.25	-0.45	2.18	-0.66	7.40	-0.45	2.18	-0.67	7.58	-0.45	2.18	-0.69	7.78	-0.45	2.18	-0.70	7.98
Cal_Inj_Band1	4	190		0.00	0.19	-0.65	7.47	0.00	0.19	-0.66	7.63	0.00	0.19	-0.67	7.80	0.00	0.19	-0.69	8.00	0.00	0.19	-0.70	8.21
LNA_Band1	1	20		26.60	1.24	25.95	8.92	26.37	1.24	25.71	9.07	26.29	1.50	25.61	9.55	26.36	1.79	25.67	10.09	26.36	1.96	25.66	10.51
Coax_086SS	4	190	0.4	-0.86	41.56	25.09	9.02	-0.91	44.09	24.80	9.19	-0.96	46.95	24.65	9.68	-1.01	49.99	24.66	10.22	-1.06	52.80	24.59	10.65
Cascaded Values:						25.1	9.0			24.8	9.2			24.7	9.7			24.7	10.2			24.6	10.7

Table 8: Cascaded gain and noise, Band 1.

Band #: 2

Component Type	#	K	m	3.41				3.88				4.40				5.00				5.70				6.45			
				G, dB	Te, K	Gcas	Tcas	G, dB	Te, K	Gcas	Tcas	G, dB	Te, K	Gcas	Tcas	G, dB	Te, K	Gcas	Tcas	G, dB	Te, K	Gcas	Tcas	G, dB	Te, K	Gcas	Tcas
Lossless Input	1	20		0.00	0.00	0.00	0.00	0.00	0.00	0.00	0.00	0.00	0.00	0.00	0.00	0.00	0.00	0.00	0.00	0.00	0.00	0.00	0.00	0.00	0.00	0.00	0.00
Weather_Radome	5	300		0.00	0.00	0.00	0.00	0.00	0.00	0.00	0.00	0.00	0.00	0.00	0.00	0.00	0.00	0.00	0.00	0.00	0.00	0.00	0.00	0.00	0.00	0.00	0.00
Vacuum_Window	5	300		-0.02	1.38	-0.02	1.38	-0.02	1.38	-0.02	1.38	-0.02	1.45	-0.02	1.45	-0.02	1.56	-0.02	1.56	-0.02	1.68	-0.02	1.68	-0.03	1.81	-0.03	1.81
IR_Filter	4	190		-0.02	0.88	-0.04	2.27	-0.02	0.88	-0.04	2.27	-0.02	0.92	-0.04	2.38	-0.02	0.99	-0.05	2.55	-0.02	1.06	-0.05	2.75	-0.03	1.15	-0.05	2.96
Feed_Horn	1	20		-0.13	0.61	-0.17	2.88	-0.15	0.68	-0.19	2.96	-0.16	0.73	-0.20	3.11	-0.16	0.76	-0.21	3.32	-0.17	0.80	-0.22	3.56	-0.18	0.85	-0.23	3.82
Coax_141Cu	1	20	0.1	-0.07	0.34	-0.24	3.23	-0.08	0.37	-0.26	3.34	-0.08	0.39	-0.28	3.53	-0.09	0.42	-0.30	3.77	-0.10	0.46	-0.32	4.05	-0.11	0.49	-0.34	4.34
Cal_Coupler	1	20		-0.45	2.18	-0.69	5.54	-0.45	2.18	-0.71	5.66	-0.45	2.18	-0.73	5.86	-0.45	2.18	-0.75	6.10	-0.45	2.18	-0.77	6.39	-0.45	2.18	-0.79	6.70
Cal_Inj_Band2	4	190		**0.00**	**0.19**	-0.69	5.77	**0.00**	**0.19**	-0.71	5.88	**0.00**	**0.19**	-0.73	6.08	**0.00**	**0.19**	-0.75	6.33	**0.00**	**0.19**	-0.77	6.62	**0.00**	**0.19**	-0.79	6.93
LNA_Band2	1	20		**37.14**	**4.36**	36.44	10.88	**37.07**	**4.04**	36.36	10.64	**36.60**	**3.68**	35.87	10.44	**36.10**	**3.62**	35.35	10.63	**36.14**	**3.57**	35.37	10.88	**36.47**	**3.40**	35.68	11.01
Coax_086SS	4	190	0.4	-1.05	52.11	35.39	10.89	-1.12	56.16	35.23	10.66	-1.20	60.30	34.67	10.46	-1.28	65.01	34.07	10.64	-1.36	70.08	34.01	10.90	-1.45	75.24	34.23	11.03
Cascaded Values:						**35.4**	**10.9**			**35.2**	**10.7**			**34.7**	**10.5**			**34.1**	**10.6**			**34.0**	**10.9**			**34.2**	**11.0**

Band #: 2

Component Type	#	K	m	7.35				8.35				9.50				10.80				12.29			
				G, dB	Te, K	Gcas	Tcas	G, dB	Te, K	Gcas	Tcas	G, dB	Te, K	Gcas	Tcas	G, dB	Te, K	Gcas	Tcas	G, dB	Te, K	Gcas	Tcas
Lossless Input	1	20		0.00	0.00	0.00	0.00	0.00	0.00	0.00	0.00	0.00	0.00	0.00	0.00	0.00	0.00	0.00	0.00	0.00	0.00	0.00	0.00
Weather_Radome	5	300		0.00	0.00	0.00	0.00	0.00	0.00	0.00	0.00	0.00	0.00	0.00	0.00	0.00	0.00	0.00	0.00	0.00	0.00	0.00	0.00
Vacuum_Window	5	300		-0.03	1.97	-0.03	1.97	-0.03	2.08	-0.03	2.08	-0.03	2.08	-0.03	2.08	-0.03	2.08	-0.03	2.08	-0.03	2.08	-0.03	2.08
IR_Filter	4	190		-0.03	1.25	-0.06	3.22	-0.03	1.32	-0.06	3.41	-0.03	1.32	-0.06	3.41	-0.03	1.32	-0.06	3.41	-0.03	1.32	-0.06	3.41
Feed_Horn	1	20		-0.19	0.90	-0.25	4.14	-0.21	0.98	-0.27	4.40	-0.23	1.11	-0.29	4.53	-0.27	1.26	-0.33	4.68	-0.30	1.43	-0.36	4.86
Coax_141Cu	1	20	0.1	-0.11	0.53	-0.36	4.70	-0.12	0.58	-0.39	5.01	-0.13	0.62	-0.43	5.20	-0.14	0.67	-0.47	5.41	-0.16	0.73	-0.52	5.65
Cal_Coupler	1	20		-0.45	2.18	-0.81	7.07	-0.45	2.18	-0.84	7.40	-0.45	2.18	-0.88	7.61	-0.45	2.18	-0.92	7.84	-0.45	2.18	-0.97	8.11
Cal_Inj_Band2	4	190		**0.00**	**0.19**	-0.81	7.30	**0.00**	**0.19**	-0.84	7.63	**0.00**	**0.19**	-0.88	7.84	**0.00**	**0.19**	-0.92	8.07	**0.00**	**0.19**	-0.97	8.34
LNA_Band2	1	20		**37.14**	**3.47**	36.33	11.49	**37.74**	**3.96**	36.90	12.44	**38.05**	**4.35**	37.17	13.16	**38.02**	**5.15**	37.10	14.44	**38.10**	**5.41**	37.13	15.10
Coax_086SS	4	190	0.4	-1.55	81.26	34.78	11.50	-1.65	87.83	35.25	12.46	-1.76	94.94	35.41	13.18	-1.88	102.71	35.22	14.46	-2.00	111.37	35.13	15.12
Cascaded Values:						**34.8**	**11.5**			**35.2**	**12.5**			**35.4**	**13.2**			**35.2**	**14.5**			**35.1**	**15.1**

Table 9: Cascaded gain and noise, Band 2.

Band #: 3

Component Type	#	K	m	12.31 G,dB	12.31 Te,K	12.31 Gcas	12.31 Tcas	12.94 G,dB	12.94 Te,K	12.94 Gcas	12.94 Tcas	13.60 G,dB	13.60 Te,K	13.60 Gcas	13.60 Tcas	14.35 G,dB	14.35 Te,K	14.35 Gcas	14.35 Tcas	15.10 G,dB	15.10 Te,K	15.10 Gcas	15.10 Tcas	15.90 G,dB	15.90 Te,K	15.90 Gcas	15.90 Tcas
Lossless Input	1	20		0.00	0.00	0.00	0.00	0.00	0.00	0.00	0.00	0.00	0.00	0.00	0.00	0.00	0.00	0.00	0.00	0.00	0.00	0.00	0.00	0.00	0.00	0.00	0.00
Weather_Radome	5	300		-0.03	2.08	-0.03	2.08	-0.03	2.08	-0.03	2.08	-0.03	2.08	-0.03	2.08	-0.03	2.08	-0.03	2.08	-0.03	2.08	-0.03	2.08	-0.03	2.08	-0.03	2.08
Vacuum_Window	5	300		-0.03	2.08	-0.06	4.17	-0.03	2.08	-0.06	4.17	-0.03	2.08	-0.06	4.17	-0.03	2.08	-0.06	4.17	-0.03	2.08	-0.06	4.17	-0.03	2.08	-0.06	4.17
IR_Filter	4	190		-0.03	1.32	-0.09	5.51	-0.03	1.32	-0.09	5.51	-0.03	1.32	-0.09	5.51	-0.03	1.32	-0.09	5.51	-0.03	1.32	-0.09	5.51	-0.03	1.32	-0.09	5.51
Feed_Horn	1	20		-0.05	0.23	-0.14	5.75	-0.05	0.23	-0.14	5.75	-0.05	0.23	-0.14	5.75	-0.05	0.23	-0.14	5.75	-0.05	0.23	-0.14	5.75	-0.05	0.23	-0.14	5.75
OMT_Band3	1	20		-0.10	0.48	-0.24	6.24	-0.09	0.42	-0.23	6.18	-0.08	0.38	-0.22	6.14	-0.08	0.35	-0.22	6.11	-0.07	0.33	-0.21	6.09	-0.07	0.31	-0.21	6.07
Cal_Coupler	1	20		-0.20	0.94	-0.44	7.24	-0.20	0.94	-0.43	7.17	-0.20	0.94	-0.42	7.13	-0.20	0.94	-0.42	7.10	-0.20	0.94	-0.41	7.08	-0.20	0.94	-0.41	7.06
WG_Band3	1	20	0.1	-0.04	0.17	-0.48	7.42	-0.03	0.15	-0.46	7.34	-0.03	0.14	-0.45	7.28	-0.03	0.12	-0.44	7.24	-0.03	0.12	-0.44	7.21	-0.02	0.11	-0.43	7.18
Cal_Inj_Band3	4	190		0.00	0.19	-0.48	7.64	0.00	0.19	-0.46	7.55	0.00	0.19	-0.45	7.49	0.00	0.19	-0.44	7.45	0.00	0.19	-0.44	7.42	0.00	0.19	-0.43	7.39
LNA_Band3	1	20		35.08	5.00	34.60	13.22	34.65	5.00	34.19	13.11	34.28	5.44	33.83	13.53	34.88	6.35	34.44	14.48	34.96	7.10	34.52	15.27	34.64	7.90	34.21	16.12
Coax_086SS	4	190	0.3	-1.50	78.62	33.09	13.25	-1.54	80.95	32.64	13.14	-1.58	83.41	32.25	13.56	-1.62	86.15	32.81	14.51	-1.67	88.80	32.86	15.30	-1.71	91.67	32.50	16.15
Cascaded Values:						33.1	13.2			32.6	13.1			32.2	13.6			32.8	14.5			32.9	15.3			32.5	16.2

Band #: 3

Component Type	#	K	m	16.70 G,dB	16.70 Te,K	16.70 Gcas	16.70 Tcas	17.60 G,dB	17.60 Te,K	17.60 Gcas	17.60 Tcas	18.50 G,dB	18.50 Te,K	18.50 Gcas	18.50 Tcas	19.50 G,dB	19.50 Te,K	19.50 Gcas	19.50 Tcas	20.50 G,dB	20.50 Te,K	20.50 Gcas	20.50 Tcas
Lossless Input	1	20		0.00	0.00	0.00	0.00	0.00	0.00	0.00	0.00	0.00	0.00	0.00	0.00	0.00	0.00	0.00	0.00	0.00	0.00	0.00	0.00
Weather_Radome	5	300		-0.03	2.20	-0.03	2.20	-0.03	2.36	-0.03	2.36	-0.04	2.51	-0.04	2.51	-0.04	2.69	-0.04	2.69	-0.04	2.82	-0.04	2.82
Vacuum_Window	5	300		-0.03	2.08	-0.06	4.30	-0.03	2.08	-0.06	4.45	-0.03	2.08	-0.07	4.61	-0.03	2.08	-0.07	4.79	-0.03	2.08	-0.07	4.92
IR_Filter	4	190		-0.03	1.32	-0.09	5.63	-0.03	1.32	-0.09	5.79	-0.03	1.32	-0.10	5.95	-0.03	1.32	-0.10	6.12	-0.03	1.32	-0.10	6.26
Feed_Horn	1	20		-0.05	0.23	-0.14	5.87	-0.05	0.23	-0.14	6.03	-0.05	0.23	-0.15	6.19	-0.05	0.23	-0.15	6.36	-0.05	0.23	-0.15	6.49
OMT_Band3	1	20		-0.07	0.30	-0.21	6.18	-0.06	0.29	-0.21	6.33	-0.06	0.29	-0.21	6.48	-0.06	0.28	-0.21	6.65	-0.06	0.27	-0.21	6.78
Cal_Coupler	1	20		-0.20	0.94	-0.41	7.17	-0.20	0.94	-0.41	7.32	-0.20	0.94	-0.41	7.47	-0.20	0.94	-0.41	7.64	-0.20	0.94	-0.41	7.77
WG_Band3	1	20	0.1	-0.02	0.11	-0.43	7.29	-0.02	0.10	-0.43	7.43	-0.02	0.10	-0.43	7.58	-0.02	0.10	-0.43	7.75	-0.02	0.10	-0.43	7.87
Cal_Inj_Band3	4	190		0.00	0.19	-0.43	7.50	0.00	0.19	-0.43	7.64	0.00	0.19	-0.43	7.79	0.00	0.19	-0.43	7.96	0.00	0.19	-0.43	8.08
LNA_Band3	1	20		34.18	7.65	33.75	15.94	34.36	6.60	33.93	14.93	34.80	6.00	34.37	14.41	34.80	7.00	34.37	15.69	34.30	8.75	33.87	17.75
Coax_086SS	4	190	0.3	-1.75	94.40	32.00	15.98	-1.80	97.49	32.13	14.97	-1.84	100.51	32.53	14.45	-1.89	103.83	32.48	15.72	-1.94	107.10	31.93	17.79
Cascaded Values:						32.0	16.0			32.1	15.0			32.5	14.5			32.5	15.7			31.9	17.8

Table 10: Cascaded gain and noise, Band 3.

Band #: 4 — Frequencies 20.5 – 26.4

Band #: 4 / Component Type	Temp. Stage #	Phys. Temp. K	T-Line Len. m	20.5 G, dB	Te, K	Gcas	Tcas	21.6 G, dB	Te, K	Gcas	Tcas	22.7 G, dB	Te, K	Gcas	Tcas	23.9 G, dB	Te, K	Gcas	Tcas	25.1 G, dB	Te, K	Gcas	Tcas	26.4 G, dB	Te, K	Gcas	Tcas
Lossless Input	1	20		0.00	0.00	0.00	0.00	0.00	0.00	0.00	0.00	0.00	0.00	0.00	0.00	0.00	0.00	0.00	0.00	0.00	0.00	0.00	0.00	0.00	0.00	0.00	0.00
Weather_Radome	5	300		-0.04	2.82	-0.04	2.82	-0.04	2.92	-0.04	2.92	-0.04	3.01	-0.04	3.01	-0.04	3.12	-0.04	3.12	-0.05	3.22	-0.05	3.22	-0.05	3.33	-0.05	3.33
Vacuum_Window	5	300		-0.03	2.08	-0.07	4.92	-0.03	2.08	-0.07	5.02	-0.03	2.08	-0.07	5.11	-0.03	2.08	-0.07	5.22	-0.03	2.08	-0.08	5.32	-0.03	2.08	-0.08	5.44
IR_Filter	4	190		-0.03	1.32	-0.10	6.26	-0.03	1.32	-0.10	6.35	-0.03	1.32	-0.10	6.45	-0.03	1.32	-0.10	6.56	-0.03	1.32	-0.11	6.66	-0.03	1.32	-0.11	6.78
Feed_Horn	1	20		-0.05	0.23	-0.15	6.49	-0.05	0.23	-0.15	6.59	-0.05	0.23	-0.15	6.69	-0.05	0.23	-0.15	6.79	-0.05	0.23	-0.16	6.90	-0.05	0.23	-0.16	7.02
OMT_Band4	1	20		-0.13	0.61	-0.28	7.12	-0.11	0.54	-0.27	7.15	-0.10	0.49	-0.26	7.19	-0.10	0.45	-0.25	7.26	-0.09	0.43	-0.25	7.34	-0.09	0.41	-0.25	7.44
Cal_Coupler	1	20		-0.20	0.94	-0.48	8.13	-0.20	0.94	-0.47	8.15	-0.20	0.94	-0.46	8.19	-0.20	0.94	-0.45	8.26	-0.20	0.94	-0.45	8.34	-0.20	0.94	-0.45	8.43
WG_Band4	1	20	0.1	-0.08	0.36	-0.56	8.53	-0.07	0.31	-0.53	8.50	-0.06	0.29	-0.52	8.51	-0.06	0.26	-0.51	8.55	-0.05	0.25	-0.50	8.61	-0.05	0.24	-0.50	8.70
Cal_Inj_Band4	4	190		0.00	0.19	-0.56	8.74	0.00	0.19	-0.53	8.71	0.00	0.19	-0.52	8.72	0.00	0.19	-0.51	8.77	0.00	0.19	-0.50	8.83	0.00	0.19	-0.50	8.91
LNA_Band4	1	20		33.65	5.65	33.09	15.17	33.04	5.48	32.51	14.91	31.89	5.88	31.37	15.35	31.50	6.00	30.99	15.51	30.90	6.47	30.40	16.09	29.16	6.00	28.66	15.63
Coax_086SS	4	190	0.3	-1.94	107.10	31.15	15.22	-1.99	110.64	30.51	14.97	-2.04	114.11	29.33	15.44	-2.10	117.85	28.90	15.61	-2.15	121.63	28.25	16.20	-2.20	125.54	26.46	15.81
Cascaded Values:						31.2	15.2			30.5	15.0			29.3	15.4			28.9	15.6			28.2	16.2			26.5	15.8

Band #: 4 — Frequencies 27.8 – 34.0

Band #: 4 / Component Type	Temp. Stage #	Phys. Temp. K	T-Line Len. m	27.8 G, dB	Te, K	Gcas	Tcas	29.2 G, dB	Te, K	Gcas	Tcas	30.7 G, dB	Te, K	Gcas	Tcas	32.4 G, dB	Te, K	Gcas	Tcas	34.0 G, dB	Te, K	Gcas	Tcas
Lossless Input	1	20		0.00	0.00	0.00	0.00	0.00	0.00	0.00	0.00	0.00	0.00	0.00	0.00	0.00	0.00	0.00	0.00	0.00	0.00	0.00	0.00
Weather_Radome	5	300		-0.05	3.46	-0.05	3.46	-0.05	3.47	-0.05	3.47	-0.05	3.47	-0.05	3.47	-0.05	3.47	-0.05	3.47	-0.05	3.47	-0.05	3.47
Vacuum_Window	5	300		-0.03	2.08	-0.08	5.56	-0.03	2.08	-0.08	5.58	-0.03	2.08	-0.08	5.58	-0.03	2.08	-0.08	5.58	-0.03	2.08	-0.08	5.58
IR_Filter	4	190		-0.03	1.32	-0.11	6.90	-0.03	1.32	-0.11	6.92	-0.03	1.32	-0.11	6.92	-0.03	1.32	-0.11	6.92	-0.03	1.32	-0.11	6.92
Feed_Horn	1	20		-0.05	0.23	-0.16	7.14	-0.05	0.23	-0.16	7.16	-0.05	0.23	-0.16	7.16	-0.05	0.23	-0.16	7.16	-0.05	0.23	-0.16	7.16
OMT_Band4	1	20		-0.08	0.39	-0.24	7.54	-0.08	0.38	-0.24	7.55	-0.08	0.37	-0.24	7.54	-0.08	0.36	-0.24	7.53	-0.08	0.35	-0.24	7.52
Cal_Coupler	1	20		-0.20	0.94	-0.44	8.54	-0.21	0.98	-0.45	8.58	-0.22	1.02	-0.46	8.62	-0.23	1.08	-0.46	8.67	-0.24	1.12	-0.47	8.71
WG_Band4	1	20	0.1	-0.05	0.23	-0.49	8.79	-0.05	0.22	-0.50	8.83	-0.05	0.22	-0.50	8.86	-0.05	0.21	-0.51	8.90	-0.04	0.21	-0.52	8.94
Cal_Inj_Band4	4	190		0.00	0.19	-0.49	9.00	0.00	0.19	-0.50	9.04	0.00	0.19	-0.50	9.07	0.00	0.19	-0.51	9.11	0.00	0.19	-0.52	9.16
LNA_Band4	1	20		27.56	5.70	27.06	15.39	28.00	6.06	27.50	15.83	28.00	6.44	27.50	16.30	28.00	6.94	27.49	16.92	28.00	7.80	27.48	17.95
Coax_086SS	4	190	0.3	-2.26	129.82	24.80	15.64	-2.32	133.95	25.19	16.07	-2.38	138.41	25.12	16.55	-2.44	143.30	25.05	17.17	-2.50	147.93	24.98	18.21
Cascaded Values:						24.8	15.6			25.2	16.1			25.1	16.5			25.0	17.2			25.0	18.2

Table 11: Cascaded gain and noise, Band 4.

Band #: 5	Temp. Stage	Phys. Temp.	T-Line Len.	30.5				32.0				33.7				35.5				37.3				39.3			
Frequency:																											
Component Type	#	K	m	G, dB	Te, K	Gcas	Tcas	G, dB	Te, K	Gcas	Tcas	G, dB	Te, K	Gcas	Tcas	G, dB	Te, K	Gcas	Tcas	G, dB	Te, K	Gcas	Tcas	G, dB	Te, K	Gcas	Tcas
Lossless Input	1	20		0.00	0.00	0.00	0.00	0.00	0.00	0.00	0.00	0.00	0.00	0.00	0.00	0.00	0.00	0.00	0.00	0.00	0.00	0.00	0.00	0.00	0.00	0.00	0.00
Weather_Radome	5	300		-0.05	3.47	-0.05	3.47	-0.05	3.47	-0.05	3.47	-0.05	3.47	-0.05	3.47	-0.05	3.47	-0.05	3.47	-0.05	3.47	-0.05	3.47	-0.05	3.47	-0.05	3.47
Vacuum_Window	5	300		-0.03	2.08	-0.08	5.58	-0.03	2.08	-0.08	5.58	-0.03	2.08	-0.08	5.58	-0.03	2.08	-0.08	5.58	-0.03	2.08	-0.08	5.58	-0.03	2.08	-0.08	5.58
IR_Filter	4	190		-0.03	1.32	-0.11	6.92	-0.03	1.32	-0.11	6.92	-0.03	1.32	-0.11	6.92	-0.03	1.32	-0.11	6.92	-0.03	1.32	-0.11	6.92	-0.03	1.32	-0.11	6.92
Feed_Horn	1	20		-0.05	0.23	-0.16	7.16	-0.05	0.23	-0.16	7.16	-0.05	0.23	-0.16	7.16	-0.05	0.23	-0.16	7.16	-0.05	0.23	-0.16	7.16	-0.05	0.23	-0.16	7.16
OMT_Band5	1	20		-0.17	0.80	-0.33	7.99	-0.15	0.70	-0.31	7.88	-0.13	0.63	-0.29	7.81	-0.12	0.57	-0.28	7.75	-0.12	0.54	-0.28	7.71	-0.11	0.51	-0.27	7.69
Cal_Coupler	1	20		-0.22	1.02	-0.55	9.09	-0.23	1.06	-0.53	9.02	-0.24	1.12	-0.53	9.00	-0.25	1.17	-0.53	9.00	-0.24	1.15	-0.52	8.93	-0.23	1.08	-0.50	8.84
Cal_Inj_Band5	4	190		**0.00**	**0.19**	-0.55	9.31	**0.00**	**0.19**	-0.53	9.24	**0.00**	**0.19**	-0.53	9.21	**0.00**	**0.19**	-0.53	9.22	**0.00**	**0.19**	-0.52	9.15	**0.00**	**0.19**	-0.50	9.05
WG_Band5	1	20	0.05	-0.08	0.36	-0.62	9.71	-0.07	0.31	-0.60	9.59	-0.06	0.28	-0.59	9.53	-0.05	0.25	-0.58	9.50	-0.05	0.24	-0.57	9.42	-0.05	0.23	-0.55	9.31
LNA_Band5	1	20		**33.25**	**7.80**	32.63	18.71	**33.00**	**7.20**	32.40	17.85	**32.50**	**7.42**	31.91	18.02	**33.90**	**7.90**	33.32	18.54	**34.00**	**8.20**	33.43	18.76	**34.13**	**8.46**	33.58	18.90
WG_Band5	4	190	0.3	-0.46	21.17	32.17	18.72	-0.40	18.27	32.00	17.86	-0.36	16.34	31.55	18.03	-0.33	14.96	32.99	18.55	-0.31	14.00	33.12	18.77	-0.29	13.25	33.29	18.91
Cascaded Values:						**32.2**	**18.7**			**32.0**	**17.9**			**31.6**	**18.0**			**33.0**	**18.5**			**33.1**	**18.8**			**33.3**	**18.9**

Band #: 5	Temp. Stage	Phys. Temp.	T-Line Len.	41.3				43.3				45.7				48.0				50.5			
Frequency:																							
Component Type	#	K	m	G, dB	Te, K	Gcas	Tcas	G, dB	Te, K	Gcas	Tcas	G, dB	Te, K	Gcas	Tcas	G, dB	Te, K	Gcas	Tcas	G, dB	Te, K	Gcas	Tcas
Lossless Input	1	20		0.00	0.00	0.00	0.00	0.00	0.00	0.00	0.00	0.00	0.00	0.00	0.00	0.00	0.00	0.00	0.00	0.00	0.00	0.00	0.00
Weather_Radome	5	300		-0.05	3.47	-0.05	3.47	-0.05	3.47	-0.05	3.47	-0.05	3.47	-0.05	3.47	-0.05	3.47	-0.05	3.47	-0.05	3.47	-0.05	3.47
Vacuum_Window	5	300		-0.03	2.08	-0.08	5.58	-0.03	2.08	-0.08	5.58	-0.03	2.08	-0.08	5.58	-0.03	2.08	-0.08	5.58	-0.03	2.08	-0.08	5.58
IR_Filter	4	190		-0.03	1.32	-0.11	6.92	-0.03	1.32	-0.11	6.92	-0.03	1.32	-0.11	6.92	-0.03	1.32	-0.11	6.92	-0.03	1.32	-0.11	6.92
Feed_Horn	1	20		-0.05	0.23	-0.16	7.16	-0.05	0.23	-0.16	7.16	-0.05	0.23	-0.16	7.16	-0.05	0.23	-0.16	7.16	-0.05	0.23	-0.16	7.16
OMT_Band5	1	20		-0.10	0.49	-0.26	7.66	-0.10	0.47	-0.26	7.65	-0.10	0.46	-0.26	7.63	-0.10	0.45	-0.26	7.62	-0.09	0.44	-0.25	7.61
Cal_Coupler	1	20		-0.22	1.02	-0.48	8.75	-0.20	0.96	-0.47	8.67	-0.20	0.94	-0.46	8.63	-0.20	0.94	-0.46	8.62	-0.20	0.94	-0.45	8.61
Cal_Inj_Band5	4	190		**0.00**	**0.19**	-0.48	8.96	**0.00**	**0.19**	-0.47	8.88	**0.00**	**0.19**	-0.46	8.84	**0.00**	**0.19**	-0.46	8.83	**0.00**	**0.19**	-0.45	8.82
WG_Band5	1	20	0.05	-0.05	0.22	-0.53	9.21	-0.05	0.21	-0.51	9.11	-0.04	0.20	-0.50	9.07	-0.04	0.20	-0.50	9.05	-0.04	0.20	-0.50	9.04
LNA_Band5	1	20		**34.40**	**9.77**	33.87	20.24	**34.70**	**11.18**	34.18	21.69	**34.97**	**12.28**	34.47	22.85	**34.80**	**13.60**	34.30	24.31	**33.13**	**14.10**	32.63	24.85
WG_Band5	4	190	0.3	-0.28	12.68	33.59	20.24	-0.27	12.25	33.91	21.69	-0.26	11.87	34.20	22.86	-0.26	11.60	34.04	24.31	-0.25	11.40	32.38	24.85
Cascaded Values:						**33.6**	**20.2**			**33.9**	**21.7**			**34.2**	**22.9**			**34.0**	**24.3**			**32.4**	**24.9**

Table 12: Cascaded gain and noise, Band 5.

Band #: 6	Temp. Stage	Phys. Temp.	T-Line Len.	70.0				73.8				77.5				81.5				85.5				90			
Component Type	#	K	m	G, dB	Te, K	Gcas	Tcas	G, dB	Te, K	Gcas	Tcas	G, dB	Te, K	Gcas	Tcas	G, dB	Te, K	Gcas	Tcas	G, dB	Te, K	Gcas	Tcas	G, dB	Te, K	Gcas	Tcas
Lossless Input	1	20		0.00	0.00	0.00	0.00	0.00	0.00	0.00	0.00	0.00	0.00	0.00	0.00	0.00	0.00	0.00	0.00	0.00	0.00	0.00	0.00	0.00	0.00	0.00	0.00
Weather_Radome	5	300		-0.05	3.56	-0.05	3.56	-0.05	3.73	-0.05	3.73	-0.06	3.89	-0.06	3.89	-0.06	4.06	-0.06	4.06	-0.06	4.24	-0.06	4.24	-0.06	4.44	-0.06	4.44
Vacuum_Window	5	300		-0.03	2.08	-0.08	5.67	-0.03	2.08	-0.08	5.83	-0.03	2.08	-0.09	6.00	-0.03	2.08	-0.09	6.17	-0.03	2.14	-0.09	6.41	-0.03	2.34	-0.10	6.81
IR_Filter	4	190		-0.03	1.32	-0.11	7.01	-0.03	1.32	-0.11	7.18	-0.03	1.32	-0.12	7.34	-0.03	1.32	-0.12	7.52	-0.03	1.36	-0.12	7.80	-0.03	1.48	-0.13	8.33
Feed_Horn	1	20		-0.05	0.24	-0.16	7.25	-0.05	0.25	-0.17	7.43	-0.06	0.26	-0.17	7.61	-0.06	0.27	-0.18	7.79	-0.06	0.28	-0.18	8.09	-0.06	0.30	-0.20	8.63
OMT_Band6	1	20		-0.24	1.12	-0.40	8.42	-0.21	0.99	-0.38	8.46	-0.19	0.90	-0.36	8.54	-0.18	0.84	-0.36	8.67	-0.17	0.79	-0.35	8.92	-0.16	0.75	-0.36	9.42
Cal_Coupler	1	20		-0.68	3.40	-1.08	12.14	-0.65	3.21	-1.02	11.95	-0.61	3.02	-0.97	11.83	-0.57	2.82	-0.93	11.73	-0.55	2.68	-0.90	11.82	-0.53	2.60	-0.89	12.24
Cal_Inj_Band6	4	190		**0.00**	**0.19**	-1.08	12.38	**0.00**	**0.19**	-1.02	12.19	**0.00**	**0.19**	-0.97	12.06	**0.00**	**0.19**	-0.93	11.97	**0.00**	**0.19**	-0.90	12.05	**0.00**	**0.19**	-0.89	12.48
WG_Band6	1	20	0.025	-0.12	0.55	-1.20	13.09	-0.10	0.49	-1.13	12.81	-0.10	0.45	-1.07	12.62	-0.09	0.41	-1.02	12.48	-0.08	0.39	-0.98	12.53	-0.08	0.37	-0.97	12.93
LNA_Band6	1	20		**19.00**	**25.00**	17.80	46.04	**19.00**	**23.45**	17.87	43.20	**19.00**	**25.75**	17.93	45.56	**19.00**	**26.13**	17.98	45.50	**19.00**	**25.69**	18.02	44.73	**19.00**	**26.00**	18.03	45.41
WG_Band6	1	20	0.025	-0.12	0.55	17.68	46.05	-0.10	0.49	17.77	43.21	-0.10	0.45	17.83	45.57	-0.09	0.41	17.89	45.51	-0.08	0.39	17.93	44.74	-0.08	0.37	17.95	45.42
LNA_Band6	1	20		**19.00**	**25.00**	36.68	46.48	**19.00**	**23.45**	36.77	43.60	**19.00**	**25.75**	36.83	45.99	**19.00**	**26.13**	36.89	45.93	**19.00**	**25.69**	36.93	45.15	**19.00**	**26.00**	36.95	45.84
WG_Band6	4	190	0.3	-1.42	73.59	35.26	46.49	-1.25	63.60	35.52	43.61	-1.15	57.46	35.69	46.01	-1.07	53.02	35.82	45.94	-1.01	49.75	35.92	45.16	-0.96	47.09	35.99	45.85
Cascaded Values:						**35.3**	**46.5**			**35.5**	**43.6**			**35.7**	**46.0**			**35.8**	**45.9**			**35.9**	**45.2**			**36.0**	**45.8**

Band #: 6	Temp. Stage	Phys. Temp.	T-Line Len.	95				100				105				110.6				116.0			
Component Type	#	K	m	G, dB	Te, K	Gcas	Tcas	G, dB	Te, K	Gcas	Tcas	G, dB	Te, K	Gcas	Tcas	G, dB	Te, K	Gcas	Tcas	G, dB	Te, K	Gcas	Tcas
Lossless Input	1	20		0.00	0.00	0.00	0.00	0.00	0.00	0.00	0.00	0.00	0.00	0.00	0.00	0.00	0.00	0.00	0.00	0.00	0.00	0.00	0.00
Weather_Radome	5	300		-0.07	4.66	-0.07	4.66	-0.07	4.87	-0.07	4.87	-0.07	5.09	-0.07	5.09	-0.08	5.34	-0.08	5.34	-0.08	5.58	-0.08	5.58
Vacuum_Window	5	300		-0.04	2.56	-0.10	7.25	-0.04	2.78	-0.11	7.70	-0.04	2.99	-0.12	8.14	-0.05	3.24	-0.12	8.64	-0.05	3.47	-0.13	9.12
IR_Filter	4	190		-0.04	1.62	-0.14	8.91	-0.04	1.76	-0.15	9.50	-0.04	1.90	-0.16	10.09	-0.05	2.05	-0.17	10.75	-0.05	2.20	-0.18	11.38
Feed_Horn	1	20		-0.07	0.31	-0.21	9.23	-0.07	0.32	-0.22	9.84	-0.07	0.34	-0.23	10.44	-0.08	0.36	-0.25	11.12	-0.08	0.37	-0.26	11.77
OMT_Band6	1	20		-0.15	0.72	-0.36	9.99	-0.15	0.70	-0.37	10.57	-0.15	0.68	-0.38	11.16	-0.14	0.67	-0.39	11.82	-0.14	0.66	-0.40	12.47
Cal_Coupler	1	20		-0.52	2.52	-0.88	12.73	-0.50	2.44	-0.87	13.23	-0.50	2.44	-0.88	13.82	-0.50	2.44	-0.89	14.49	-0.50	2.44	-0.90	15.14
Cal_Inj_Band6	4	190		**0.00**	**0.19**	-0.88	12.96	**0.00**	**0.19**	-0.87	13.46	**0.00**	**0.19**	-0.88	14.05	**0.00**	**0.19**	-0.89	14.72	**0.00**	**0.19**	-0.90	15.38
WG_Band6	1	20	0.025	-0.08	0.36	-0.95	13.40	-0.07	0.35	-0.94	13.88	-0.07	0.34	-0.95	14.46	-0.07	0.33	-0.96	15.13	-0.07	0.33	-0.97	15.78
LNA_Band6	1	20		**19.00**	**26.75**	18.05	46.72	**19.00**	**27.50**	18.06	48.05	**19.00**	**26.38**	18.05	47.29	**19.00**	**25.68**	18.04	47.16	**19.00**	**42.00**	18.03	68.29
WG_Band6	1	20	0.025	-0.08	0.36	17.97	46.72	-0.07	0.35	17.98	48.06	-0.07	0.34	17.98	47.30	-0.07	0.33	17.97	47.16	-0.07	0.33	17.96	68.30
LNA_Band6	1	20		**19.00**	**26.75**	36.97	47.15	**19.00**	**27.50**	36.98	48.49	**19.00**	**26.38**	36.98	47.72	**19.00**	**25.68**	36.97	47.57	**19.00**	**42.00**	36.96	68.97
WG_Band6	4	190	0.3	-0.92	44.94	36.05	47.16	-0.89	43.36	36.09	48.50	-0.87	42.24	36.11	47.73	-0.85	41.30	36.11	47.58	-0.84	40.64	36.12	68.98
Cascaded Values:						**36.0**	**47.2**			**36.1**	**48.5**			**36.1**	**47.7**			**36.1**	**47.6**			**36.1**	**69.0**

Table 13: Cascaded gain and noise, Band 6.

7.3 Low Noise Amplifier Data, Bands 1–6

1			2			3			4			5			6		
Freq. (GHz)	Ga [1] (dB)	Tn [1] (K)	Freq. (GHz)	Ga [2] (dB)	Tn [2] (K)	Freq. (GHz)	Ga [3] (dB)	Tn [3] (K)	Freq. (GHz)	Ga [4] (dB)	Tn [4] (K)	Freq. (GHz)	Ga [5] (dB)	Tn [5] (K)	Freq. (GHz)	Ga [6] (dB)	Tn [6] (K)
1.0	23.0	9.5	3.0	36.4	4.6	12.0	35.2	5.0	20	33.9	6.0	30	33.0	8.0	70	19.0	25.0
1.2	26.0	4.0	3.5	37.3	4.3	12.5	35.0	5.0	21	33.4	5.3	31	33.5	7.6	72	19.0	23.0
1.4	27.7	2.5	4.0	37.0	4.0	13.0	34.6	5.0	22	32.8	5.6	32	33.0	7.2	74	19.0	23.5
1.6	27.5	1.7	4.5	36.5	3.6	13.5	34.2	5.3	23	31.5	6.0	33	32.5	7.0	76	19.0	25.0
1.8	27.2	1.5	5.0	36.1	3.6	14.0	34.6	6.0	24	31.5	6.0	34	32.5	7.6	78	19.0	26.0
2.0	26.8	1.1	5.5	36.1	3.6	14.5	35.0	6.5	25	31.0	6.5	35	34.0	7.8	80	19.0	26.5
2.2	26.8	1.2	6.0	36.2	3.5	15.0	35.0	7.0	26	30.0	6.2	36	33.8	8.0	84	19.0	25.5
2.4	26.3	1.2	6.5	36.5	3.4	16.0	34.6	8.0	27	27.9	5.7	37	34.0	8.2	88	19.0	26.0
2.6	26.4	1.2	7.0	37.0	3.4	17.0	34.0	7.5	28	27.5	5.7	38	34.0	8.2	92	19.0	26.0
2.8	26.3	1.5	7.5	37.2	3.5	18.0	34.6	6.0	29	28.0	6.0	40	34.2	8.6	96	19.0	27.0
3.0	26.2	1.7	8.0	37.6	3.8	19.0	35.0	6.0	30	28.0	6.3	42	34.5	10.4	100	19.0	27.5
3.2	26.4	1.8	9.0	38.0	4.2	20.0	34.6	8.0	31	28.0	6.5	44	34.8	11.6	104	19.0	26.5
3.4	26.4	1.8	10.0	38.1	4.5	21.0	34.0	9.5	32	28.0	6.7	46	35.0	12.4	108	19.0	26.0
3.6	26.3	2.1	11.0	38.0	5.3	22.0	33.0	8.5	33	28.0	7.3	48	34.8	13.6	112	19.0	25.5
3.8	26.1	2.4	12.0	38.1	5.3	23.0	32.5	9.0	34	28.0	7.8	50	33.5	14.0	114	19.0	27.0
4.0	25.6	3.4	13.0	38.1	5.7	24.0	33.0	10.0	35	28.0	8.0	52	32.0	14.4	115	19.0	28.0
															116	19.0	42.0

NOTES:

[1] - Band 1 LNA data is a Low Noise Factory LNF-LNC1.5_3.5A (1.5-3.5 GHz). Data has been derated per [8] to account for 20K vs. 4K operation.
N. Wadefalk at LNF states (4/2/20) that the noise temp at 1.2 could be improved to from 3.5K to 2K, with a quick redesign.

[2] - Band 2 LNA data is a Low Noise Factory LNF-LNC0.3_14 (0.6-14 GHz). Data has been derated per [8], to account for 20K vs. 4K operation.

[3] - Band 3 LNA data is a Caltech 1-18 GHz GaAs MMIC LNA (p/n CIT-118), based on OMMIC WBA118B device, T=19K (August 2014).
A version with a waveguide input, or an NRAO or Low Noise Factory (LNF) amp would likely perform better, by ~0.5 - 2K.

[4] - Band 4 LNA is a combination of data from Low Noise Factory LNF-LNC16_28WB (20-26 GHz) and LNF-LNC23_42WB (27-35 GHz),
assuming a custom WR-34 housing. A custom MMIC from LNF will be required for Band 4

[5] - Band 5 LNA data is a Low Noise Factory LNF-LNC28_52WB, 28-52 GHz, in a WR-22 housing.

[6] - Band 6 LNA data is of a 35nm MMIC LNA based on 35nm NGIC devices, from David Quadrado-Calle, U. of Manchester.

[7] - Numbers highlighted in yellow are either undetermined or rough estimates.

[8] - McCullock, Grahn, Melhuish, Nilsson, Piccirillo, Schleeh, Wadefalk, "Dependence of noise temperature on physical temperature for
cryogenic low-noise amplifiers", SPIE J. Astron. Telesc. Instrum. Syst. 3(1), 014003 (2017).

Table 14: LNA gain and noise temperature vs. frequency, Bands 1–6. A physical temperature of 20 Kelvin is assumed for all devices.

7.4 Single-Antenna Sensitivity Data Table, Bands 1–6

Freq. (GHz)	Aeff/Tsys vs. Antenna Elevation (deg)					Freq. (GHz)	Aeff/Tsys vs. Antenna Elevation (deg)				
	15	30	45	60	90		15	30	45	60	90
1.20	8.1	8.4	8.4	8.3	7.7	20.5	4.9	6.6	7.5	8.0	7.9
1.32	8.9	9.4	9.4	9.3	8.6	21.6	3.7	5.4	6.4	6.9	6.9
1.49	9.9	10.5	10.6	10.5	9.8	22.7	3.3	4.9	5.8	6.3	6.4
1.65	10.7	11.6	11.7	11.7	11.0	23.9	3.9	5.6	6.5	7.0	7.1
1.84	11.4	12.5	12.7	12.7	12.1	25.1	4.6	6.3	7.2	7.7	7.6
2.05	12.2	13.7	14.1	14.2	13.7	26.4	5.2	7.0	7.8	8.2	8.2
2.28	12.2	13.7	14.3	14.4	14.1	27.8	5.5	7.3	8.1	8.5	8.5
2.54	11.9	13.4	14.0	14.1	13.9	29.2	5.5	7.2	8.0	8.4	8.4
2.83	11.2	12.8	13.3	13.5	13.3	30.7	5.4	7.1	7.8	8.2	8.2
3.16	10.2	11.6	12.1	12.4	12.4	32.4	5.1	6.8	7.5	7.9	7.9
3.49	8.5	9.7	10.1	10.3	10.4	34.0	4.8	6.3	7.1	7.4	7.5
3.41	8.2	9.0	9.5	10.0	11.5	30.5	5.0	6.4	7.1	7.4	7.3
3.88	8.9	9.9	10.3	10.8	12.1	32.0	5.0	6.5	7.2	7.6	7.4
4.40	9.7	10.8	11.3	11.6	12.8	33.7	4.8	6.3	7.0	7.4	7.3
5.00	9.9	11.0	11.6	11.9	12.9	35.5	4.5	6.0	6.7	7.0	7.0
5.70	9.6	10.7	11.3	11.8	12.9	37.3	4.1	5.6	6.3	6.7	6.7
6.45	9.8	11.0	11.6	12.1	13.2	39.3	3.8	5.2	5.9	6.3	6.4
7.35	10.0	11.3	11.9	12.3	13.2	41.3	3.3	4.6	5.3	5.7	5.8
8.35	9.5	10.7	11.1	11.6	12.4	43.3	2.9	4.0	4.7	5.1	5.2
9.50	9.0	10.1	10.6	11.1	11.9	45.7	2.3	3.3	4.0	4.3	4.5
10.80	8.5	9.6	10.1	10.4	11.1	48.0	1.8	2.6	3.2	3.5	3.7
12.29	8.2	9.3	9.8	10.1	10.7	50.5	1.3	1.8	2.2	2.5	2.7
12.31	9.6	10.9	11.4	11.6	11.2	70.0	1.0	1.4	1.6	1.8	1.9
12.94	9.5	11.0	11.5	11.7	11.3	73.8	1.4	1.9	2.2	2.4	2.5
13.60	9.3	10.7	11.2	11.4	11.1	77.5	1.7	2.2	2.4	2.6	2.6
14.35	8.8	10.2	10.7	10.9	10.7	81.5	1.8	2.3	2.6	2.7	2.8
15.10	8.4	9.8	10.3	10.5	10.3	85.5	2.0	2.5	2.7	2.8	2.8
15.90	7.9	9.3	9.8	10.0	9.9	90.0	2.0	2.4	2.6	2.7	2.8
16.70	7.7	9.2	9.7	10.0	9.8	95.0	2.0	2.4	2.5	2.6	2.7
17.60	7.5	9.2	9.9	10.2	10.0	100.0	1.8	2.2	2.4	2.4	2.5
18.50	7.0	8.9	9.7	10.1	9.9	105.0	1.7	2.1	2.2	2.3	2.4
19.50	6.0	7.8	8.6	9.0	9.0	110.6	1.3	1.7	1.8	1.9	2.0
20.50	4.7	6.4	7.2	7.6	7.6	116.0	0.5	0.6	0.7	0.8	0.8

Table 15: Single-dish antenna sensitivity, Bands 1–6, for six elevation angles: 15, 30, 45, 60, and 90 degrees.

7.5 Abbreviations and Acronyms

Acronym	Description
AD	Applicable Document
ALMA	Atacama Large Millimeter sub-millimeter Array (telescope)
CDL	Central Development Laboratory
CW	Continuous Wave
DR	Dynamic Range
FEA	Finite Element Analysis
GPS	Global Positioning System
HEMT	High Electron Mobility Transistor
HAA	Herzberg Astronomy and Astrophysics Research Centre
IR	Infrared
IRD	Integrated Receiver Downconverter/Digitizer (Subsystem)
LNA	Low Noise Amplifier
LO	Local Oscillator
LRU	Line Replaceable Unit
M&C, M/C	Monitor and Control
MMIC	Monolithic Microwave Integrated Circuit
MTBM	Mean Time Between Maintenance
ngVLA	Next Generation Very Large Array
NRAO	National Radio Astronomy Observatory
NRC	National Research Council (Canada)
OFHC	Oxygen-Free High Conductivity (copper)
OMT	Ortho Mode Transducer
PWV	Precipitable Water Vapor
QRFH	Quad-Ridged Feed Horn
RD	Reference Document
RF	Radio Frequency
SEFD	System Equivalent Flux Density
SKA	Square Kilometer Array (telescope)
TBD	To Be Determined
VLA	Jansky Very Large Array
VLBA	Very Long Baseline Array

020.30.05.00.00-0006-DSN-C-FRONT_END_C ONCEPTUAL_DESIGN

Final Audit Report   2022-09-07

Created:	2022-09-06
By:	Alicia Kuhn (akuhn@nrao.edu)
Status:	Signed
Transaction ID:	CBJCHBCAABAA6Vrs0hqqhIkCVyXgPYrfX5J7Mg3DRj78

"020.30.05.00.00-0006-DSN-C-FRONT_END_CONCEPTUAL_D ESIGN" History

📄 Document created by Alicia Kuhn (akuhn@nrao.edu)
2022-09-06 - 6:10:02 PM GMT

✉ Document emailed to plopez@nrao.edu for signature
2022-09-06 - 6:11:25 PM GMT

📄 Email viewed by plopez@nrao.edu
2022-09-06 - 6:17:13 PM GMT

🖊 Signer plopez@nrao.edu entered name at signing as Phillip Lopez
2022-09-06 - 6:30:57 PM GMT

🖊 Document e-signed by Phillip Lopez (plopez@nrao.edu)
Signature Date: 2022-09-06 - 6:30:59 PM GMT - Time Source: server

✉ Document emailed to Thomas Kusel (tkusel@nrao.edu) for signature
2022-09-06 - 6:31:03 PM GMT

📄 Email viewed by Thomas Kusel (tkusel@nrao.edu)
2022-09-06 - 6:35:26 PM GMT

🖊 Document e-signed by Thomas Kusel (tkusel@nrao.edu)
Signature Date: 2022-09-06 - 6:36:17 PM GMT - Time Source: server

✉ Document emailed to rselina@nrao.edu for signature
2022-09-06 - 6:36:22 PM GMT

📄 Email viewed by rselina@nrao.edu
2022-09-06 - 6:37:07 PM GMT

Signer rselina@nrao.edu entered name at signing as R. Selina

2022-09-07 - 0:03:32 AM GMT

Document e-signed by R. Selina (rselina@nrao.edu)

Signature Date: 2022-09-07 - 0:03:33 AM GMT - Time Source: server

Document emailed to westerhu@nrao.edu for signature

2022-09-07 - 0:03:37 AM GMT

Email viewed by westerhu@nrao.edu

2022-09-07 - 7:11:21 AM GMT

Signer westerhu@nrao.edu entered name at signing as Willem Esterhuyse

2022-09-07 - 7:11:43 AM GMT

Document e-signed by Willem Esterhuyse (westerhu@nrao.edu)

Signature Date: 2022-09-07 - 7:11:44 AM GMT - Time Source: server

Agreement completed.

2022-09-07 - 7:11:44 AM GMT